# Recommended Method to Account for Uncertainty in the Fracture Toughness Characterization Used to Re-Evaluate the Pressurized Thermal Shock (PTS) Screening Criteria

Mark Kirk, *USNRC*

Paul Williams, *ORNL*

**October 5th, 2001**

# Executive Summary

To maintain their operating licenses, nuclear plant operators must demonstrate that the effects of irradiation embrittlement do not compromise the structural integrity of their reactor pressure vessel (RPV) during both routine operations and under postulated accident conditions. One of the most severe accidents is a pressurized thermal shock, or PTS, event wherein severe cooling of the core occurs on the inner diameter or the reactor together with, or followed by, pressurization. To protect against vessel failure under such circumstances, it is prudent to require a degree of toughness from the reactor pressure vessel steel adequate to stop a running crack. This idea led to the development of the "PTS Rule" [10CFR50.61], which contains just such a toughness requirement.

As pressurized water reactors (PWRs) approach the end of their original 40 year operating licenses, and consider requesting a 20 year license extension, compliance with the PTS Rule [10CFR50.61] can become a factor that limits the operational life of the plant. Addressing this issue on a plant-specific basis has consumed considerable resources. Additionally, it is now widely recognized that state of knowledge and data limitations in the early 1980's necessitated a conservative treatment of several key parameters and models used in the probabilistic calculations that provide the technical basis [SECY-82-465] of the current PTS rule [10CFR50.61]. One of the most prominent conservatisms is the characterization of fracture toughness using $RT_{NDT}$, which has an intentional conservative bias [ASME NB-2331].

The cost associated with demonstrating compliance with the current PTS screening criteria, the conservatisms known to underlie the screening criteria, and the considerable technical advancements that have occurred in the 20 years since the PTS Rule was established all combined to motivate the NRC Office of Nuclear Regulatory Research to undertake a project aimed at developing the technical basis to support a fundamental revision of the PTS rule, and the associated PTS screening criteria.

The PTS Re-Evaluation Project was initiated in 1998. Probabilistic calculations will be performed to establish the technical basis for a revised PTS rule within the framework established by probabilistic risk assessment (PRA) techniques. These techniques consider all of the factors that influence the risk of vessel failure during a PTS event while accounting for uncertainties in these factors in a consistent manner across a breadth of technical disciplines. A central feature of modern PRA techniques is an *explicit* treatment of uncertainties. These techniques distinguish between two types of uncertainties: aleatory and epistemic [Siu 99]. Aleatory uncertainties arise due to the randomness inherent to a physical or human process, whereas epistemic uncertainties are caused by a limitation in our current state of knowledge (or understanding) of that process. A practical way to distinguish between aleatory and epistemic uncertainties is that epistemic uncertainties can, in principle, be reduced by an increased state of knowledge. Conversely, because aleatory uncertainties arise due to inherent randomness at a level below which a particular process is modeled in the PRA, they are fundamentally irreducible. Distinction between aleatory and epistemic uncertainties is a crucial precursor to PRA calculations because the mathematical procedures used to account for uncertainties treat aleatory and epistemic uncertainties differently [Siu 01].

Currently, NRC regulations adopt a model of fracture toughness based on linear elastic fracture toughness values: $K_{Ic}$ for crack initiation toughness and $K_{Ia}$ for crack arrest toughness. The temperature dependency of these toughness values was established based on an empirical fit to a database of $K_{Ia}$ and

$K_{Ia}$ values. This temperature dependency is expressed as a function of temperature measured relative to an index temperature called $RT_{NDT}$, which is established based on testing of nil-ductility temperature (NDT) and Charpy V-notch (CVN) specimens. Use of $RT_{NDT}$ as an index temperature was intended to account for heat-to-heat differences in the fracture toughness transition temperature, thereby allowing a single toughness transition curve to represent all RPV steels. However, neither NDT nor CVN tests actually measure fracture toughness, so $RT_{NDT}$ can only be correlated with the true toughness transition temperature. As a consequence, $RT_{NDT}$-based models of fracture toughness have a known and intentional conservative bias [ASME NB-2331]. Despite these well-recognized shortcomings, the fracture toughness of the RPV will be estimated from CVN and NDT data in the PTS re-evaluation project so that all operators of pressurized water reactors can assess the state of their RPV relative to the new PTS screening criteria without the need to make new measurements of their reactor pressure vessel steels. Also, resource limitations on the PTS re-evaluation project dictate that calculations of fracture driving force will still rely on LEFM principles, rather than on more advanced elastic-plastic fracture mechanics techniques.

In summary, modern PRA techniques require an explicit treatment of uncertainties. However, the correlative and inexact nature of $RT_{NDT}$ produces an implicit treatment of uncertainty in current toughness models. Moreover, current toughness models, being empirical by nature, lack the theoretical underpinnings necessary to establish a view of how the data *should* behave, making discrimination between aleatory and epistemic uncertainties impossible. To structure a $RT_{NDT}$ / $K_{Ic}$ / $K_{Ia}$ toughness model in a manner compatible with PRA techniques, it is therefore necessary to first establish an independent, physically motivated, model of crack initiation and arrest toughness that also accounts for the effects of irradiation damage. Such models are established in this report, and are used to identify, classify, and quantify uncertainties in the $RT_{NDT}$ / $K_{Ic}$ / $K_{Ia}$ toughness model. Detailed instructions concerning how to incorporate this uncertainty framework into the probabilistic fracture mechanics code FAVOR (*F*racture *A*nalysis of *V*essels, *O*ak *R*idge) are also provided.

# Acknowledgements

The authors are indebted to their many colleagues who provided invaluable editorial and technical assistance in the preparation of this document. These individuals included Drs. Randy Nanstad and Richard Bass and Messrs. Terry Dickson and John Merkle, all of the Oak Ridge National Laboratory. Additionally Mr. Tanny Santos of the USNRC and Dr. Mohammad Modarres of the University of Maryland also provided editorial and technical assistance. We also extend our thanks to Mr. Stan Rosinski of the Electric Power Research Institute for providing access to the EPRI databases RPVDATA and PREP4. Finally, and most importantly, the recommendations provided herein could not have been established without the underlying methodology and technical basis, which is described in a separate document (referenced herein) authored by Dr. Marjorie Natishan of Phoenix Engineering Associates Inc.

# Table of Contents

# List of Tables

# List of Figures

# 1. Introduction

## 1.1 Background and Motivation

To maintain their operating licenses, nuclear plant operators must demonstrate that the effects of irradiation embrittlement do not compromise the structural integrity of their reactor pressure vessel (RPV) during both routine operations and under postulated accident conditions. One of the most severe accidents is a pressurized thermal shock, or PTS, event wherein severe cooling of the core occurs on the inner diameter or the reactor together with, or followed by, pressurization. Several operational sequences can generate a PTS, including a break of the main steam line, a rupture of a steam generator tube, a small break loss of coolant accident (LOCA), or extended injection of high-pressure water. In these situations, the tensile stresses produced by sudden cooling could be high enough to initiate a running cleavage crack, a crack that could propagate all the way through the vessel given adequate internal pressure. To protect against vessel failure under such circumstances, it is prudent to require a degree of toughness from the reactor pressure vessel steel adequate to stop a running crack. This idea led to the development of the "PTS Rule" [10CFR50.61], which contains just such a toughness requirement.

Clearly, factors other than the fracture toughness (e.g. operator response, plant design, etc.) can influence significantly the outcome (failure or non-failure) of a PTS event. To account for all of these factors and their interaction, probabilistic calculations were performed [SECY-82-465]. These calculations established a relationship between the probability of the RPV developing a through wall crack, and the index temperature for the fracture toughness transition curve ($RT_{NDT}$). This result, combined with the judgment that a $5x10^{-6}$ yearly probability of developing a through wall crack is tolerable, led to the establishment of +300°F (for circumferential welds) or +270°F (for all other materials) as screening limits for PTS [10CFR50.61]. Should these screening limits be exceeded before EOL, licensees are required to submit to the NRC a plant-specific analysis indicating how safe operation beyond the PTS screening limit will be ensured.

As pressurized water reactors (PWRs) approach the end of their original 40 year operating licenses, and consider requesting a 20 year license extension, compliance with the PTS Rule [10CFR50.61] can become a factor that limits the operational life of the plant. Addressing this issue on a plant-specific basis has consumed considerable resources. Additionally, it is now widely recognized that state of knowledge and data limitations in the early 1980's necessitated a conservative treatment of several key parameters and models used in the probabilistic calculations that provide the technical basis [SECY-82-465] of the current PTS rule [10CFR50.61]. The most prominent of these conservatisms include:

1. Characterization of fracture toughness using $RT_{NDT}$, which has an intentional conservative bias [ASME NB-2331],
2. The use of a flaw distribution that placed *all* of the flaws on the interior surface of the RPV, and, in general, contains larger flaws than those usually detected in service, and

3. The assumption that the peak fluence occurs over the entire interior surface of the RPV.

The cost associated with demonstrating compliance with the current PTS screening criteria, the conservatisms known to underlie the screening criteria, and the considerable technical advancements that have occurred in the 20 years since the PTS Rule was established all combined to motivate the NRC Office of Nuclear Regulatory Research to undertake a project aimed at developing the technical basis to support a fundamental revision of the PTS rule, and the associated PTS screening criteria.

## 1.2 The PTS Re-Evaluation Project

The PTS Re-Evaluation Project was initiated in 1998. Probabilistic calculations will be performed to establish the technical basis for a revised PTS rule within the framework established by probabilistic risk assessment (PRA) techniques. These techniques consider all of the factors that influence the risk of vessel failure during a PTS event while accounting for uncertainties in these factors in a consistent manner across a breadth of technical disciplines. A central feature of modern PRA techniques is an *explicit* treatment of uncertainties. These techniques distinguish between two types of uncertainties: aleatory and epistemic [Siu 99]. Aleatory uncertainties arise due to the randomness inherent to a physical or human process, whereas epistemic uncertainties are caused by a limitation in our current state of knowledge (or understanding) of that process. A practical way to distinguish between aleatory and epistemic uncertainties is that epistemic uncertainties can, in principle, be reduced by an increased state of knowledge. Conversely, because aleatory uncertainties arise due to inherent randomness at a level below which a particular process is modeled in the PRA, they are fundamentally irreducible. Distinction between aleatory and epistemic uncertainties is a crucial precursor to PRA calculations because the mathematical procedures used to account for uncertainties treat aleatory and epistemic uncertainties differently [Siu 01].

Currently, both NRC regulations and ASME Code adopt a model of fracture toughness based on linear elastic fracture toughness values: $K_{Ic}$ for crack initiation toughness and $K_{Ia}$ for crack arrest toughness. The temperature dependency of these toughness values was established based on an empirical fit to a database of $K_{Ia}$ and $K_{Ia}$ values. This temperature dependency is expressed as a function of temperature measured relative to an index temperature called $RT_{NDT}$, which is established based on testing of nil-ductility temperature (NDT) and Charpy V-notch (CVN) specimens. Use of $RT_{NDT}$ as an index temperature was intended to account for heat-to-heat differences in the fracture toughness transition temperature, thereby allowing a single toughness transition curve to represent all RPV steels. However, neither NDT nor CVN tests actually measure fracture toughness, so $RT_{NDT}$ can only be correlated with the true toughness transition temperature. As a consequence, $RT_{NDT}$-based models of fracture toughness have a known and intentional conservative bias [ASME NB-2331]. Despite these well recognized shortcomings, the fracture toughness of the RPV will be estimated from CVN and NDT data in the PTS re-evaluation project so that all operators of pressurized water reactors can assess the state of their RPV relative to the new PTS screening criteria without the need to make new measurements of their reactor pressure vessel steels. Also, resource limitations on the PTS re-evaluation project dictate that calculations of fracture driving force will still rely on LEFM principles, rather than on more advanced elastic-plastic fracture mechanics techniques.

In summary, modern PRA techniques require an explicit treatment of uncertainties. However, the correlative and inexact nature of $RT_{NDT}$ produces an implicit treatment of uncertainty in current toughness models. Moreover, current toughness models, being empirical by nature, lack the theoretical underpinnings necessary to establish a view of how the data *should* behave, making discrimination between aleatory and epistemic uncertainties impossible. To structure a $RT_{NDT}$ / $K_{Ic}$ / $K_{Ia}$ toughness model in a manner compatible with PRA techniques, it is therefore necessary to first establish an independent, physically motivated, model of crack initiation and arrest toughness that also accounts for the effects of irradiation damage.

## 1.3 Technical Evaluation of a Physically Motivated Toughness Model

A working party including representatives from both the NRC and from the commercial nuclear power industry recently completed a comprehensive *Evaluation and Characterization of Uncertainty in Fracture Toughness Models for Ferritic Reactor Pressure Vessel Steels*. The report of this working party [WRC Bulletin xxxx] provides the technical justification for a physically motivated model of linear elastic fracture toughness, and also provides an assessment of uncertainties relative to this model. In this report we summarize the main findings from WRC Bulletin xxxx, and use this information as the basis for recommending a treatment of uncertainties for incorporation into FAVOR that is consistent with PRA requirements. To provide a fully specified toughness model for FAVOR it has been necessary to integrate information from sources outside of WRC Bulletin xxxx. Table 1.1 lists the main source documents used in the preparation of this report. The references for minor source documents and background documents are detailed in Section 8.

Table 1.1. Source documents.

| First Author | Title | Date | Use in this NUREG |
|---|---|---|---|
| Natishan | Evaluation and Characterization of Uncertainty in Fracture Toughness Models for Ferritic Reactor Pressure Vessel Steels (WRC Bulletin xxxx [Natishan 01b]) | 11/2001 | Framework for uncertainty evaluation, physical models of fracture toughness |
| Eason | Updated Transition Temperature Shift Model (NRC Internal Document) | 2/2001 | Embrittlement trend curve |
| Santos | Development of Statistical Distributions for Copper, Nickel, and Phosphorus for the PTS Re-Evaluation Program (NRC Internal Document) | 7/2000 | Generic distributions of chemical composition |
| NRC RVID | Reactor Vessel Integrity Database (NRC Database) | 2000 | Best estimate values of Cu, Ni, and P |

## 1.4 Structure of this Report

In Section 2 we describe the existing $RT_{NDT}$ / $K_{Ic}$ / $K_{Ia}$ toughness model. Section 3 describes the procedure employed by the authors of WRC ???? to develop physically motivated models and assess uncertainties in a manner consistent with the requirements of modern PRA techniques. Sections 4, 5, and 6 contain more details regarding crack initiation toughness ($K_{Ic}$), transition temperature shift ($\Delta T_{30}$), and crack arrest toughness ($K_{Ia}$), respectively. In each section we summarize the physically motivated model developed in WRC Bulletin xxxx for each of these variables, and, based on this model, recommend an uncertainty treatment for use in FAVOR.

# 2. The Current Toughness Model and its Technical Basis

## 2.1 The Model

In the early 1970s, a set of LEFM-valid initiation ($K_{Ic}$) and arrest ($K_{Ia}$) fracture toughness data was developed for ferritic nuclear RPV steels [WRC 175]. These data, with test temperature normalized to $RT_{NDT}$, provide the basis for the ASME $K_{Ic}$ and $K_{Ia}$ curves. These curves were hand-drawn as lower bounds to the fracture toughness data (See Figure 2.1); they are represented mathematically as follows:

Eq. 2-1
$$K_{Ic} = 33.2 + 2.806 \cdot \exp\left[0.02 \cdot \left(T - RT_{NDT} + 100\right)\right] \quad \text{(a)}$$
$$K_{Ia} = 26.78 + 1.223 \cdot \exp\left[0.0145 \cdot \left(T - RT_{NDT} + 160\right)\right] \quad \text{(b)}$$

where

$RT_{NDT}$ is defined as per ASME NB-2331, i.e. $RT_{NDT} = MAX\left\{T_{NDT}, T_{35/50} - 60\right\}$,

$T_{NDT}$ is the nil-ductility temperature determined by testing NDT specimens as per ASTM E208,

$T_{35,50}$ is the transition temperature at which Charpy-V notch (CVN) specimens tested as per ASTM E23 exhibit at least 35 mills lateral expansion and 50 ft-lbs absorbed energy.

In Eq. 2-1 stress intensity factor ($K$) values are expressed in units of ksi√in and temperature values are expressed in units of °F. When the technical basis for the current PTS rule was established [SECY 82 465], Eq. 2-1 was used to establish the statistical models of fracture toughness used in the probabilistic calculations. At the time it was assumed that Eq. 2-1 represents the mean-minus-2σ curves, and that the scatter in fracture toughness could be modeled using a truncated normal distribution. On the basis of these assumptions, the following mathematical model of the linear elastic fracture toughness of an irradiation embrittled reactor pressure vessel steel, was developed:

Eq. 2-2
$$\overline{K_{Ic}} = \frac{1}{0.7}\left\langle 33.2 + 2.806 \cdot \exp\left[0.02 \cdot \left(T - \left\{RT_{NDT} + \Delta T_{30}\right\} + 100\right)\right]\right\rangle, \ \sigma_{Ic} = 0.15\overline{K_{Ic}} \quad \text{(a)}$$
$$\overline{K_{Ia}} = \frac{1}{0.8}\left\langle 26.78 + 1.223 \cdot \exp\left[0.0145 \cdot \left(T - \left\{RT_{NDT} + \Delta T_{30}\right\} + 100 + \Delta RT_{ARREST}\right)\right]\right\rangle, \ \sigma_{Ia} = 0.10\overline{K_{Ia}} \quad \text{(b)}$$
$$\Delta T_{30} = (CF) f^{(0.28 - 0.1 \log f)} \quad \text{(c)}$$

where

$\left\{\overline{K_{Ic}}, \sigma_{Ic}\right\}$ are, respectively, the mean and standard deviation of the crack initiation fracture toughness ($K_{Ic}$). In the calculations reported in SECY-82-465, $K_{Ic}$ was truncated at ±3σ.

$\left\{\overline{K_{Ia}}, \sigma_{Ia}\right\}$ are, respectively, the mean and standard deviation of the crack arrest fracture toughness ($K_{Ia}$). In the calculations reported in SECY-82-465, $K_{Ia}$ was truncated at ±3σ.

$\Delta T_{30}$ is the irradiation-induced shift in the 30 ft-lb CVN transition temperature
$\Delta RT_{ARREST}$ is 60°F as defined by Eq. 2-1.
*CF* (chemistry factor) expresses the aggregate effect of Cu, Ni, and product form on irradiation sensitivity. *CF* values are determined from tables in Reg. Guide 1.99 Rev. 2.
*f* is the neutron fluence (/ $1x10^{19}$ n/cm$^2$)

Figure 2.2 compares the statistical models for $K_{Ic}$ and $K_{Ia}$, Eq. 2-2 (a) and (b) respectively, to the fracture toughness data they were intended to represent. While a reasonable representation, it is clear that these models do not represent "best fits" to the data. Figure 2.3 compares the CVN transition temperature shift model of Eq. 2-2(c) with available $\Delta T_{30}$ data from commercial reactor surveillance programs. There is both considerable uncertainty and a systematic over-prediction associated with the Reg. Guide 1.99 (Revision 2) model. Furthermore, Eq. 2-2(c) implicitly assumes that $\Delta T_{30}$ represents accurately the transition temperature shift in fracture toughness (i.e. $K_{Ic}$ and $K_{Ia}$) data.

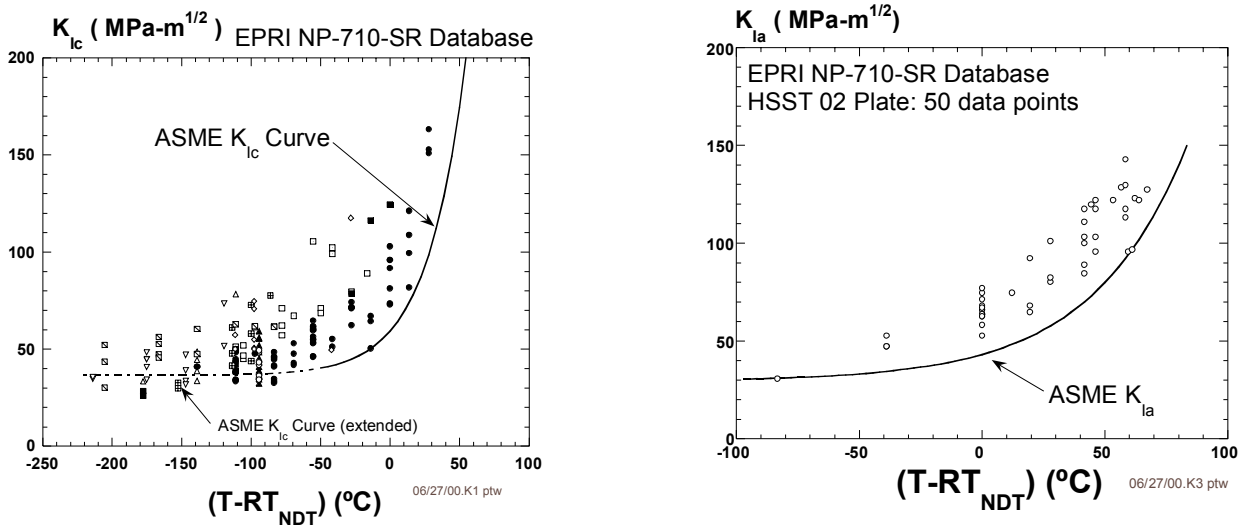


Figure 2.1. Experimental database of $K_{Ic}$ and $K_{Ia}$ values used to establish the ASME $K_{Ic}$ and $K_{Ia}$ curves.

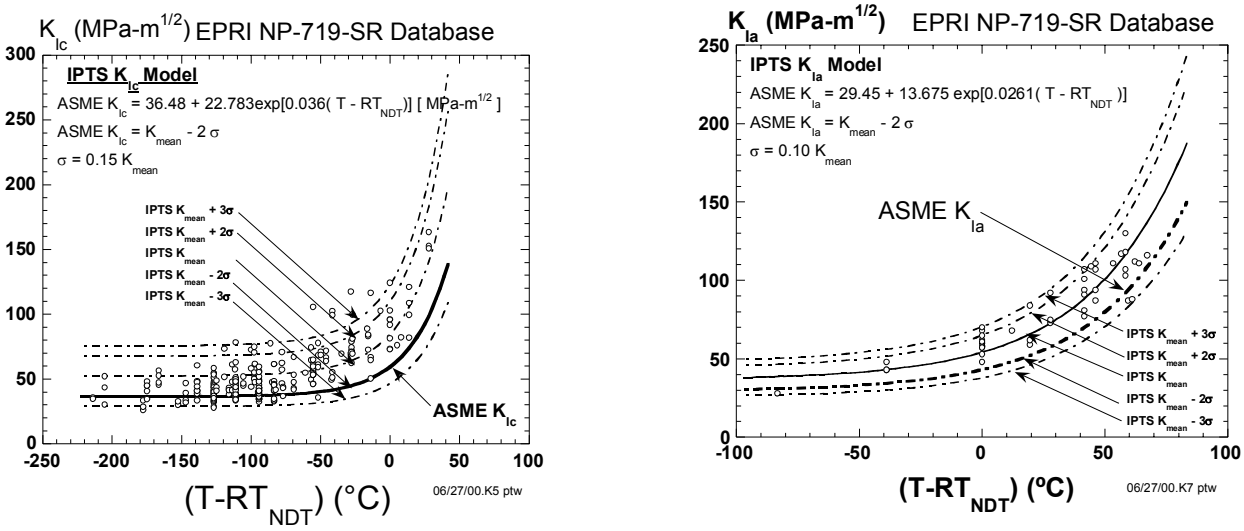


Figure 2.2. Comparison of the statistical toughness models used in the IPTS studies with the experimental database of $K_{Ic}$ and $K_{Ia}$ values used to establish the ASME $K_{Ic}$ and $K_{Ia}$ curves.

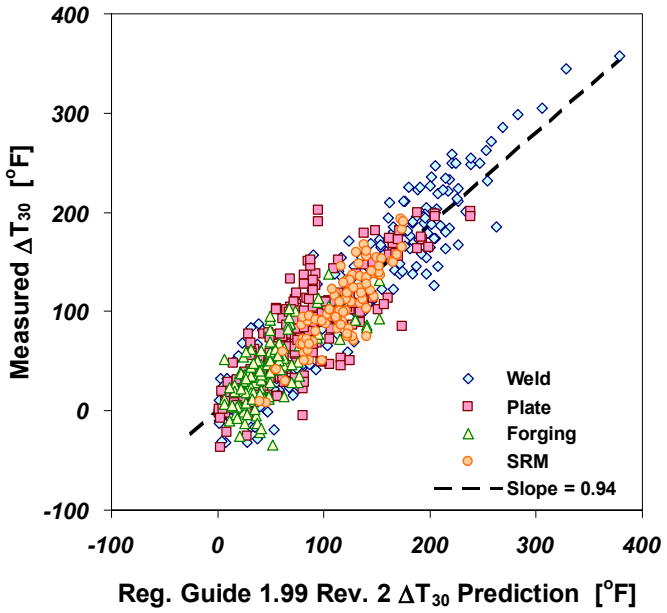


Figure 2.3. Comparison of Regulatory Guide 1.99 (Revision 2) predictions of $\Delta T_{30}$ with measured values.

Figure 2.4 provides a diagrammatic representation of the statistical toughness model (Eq. 2-2), and illustrates that it includes five key variables:

1. Fracture Toughness Variables
   a. $K_{Ic}$: Crack initiation fracture toughness
   b. $K_{Ia}$: Crack arrest fracture toughness
2. Index Temperature Variables
   a. $RT_{NDT}$: Establishes the location of un-irradiated crack initiation toughness ($K_{Ic}$) data on the temperature axis.
   b. $\Delta RT_{ARREST}$: Establishes the separation between crack initiation toughness ($K_{Ic}$) data and crack arrest toughness data ($K_{Ia}$) on the temperature axis
   c. $\Delta T_{30}$: Establishes the degree to which the transition temperatures of both the $K_{Ic}$ and $K_{Ia}$ data are shifted due to irradiation.

In subsequent Sections, the uncertainty associated with each of these variables will be discussed.

## 2.2 Applications of the Model

Both deterministic and stochastic applications of this toughness model exist. Deterministically, ASME code adopts the {mean–2σ} $K_{Ic}$ and $K_{Ia}$ curves (Eq. 2-1) as representations of fracture toughness for use in calculations that establish the window of allowable pressures and temperatures for routine heat-up and cool-down of a nuclear pressure vessel performed as per 10CFR50 Appendix G [10CFR50G]. However, the stochastic representations of this toughness model, Eq. 2-2, are of greater relevance to the topic at hand, for these have been used in the PFM calculations reported in SECY-82-465. Since SECY-82-465 provides the technical basis for the current PTS rule [10CFR50.61], Eq. 2-2 describes the toughness assumed by this rule. Eq. 2-2 was also used in the Integrated Pressurized Thermal Shock (IPTS) studies [Dickson 99]. Therefore, when discussing PTS, Eq. 2-2 establishes both the model of fracture toughness and the treatment of uncertainty used currently.

## 2.3 Technical Basis, Assumptions, and Treatment of Uncertainties

Eq. 2-2, was based on a database of $K_{Ic}$ and $K_{Ia}$ values expressed as a function of $T$-$RT_{NDT}$ (see Figure 2.2). Eq. 2-2 therefore assumes that both the variation of $K_{Ic}$ and $K_{Ia}$ with temperature and the scatter of $K_{Ic}$ and $K_{Ia}$, shown in Figure 2.2, is characteristic of all RPV steels. Taken in combination, $RT_{NDT}$ and the fracture toughness ($K_{Ic}$ and $K_{Ia}$) relationships of Eq. 2-2 were defined to account conservatively for the various material variables that influence the ductile to brittle transition temperature of a specific steel. As illustrated in Figure 2.5, the degree of conservatism achieved by this process can vary greatly from one heat of steel to the next. Eq. 2-2 therefore accounts *implicitly* for uncertainties, and in no way accounts for the source of these uncertainties, or even indicates in relation to what variable (i.e. to $K_{Ic}$, $K_{Ia}$, $RT_{NDT}$, $\Delta T_{30}$, $\Delta RT_{ARREST}$) the uncertainties arise.

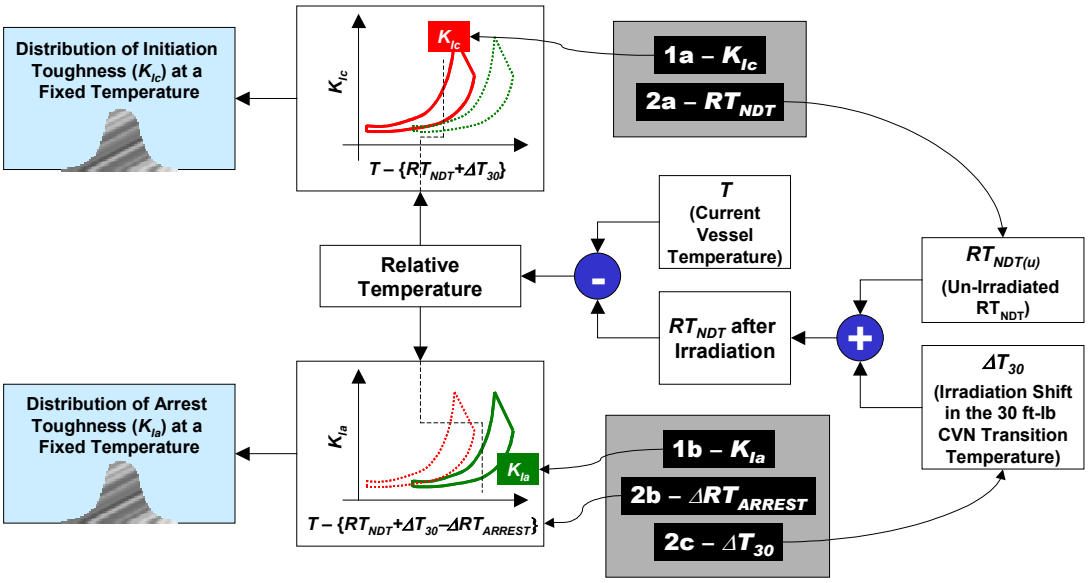


Figure 2.4. Schematic illustrating how the existing toughness model combines values of five key variables (see shaded boxes). Three index temperatures ($RT_{NDT}$, $\Delta RT_{ARREST}$, and $\Delta$T30) are combined with initiation ($K_{Ic}$) and arrest ($K_{Ia}$) transition fracture toughness curves to estimate distributions of $K_{Ic}$ and $K_{Ia}$ at a fixed temperature.

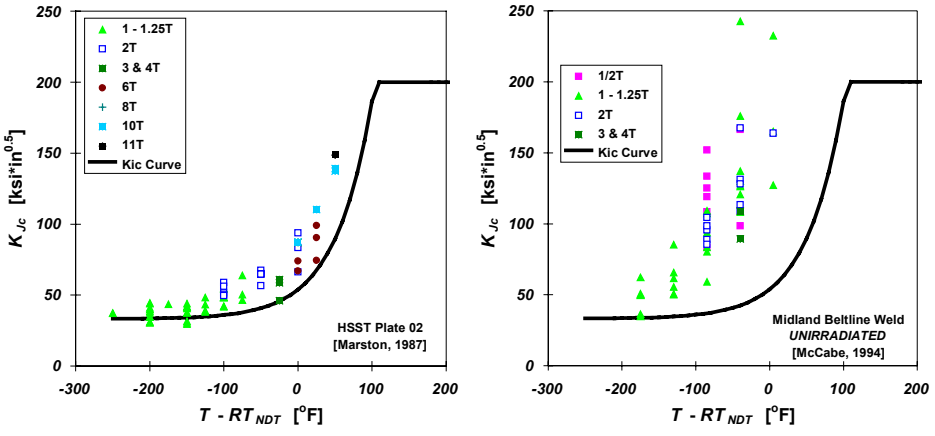


Figure 2.5. Illustration of the inconsistency with which $RT_{NDT}$ positions a $K_{Ic}$ curve relative to as-measured fracture toughness data.

# 3. Approach to Uncertainty Characterization for Fracture Toughness Models

As stated earlier, PRA procedures require an explicit identification of the type of uncertainty present. To do this it is first necessary to establish an independent, physically motivated, model of crack initiation and arrest toughness that accounts also for the effects of irradiation damage. A working party including representatives from both the NRC and from the commercial nuclear power industry recently completed a document entitled *Evaluation and Characterization of Uncertainty in Fracture Toughness Models for Ferritic Reactor Pressure Vessel Steels* that does this. The approach used in that report to identify, classify, and quantify uncertainty is summarized below.

Step #1 Uncertainty Identification: The working party began by constructing a graphical description of the current toughness model. This description, called a "root cause diagram," is illustrated schematically in Figure 3.1. Diagrams of this type show *all* of the parameters (shaded boxes) and *all* of the relationships (nodes) combined by the current model to estimate the fracture toughness for a particular set of conditions. Decomposing the model in this way permitted identification of individual sources of uncertainty, both in the parameters and in the relationships assumed between the parameters.

Step #2 Uncertainty Classification: Uncertainties were classified through an understanding of the basic physical mechanisms responsible for crack initiation, for crack arrest, and for irradiation damage. Without this physical understanding, it was impossible to distinguish the irreducible (i.e. aleatory) uncertainties associated with variability of the material from reducible (i.e. epistemic) uncertainties caused by limited data, imperfect models, and so on.

Step #3 Uncertainty Quantification: The physical understanding developed to classify uncertainty types also played a pivotal role in uncertainty quantification, because a model of fracture toughness that can be regarded as representing the true behavior of the material is needed to quantify the uncertainties present in any other model. Therefore, uncertainty quantification was achieved by comparing the $RT_{NDT}$-based toughness model developed for use in the PTS re-evaluation project to this best-estimate model.

To be consistent with LEFM principles, LEFM-valid $K_{Ic}$ and $K_{Ia}$ values are the preferred data that the working party used to calibrate the parameters of this best estimate model. However, the best-estimate model cannot be constructed as a purely empirical fit to these $K_{Ic}$ and $K_{Ia}$ values. Without the insights available from a physically based understanding it is impossible to discern if the trends demonstrated by the laboratory data can be expected to apply to the material and loading conditions of interest in commercial pressurized water reactors. Consequently, the "best estimate models" developed by the working party each had a form motivated by the physical processes responsible for crack initiation, crack arrest, or irradiation damage. Depending on the sophistication of this physical understanding, the parameters of the toughness model were sometimes derivable directly from the underlying physics.

However, most of the time the parameters of the toughness model were calibrated by fitting experimental data using the physically expected functional form.

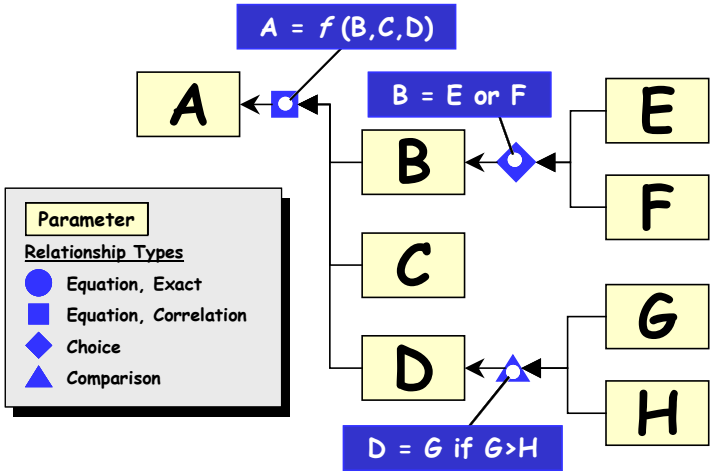


Figure 3.1. Illustration of a root cause diagram showing how uncertainties in input variables (E, F, G, and H) propagate through models (nodes), themselves potentially having uncertainty, to produce uncertainty in a resultant value (A).

# 4. Model of Crack Initiation Toughness

## 4.1 Requirements of the Model

To enable all commercial operators of pressurized water reactors to assess the state of their RPV relative to the new PTS screening criteria without the need to make new material property measurements, the initiation fracture toughness of the RPV needs to be estimated using only currently available $RT_{NDT}$ values. Moreover, to be consistent with the LEFM principles on which the FAVOR code is based, this $RT_{NDT}$ -based model needs to estimate $K_{Ic}$ values. These restrictions suggest that only very limited information, specifically a value of $RT_{NDT}$, is available to define the initiation fracture toughness model appropriate to a particular steel in a particular RPV. Consequently, the temperature dependency and uncertainty of the initiation fracture toughness model will either have to be demonstrated or assumed to be invariant over a wide range of conditions because sufficient information is not available to establish these features on a material heat specific basis.

## 4.2 The Findings of the Working party Presented in WRC Bulletin xxxx

The information presented in WRC Bulletin xxxx demonstrates that the scatter in and temperature dependency of $K_{Ic}$ data are features universal to all reactor pressure vessel steels, features that within this class of materials are insensitive to all individual and combined effects of alloying, heat treatment (and other thermal processing), mechanical processing, and irradiation. The only effect of these variables is one of influencing the temperature range over which a particular steel experiences a transition from brittle behavior (at low temperatures) to ductile behavior (at higher temperatures), this being quantified by a heat specific index temperature value. Thus, knowledge of only an index temperature, such as $RT_{NDT}$, for a particular steel is sufficient, at least in concept, to define fully the initiation fracture toughness model for that material.

Sections 4.2.1 and 4.2.2 summarize the physical bases for a temperature dependency of and scatter in fracture toughness that is universal to all RPV steels put forward by the Working Party. Section 4.2.3 then summarizes a mathematical model that incorporates these features.

### 4.2.1 Physical Basis for a Universal Temperature Dependency in Initiation Fracture Toughness Data

Physically, the only feature of the steel that can produce a temperature dependency in its properties are the short-range barriers to dislocation motion established by the lattice structure, which is body-centered cubic (BCC) for the ferritic steel used in nuclear RPV construction. Other features that vary with steel composition, heat treatment, and irradiation include grain size/boundaries, point defects, inclusions, precipitates, and dislocation substructures. These features all influence dislocation motion, and thereby both strength and toughness, but their large inter-barrier spacing relative to the atomic scale associated with the lattice structure makes these effects completely athermal. This understanding suggests that the myriad of metallurgical factors that can influence absolute strength and toughness values, and thereby

the transition temperature, exert no control over the temperature dependency of toughness in fracture mode transition.

### 4.2.2 Physical Basis for a Universal Scatter in Initiation Fracture Toughness Data

Cleavage cracks initiate when the dislocations accumulated at non-coherent particles or other barriers to dislocation motion (i.e. carbides, grain boundaries, twin boundaries, etc.) generate sufficient strain to elevate the local stress at the barrier above that needed to fracture the barrier or cause its decohesion from the matrix. These barriers are distributed in a random fashion throughout the BCC iron lattice. The interaction of these randomly distributed barriers with the varying stress field along the crack front gives rise to the experimentally observed scatter in toughness data.

In order for fracture to occur by cleavage, high stress triaxiality is needed to inhibit crack-tip blunting by dislocation motion. Thus, for cleavage to occur the stress fields much be in a state of small-scale yielding (SSY), conditions that are ensured by the LEFM assumption. High triaxiality occurs under SSY conditions because the crack-tip stress field is not affected by the specimen boundaries. This means that dislocations are fully contained within a finite volume at the crack tip and cannot escape to blunt the crack or dissipate energy. Under SSY conditions, the volume in which dislocations are moving can be described relative only to the length $L=(K_I/\sigma_y)^2$, making the total volume of the plastic fracture process zone proportional to $L^2 \cdot B$, or (substituting for $L$) proportional to $K_I^4$. Since the probability of failure by cleavage is the compliment of the joint probability of non-failure of all the volume elements sampled by the crack-tip stress fields, the probability of failure scales in proportion to the plastically deformed volume (i.e., in proportion to $K_I^4$). Thus, the scatter in the cleavage fracture toughness of *all* ferritic steels is expected, on theoretical grounds, to be described by a Weibull distribution having a shape parameter of 4 provided only that failure occurs under the small scale yielding conditions assured by LEFM.

### 4.2.3 Best Estimate Model

As described in Sections 4.2.1 and 4.2.2, strong physical bases supports a temperature dependency of and scatter in initiation fracture toughness data that is universal to all ferritic steels. Overwhelming empirical evidence testifies that these physical expectations manifest in reality (see Figure 4.1 and Figure 4.2). Mathematically, these features have been captured in a model of initiation fracture toughness proposed by Wallin and co-workers that is widely referred to as the Master Curve:

Eq. 4-1 $$K_{Jc(median)} = 27.30 + 63.71 \cdot \exp\left[0.0106\left(T - T_o\right)\right]$$

Eq. 4-2 $$P_f = 1 - \exp\left\{-\frac{B}{B_o}\left(\frac{K_I - 18.20}{K_o - 18.20}\right)^4\right\}$$

Eq. 4-1 describes the temperature ($T$) dependency of the median fracture toughness ($K_{Jc(median)}$). In this equation, temperature is normalized to the index temperature $T_o$. $T_o$ is defined as the temperature at which the median toughness of a fracture specimen having the reference thickness ($B_o$, which is defined to be 1-in.) is 91.01 ksi√in. Eq. 4-2 provides the three-parameter Weibull distribution that describes the distribution of toughness values about this median at all temperatures in transition. Of these three parameters, two are fixed: the shape parameter is fixed at 4 and the minimum value is set to 18.18 ksi√in. The parameter $K_o$, which corresponds to a 63.2% probability of failure, is determined by fracture toughness testing as described by ASTM Standard E1921. $K_o$ and $K_{Jc(median)}$ are related as follows:

Eq. 4-3 $$K_{Jc(median)} = 0.9124\left(K_o - 18.20\right) + 18.20$$

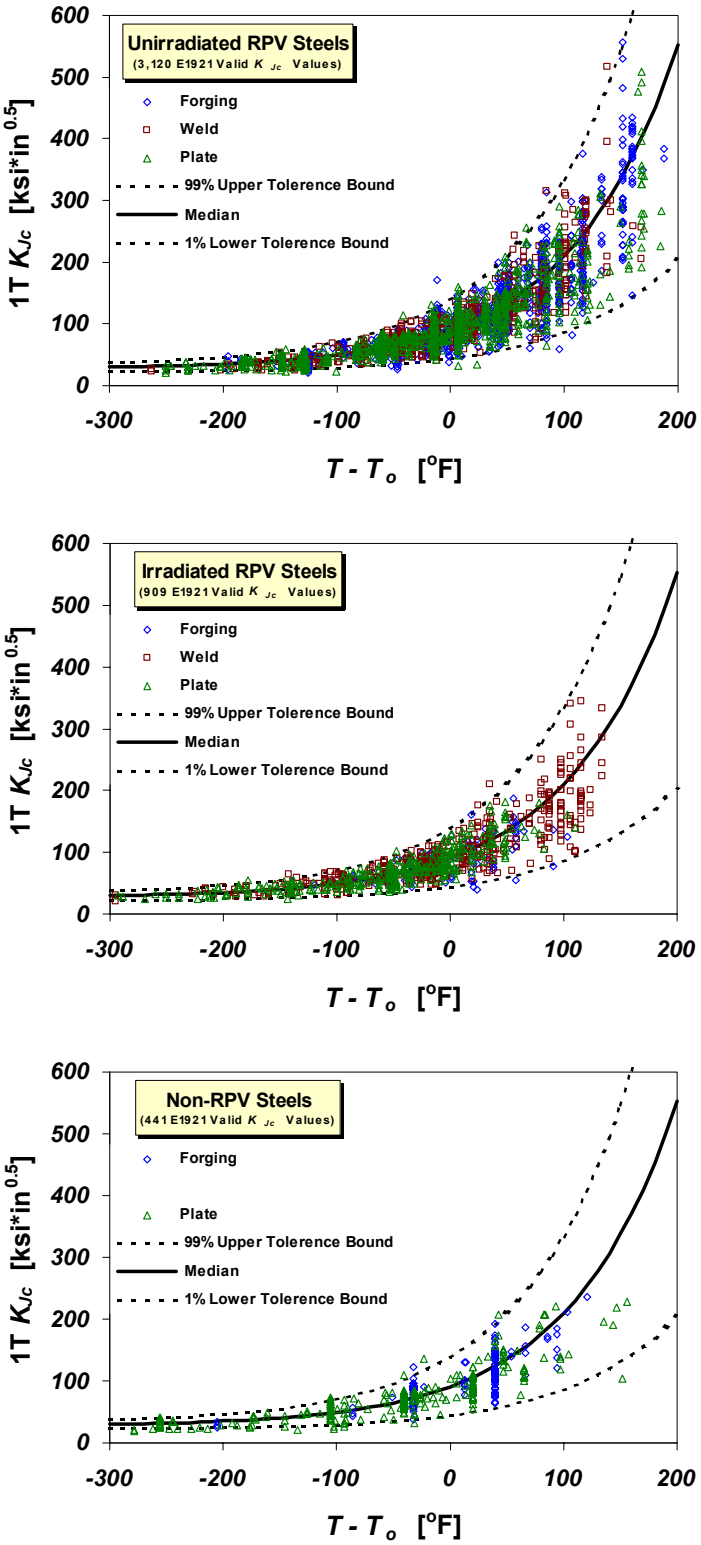


Figure 4.1. The uniform variation of cleavage fracture toughness with temperature noted by Wallin for (top) unirradiated reactor pressure vessel steels, (middle) irradiated reactor pressure vessel steels, (bottom) other ferritic steels.

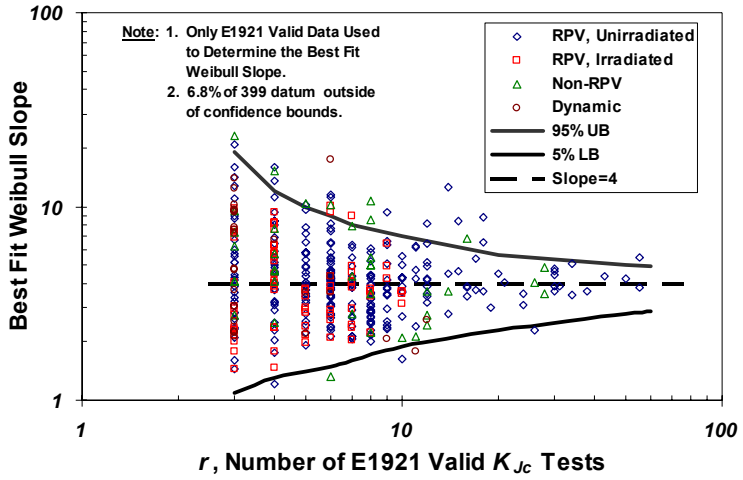


Figure 4.2. Comparison of Weibull shape parameters calculated from fracture toughness data with 5%/95% confidence bounds on the expected shape parameter of 4 predicted by Wallin.

### 4.2.4 Toughness Model Suggested for use in the PTS Re-Evaluation Project

As detailed in the preceding Sections, the Master Curve enjoys both a strong physical basis and considerable empirical support. However, two factors make its direct use in the PTS re-evaluation inappropriate, specifically:

1. Unlike $RT_{NDT}$, Master Curve index temperature ($T_o$) values are not known for most of the steels in nuclear RPVs. Using the Master Curve directly would thus require licensees to make new measurements on their irradiated materials, which is to be avoided, and
2. The Master Curve includes an explicit treatment of size effects (via Eq. 4-2), and is based on elastic-plastic fracture toughness ($K_{Jc}$) values. Neither feature is compatible with the LEFM basis of FAVOR.

To account for these inconsistencies yet still recommend a toughness model that fulfils the needs of the PTS re-evaluation project, the Working party used the insights from the Master Curve and the physical basis described in Sections 4.2.1 and 4.2.2 to classify uncertainty type, and to establish the form of the toughness model, but calibrated the model using only LEFM-valid $K_{Ic}$ data. Their recommendations on the classification and quantification of uncertainty for both the index temperature ($RT_{NDT}$) and for initiation fracture toughness ($K_{Ic}$) are summarized in the following sections

#### 4.2.4.1 Index Temperature ($RT_{NDT}$) Uncertainty Classification and Quantification

$RT_{NDT}$ values are uncertain both due to epistemic (i.e., the conservative bias implicit in the ASME NB-2331 definition of $RT_{NDT}$, the variety of inconsistent transition temperature metrics used to define $RT_{NDT}$, the lack of prescription in the test methods used to define $RT_{NDT}$, and the fact that the CVN and NDT values used to define $RT_{NDT}$ do not themselves measure fracture toughness) and aleatory (i.e. material variability) causes. Certainly epistemic uncertainty sources far outnumber aleatory ones. However, this information alone is inadequate to classify the uncertainty in $RT_{NDT}$ as being primarily aleatory or primarily epistemic. To make this distinction a comparison of the $RT_{NDT}$ index temperature to an index temperature ($T_o$) associated with a physically motivated model of crack initiation toughness (i.e., the Master Curve) is needed.

The Master Curve model of initiation fracture toughness is supported by strong physical insights, which demonstrates that the trends revealed by the empirical data (see Figure 4.1 and Figure 4.2) are expected, and more importantly are expected to apply to the entire range of material and irradiation conditions characteristic of PWR service. This, combined with the fact that the Master Curve index temperature $T_o$ is estimated directly from fracture toughness data, and so, by definition, must be associated with the same location on the transition temperature curve of every steel, suggest that the epistemic uncertainty sources that plague $RT_{NDT}$ do not influence $T_o$. Thus, the uncertainty in $T_o$ is expected to be primarily aleatory, so a comparison of $T_o$ and $RT_{NDT}$ values can be used to quantify the epistemic uncertainty in $RT_{NDT}$. Since $T_o$ represents the same point on the transition curve for all materials, $T_o$ *must* correspond to the position of fracture toughness data. The numerical difference between $RT_{NDT}$ and $T_o$ therefore quantifies how far away from measured fracture toughness data $RT_{NDT}$ positions a model of fracture toughness, as illustrated in Figure 4.3. Figure 4.4 shows the cumulative distribution function (CDF) constructed from the difference between values of $RT_{NDT}$ and $T_o$ reported in the literature for the same RPV steels that were collected by the Working Party. These data demonstrate that the epistemic uncertainty in $RT_{NDT}$ almost always produces a conservative estimate of the actual fracture toughness transition temperature.

While it quantifies the epistemic uncertainty in $RT_{NDT}$, the CDF illustrated in Figure 4.4 cannot be used directly in FAVOR because of the previously noted inconsistencies between $T_o$ and the requirements of the PTS re-evaluation project. Consequently, the Working Party developed an alternative CDF that avoids the explicit treatment of size effects and the use of EPFM toughness data, but retains the important concept from the Master Curve that the measured toughness data quantify the "truth" that a $RT_{NDT}$-based model needs to represent. This alternative CDF, illustrated in Figure 4.5, was determined based on the temperature shift values ($\Delta RT_{LB}$) needed to make a NB-2331 $RT_{NDT}$-positioned $K_{Ic}$ curve lower bound a set of LEFM-valid $K_{Ic}$ data for each of 18 heats of RPV steel.

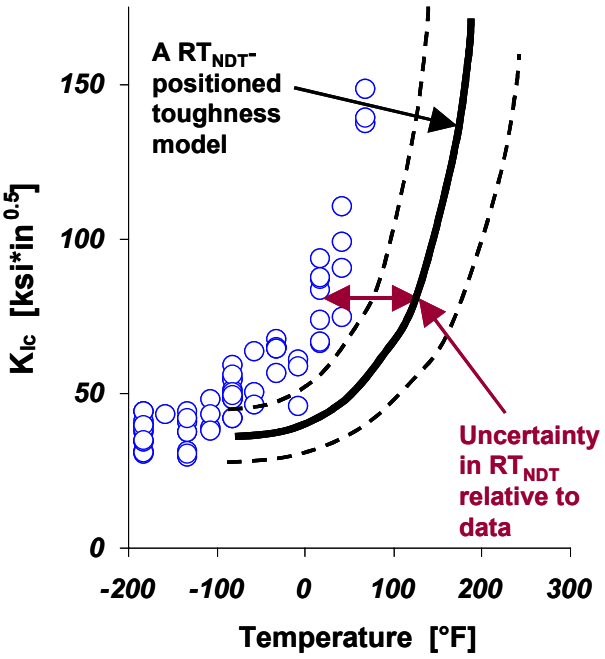


Figure 4.3. Illustration of how the error in a $RT_{NDT}$-based model of fracture toughness transition is determined.

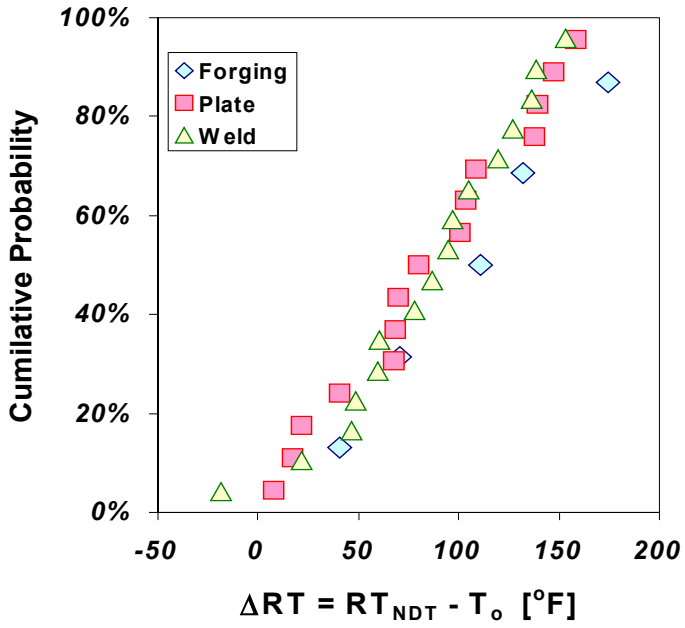


Figure 4.4. Cumulative distribution function showing the difference between $T_o$ and $RT_{NDT}$.

Figure 4.6 shows the cumulative distribution function (*CDF*) determined from these $\Delta RT_{LB}$ values.

Eq. 4-4 $$\Delta RT_{LB} = -40.02 + 124.88\left[-\ln(1-P)\right]^{0.51}$$

This CDF quantifies the epistemic uncertainty in $RT_{NDT}$ in a manner fully consistent with the constraints placed on toughness models used in the PTS re-evaluation effort. In Figure 4.6 we also compare this quantification of epistemic uncertainty with that based on the Master Curve (from Figure 4.4). This comparison illustrates that the implicit treatment of size effects adopted when developing the alternative CDF produces a result quite similar in form to that based on the Master Curve. The similarity of the alternative CDF (in Figure 4.5) to the Master Curve-based CDF (in Figure 4.4) provides a link between the $RT_{LB}$ concept developed to conform to the requirements of the PTS re-evaluation and the physical and empirical underpinnings of the Master Curve, thereby demonstrating that aleatory and epistemic uncertainties can be reasonably distinguished using $RT_{LB}$ and $\Delta RT_{LB}$.

### 4.2.4.2 Initiation Fracture Toughness ($K_{Ic}$) Uncertainty Classification and Quantification

From the physical model of cleavage crack initiation toughness developed by the Working Party in WRC Bulletin ???, one concludes that the distribution of non-coherent particles throughout the BCC iron lattice alone establishes the scatter in $K_{Ic}$ data. It is possible, at least in principle, to know if a non-coherent particle exists at a particular point in the matrix, or not. This might suggest an epistemic nature to $K_{Ic}$ scatter, were it not for the fact that $K_{Ic}$ does not exist as a point property. A $K_{Ic}$ value always has a size scale associated with it, that being the plastically deformed volume. Upon loading, the presence of the crack elevates the stress state along the entire length of the crack front to the point that dislocations begin to move in the surrounding volume of material, which contains a distribution of dislocation barriers (e.g. non-coherent particles, grain boundaries, twin boundaries, etc.). Sufficient accumulation of dislocations at a barrier can elevate the local stress-state sufficiently to initiate a crack in the barrier, and, if the criteria for fracture are satisfied, propagate the crack through the entire surrounding test specimen or structure. Thus, the existence of a particular dislocation barrier at a particular location does not control $K_{Ic}$. Rather $K_{Ic}$ is controlled by the distribution of these barriers throughout the lattice, and how

this distribution interacts with the elevated stresses along the crack front. Since the distribution of these barriers throughout the lattice is random and occurs at a size-scale below that considered by the $K_{Ic}$ model of toughness, the uncertainty in $K_{Ic}$ data is irreducible. For this reason, the uncertainty in $K_{Ic}$ should be treated as aleatory.

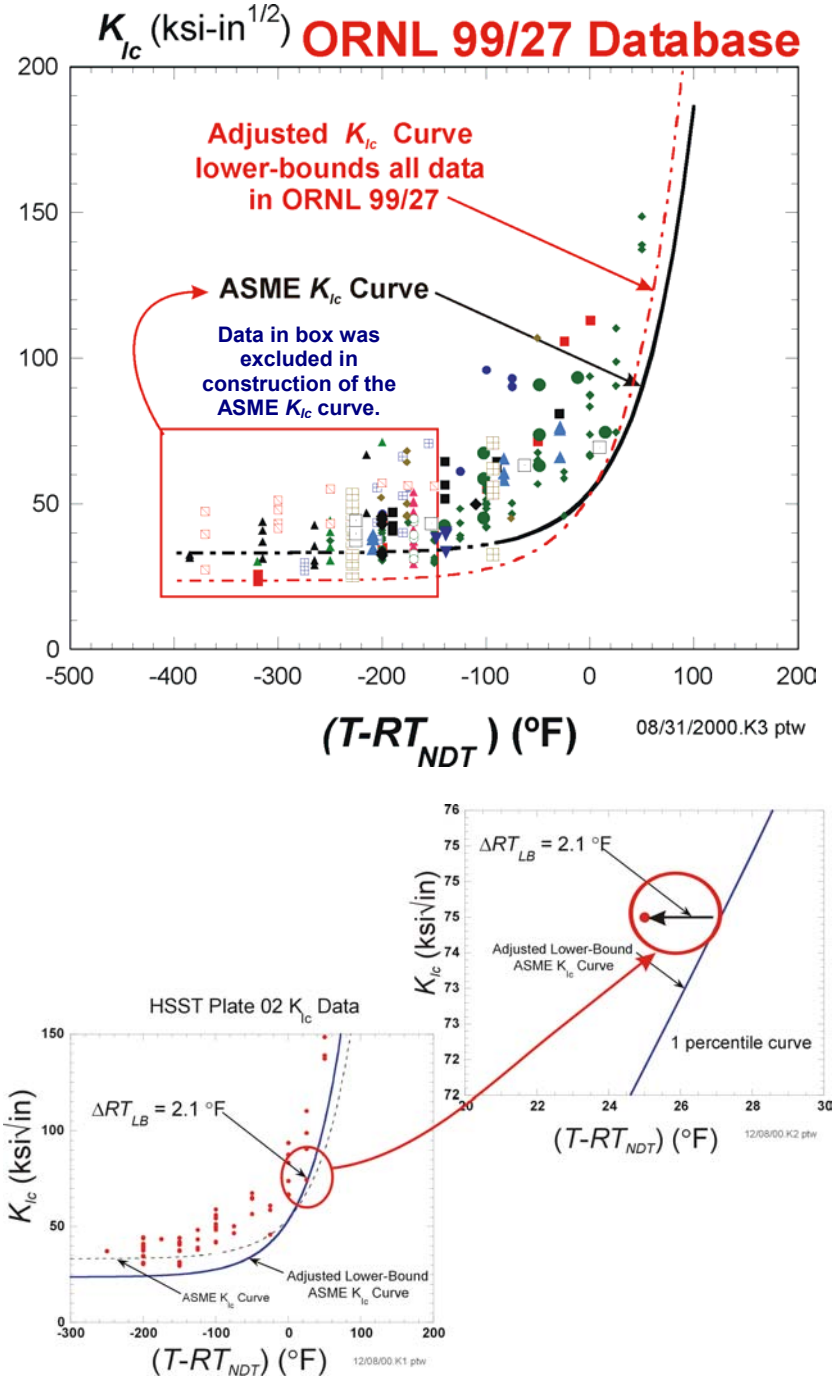


Figure 4.5. (TOP) Extended $K_{Ic}$ fracture toughness database (ORNL/NRC/LTR-99/27) [Bowman 00] of ASTM E399 valid data compared with adjusted ASME $K_{Ic}$ curve [Nanstad 93]. (BOTTOM) Illustration of the lower-bounding methodology used to generate the uncertainty term ($\Delta RT_{LB}$) for $RT_{NDT(0)}$.

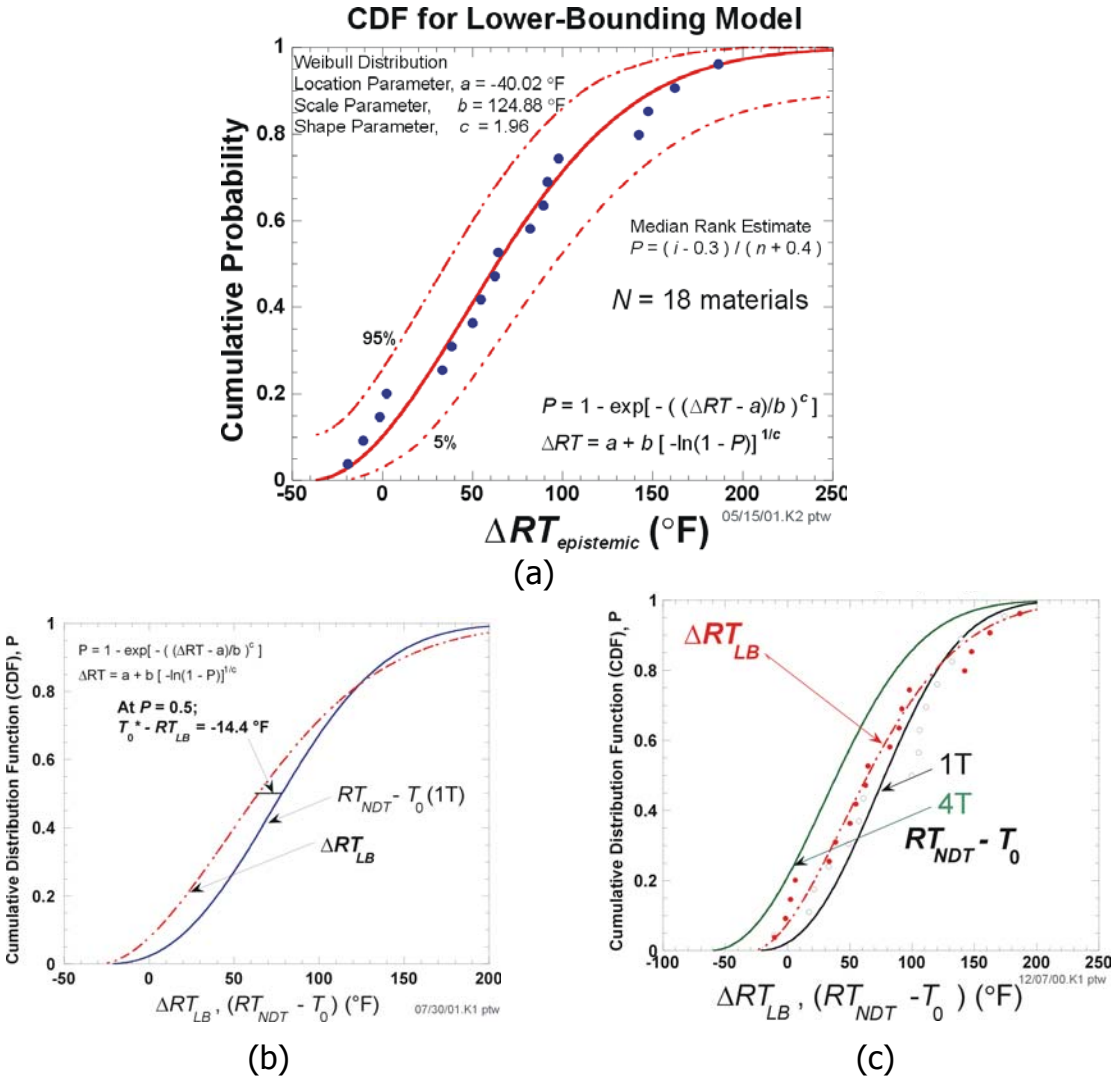


Figure 4.6. (a) Illustration of $\Delta RT_{LB}$ that quantifies both the epistemic uncertainty in $RT_{NDT(u)}$ and the intentional bias in $RT_{NDT(u)}$ values. (b-c) Comparison of $\Delta RT_{LB}$ adjustment with Master Curve-based ($RT_{NDT}$-$T_o$) adjustment.

As summarized in Section 4.2.1, the physical explanation of cleavage fracture proposed by the Working Party explains why the uncertainty (scatter) in $K_{Ic}$ data is expected to follow a Weibull distribution having a shape parameter of 4. This distribution was therefore assumed when fitting a data set of ??? LEFM valid $K_{Ic}$ values from 18 heats of RPV steel to establish the temperature dependence of $K_{Ic}$ relative to the normalized temperature $T$-$RT_{LB}$. This best-fit model, which describes the aleatory uncertainty in $K_{Ic}$, is illustrated in Figure 4.7. Mathematically, this $K_{Ic}$ model is as follows:

Eq. 4-5 $$K_{Ic}(\Delta T) = a_{K_{Ic}}(\Delta T) + b_{K_{Ic}}(\Delta T)\left[-\ln(1-P)\right]^{1/c_{K_{Ic}}} \quad \text{for } 0 \le P < 1$$

Where

$K_{Ic}$ is in ksi√in
$\Delta T$ is ($T$-$RT_{LB}$), in °F,
$P$ is the fracture probability, and

$$a_{K_{Ic}}(\Delta T) = 19.35 + 8.335\exp\left[0.02254(\Delta T)\right] \ [\text{ksi}\sqrt{\text{in.}}]$$
$$b_{K_{Ic}}(\Delta T) = 15.61 + 50.132\exp\left[0.008(\Delta T)\right] \ [\text{ksi}\sqrt{\text{in.}}]$$
$$c_{K_{Ic}} = 4$$
$$-250°\text{F} \le \Delta T \le +50°\text{F}$$

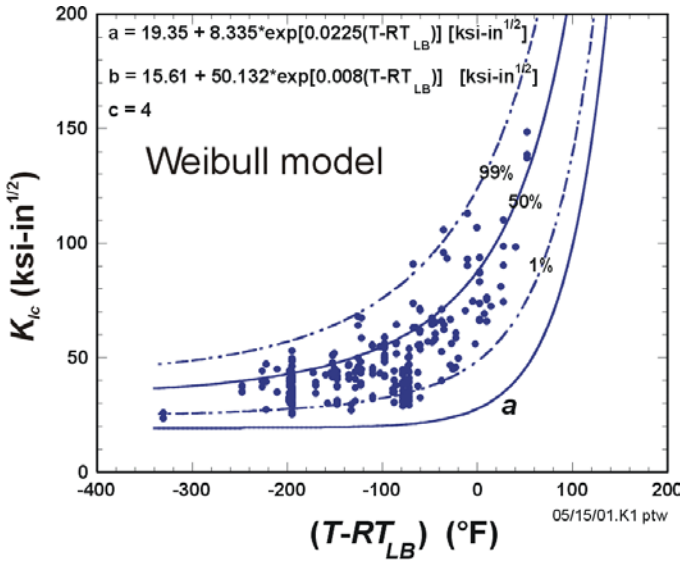


Figure 4.7. $K_{Ic}$ model proposed for use in the PTS re-evaluation effort.

### 4.3 Recommended FAVOR Coding Logic

Figure 4.8 illustrates the procedure that is recommended for use in FAVOR to represent the crack initiation toughness model, and the associated uncertainties in crack initiation fracture toughness values:

1) Determine the un-irradiated $RT_{NDT}$ value, $RT_{NDT(u)}$, and $RT_{NDT}$ uncertainty, $\sigma_{(u)}$, from the information in Appendix A.
   a) If $\sigma_{(u)}$ is other than 0, randomly select a value of $RT_{NDT}$* from a standard normal distribution having a mean value of a $RT_{NDT(u)}$ and a standard deviation of $\sigma_{(u)}$.
   b) If $\sigma_{(u)}$ is 0, let $RT_{NDT}$* = $RT_{NDT(u)}$.
2) Generate a random number, P, between 0 and 1. P represents the cumulative probability that $\Delta RT_{LB}$ is less than a particular value.
3) Use this random number to select a value of $\Delta RT_{LB}$ from the CDF in Figure 4.6 using the following equation:
   $$\Delta RT_{LB} = -40.02 + 124.88\left[-\ln(1-P)\right]^{0.51}$$
   $\Delta RT_{LB}$ quantifies both the epistemic uncertainty in $RT_{NDT}$* and the intentional bias in $RT_{NDT}$* values.
4) The best estimate of the initiation fracture toughness transition temperature for the material of interest is defined as follows:
   $$RT_{initiation} = RT_{NDT}\,^{*} - \Delta RT_{LB}$$
5) Determine the temperature of the vessel at the location of interest ($T_{vessel}$). Determine the difference between the vessel temperature and the initiation reference temperature as follows.

$$\Delta T = T_{vessel} - RT_{initiation}$$

6) The aleatory distribution of $K_{Ic}$ at $\Delta T$ is described by the following equation:

$$K_{Ic}(\Delta T) = a_{K_{Ic}}(\Delta T) + b_{K_{Ic}}(\Delta T)\left[-\ln(1-P)\right]^{1/c_{K_{Ic}}} \quad \text{for } 0 \le P < 1$$

$$a_{K_{Ic}}(\Delta T) = 19.35 + 8.335\exp\left[0.02254(\Delta T)\right] \ [\text{ksi}\sqrt{\text{in.}}]$$

$$b_{K_{Ic}}(\Delta T) = 15.61 + 50.132\exp\left[0.008(\Delta T)\right] \ [\text{ksi}\sqrt{\text{in.}}]$$

$$c_{K_{Ic}} = 4$$

$$-250°\text{F} \le \Delta T \le +50°\text{F}$$

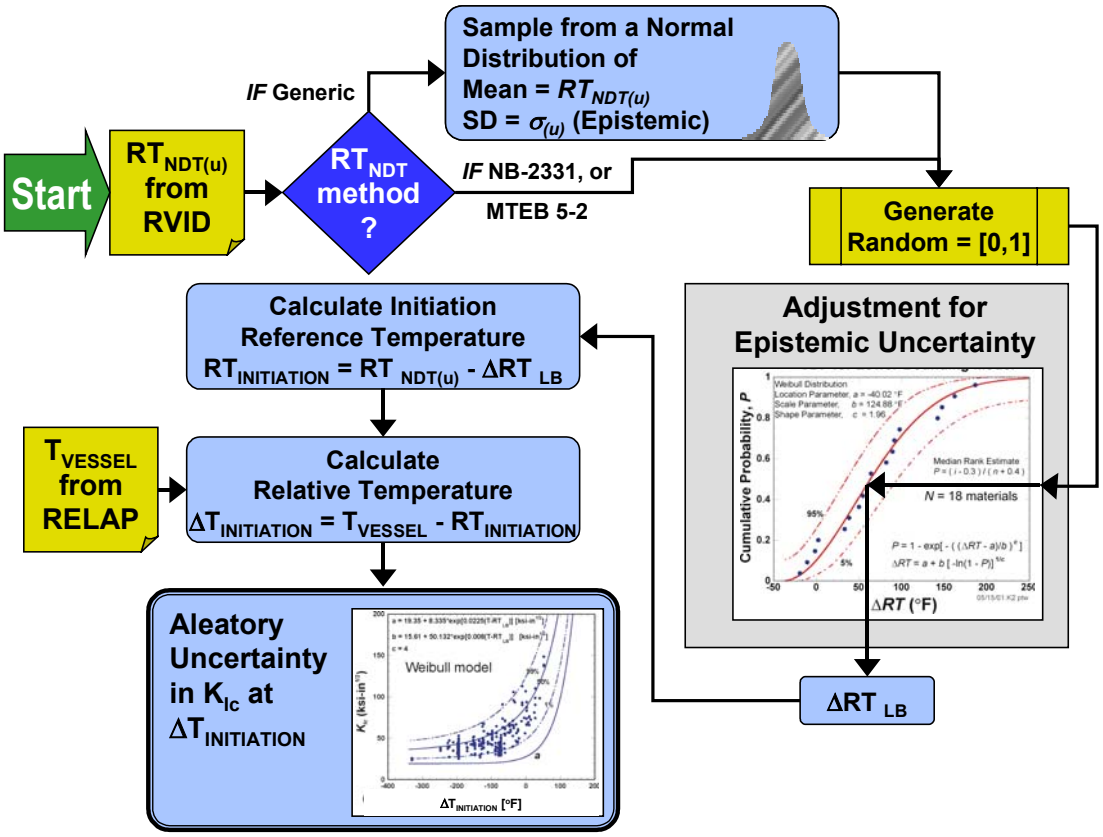


Figure 4.8. Illustration of the proposed procedure to account for epistemic uncertainty in $RT_{NDT(u)}$ and quantify aleatory uncertainty in $K_{Ic}$.

# 5. Model of the Shift in Toughness Transition Temperature Caused by Irradiation

## 5.1 Requirements of the Model

To enable all commercial operators of pressurized water reactors to assess the state of their RPV relative to the new PTS screening criteria without the need to make new material property measurements, the shift in the $K_{Ic}$ fracture toughness transition temperature produced by irradiation needs to be estimated using only currently available data on composition (e.g. Cu, Ni, P) and irradiation conditions (e.g. flux, time, temperature, fluence).

## 5.2 The Findings of the Working party Presented in WRC Bulletin ????

The information presented in WRC Bulletin xxxx suggests that two models link the influence of composition and irradiation variables to the change in fracture toughness transition temperature ($\Delta T_o$) produced by irradiation. As illustrated in Figure 5.1, these include an irradiation model (M1) describing how irradiation hardening influences the yield strength†, and a toughness model (M2) relating changes in yield strength to changes in transition temperature. The Working Party found that physical arguments to link basic composition and irradiation variables to yield strength elevation (M1: Irradiation Model), and also link yield strength elevation to the change in the toughness transition temperature (M2: Toughness Model). This physical understanding provides, at least in concept, the ability to characterize and quantify uncertainties in a manner consistent with PRA requirements. However, the current state of knowledge supporting these models is not sufficient to make them fully predictive. Moreover, the most comprehensive irradiation effects models available today relate basic compositional and irradiation variables to the shift in CVN energy transition temperature ($\Delta T_{30}$) rather than to shifts in the toughness transition temperature ($\Delta T_o$). This focus on $\Delta T_{30}$ occurs due to the historical practices of measuring Charpy shift as part of RPV surveillance programs, and of using $\Delta T_{30}$ as an approximate measure of the effect of irradiation on the shift in the fracture toughness transition temperature. This situation necessitated consideration by the Working Party of evidence other than that contained in the irradiation model and in the toughness model, including a physically motivated but empirically derived embrittlement trend curve (M3 on Figure 5.1), and empirical supporting relationships between $\Delta\sigma_{ys}$, $\Delta T_{30}$, and $\Delta T_o$ (M4 and M5 on Figure 5.1). Their findings are summarized in the following Sections.

---

† As discussed in WRC Bulletin???? (and within many other sources), irradiation can produce grain boundary segregation of tramp elements such as phosphorus. This leads to a non-hardening form of embrittlement (i.e. one that elevates the toughness transition temperature without increasing the yield strength) that is not captured by the models illustrated in Figure 5.1. Nevertheless, the consensus of the technical community is that US RPV steels have sufficiently low impurity levels that non-hardening embrittlement is not expected for the operational conditions of US RPVs.

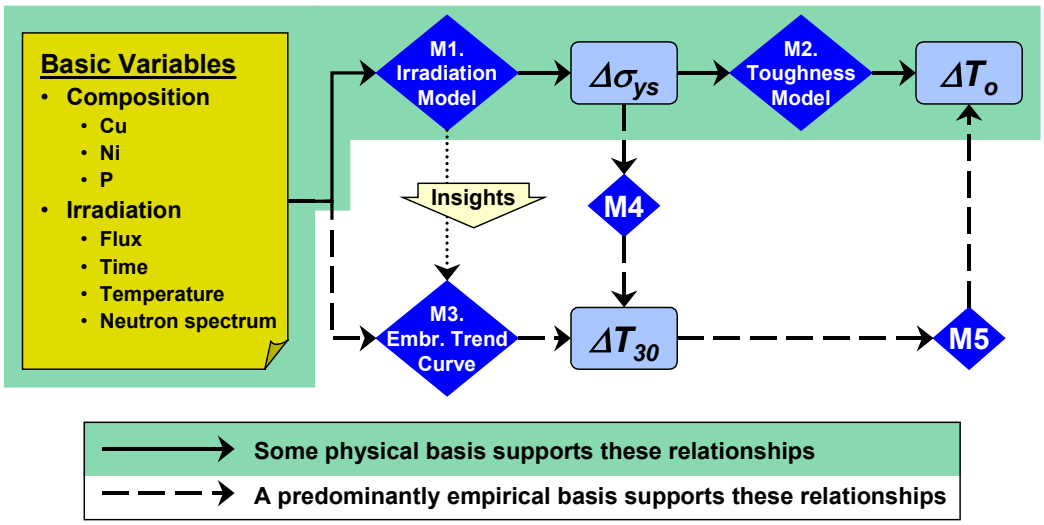


Figure 5.1. Illustration of two different models by which the shift in fracture toughness transition temperature produced by irradiation can be estimated.

### 5.2.1 A Physical Understanding of Damage Caused by Irradiation in Ferritic Steels

Neutron irradiation of RPV steels causes embrittlement effects marked by an increase in yield strength due to the fine scale microstructures produced by irradiation. These microstructures obstruct dislocation motion, thereby increasing the stress required to move dislocations past these obstacles. The mechanisms that produce these obstacles are as follows:

1. Matrix hardening due to irradiation produced point defect clusters and dislocation loops,
2. Age hardening due to irradiation-enhanced formation of copper-rich precipitates, and
3. Grain boundary segregation of embrittling elements such as phosphorous[‡].

The microstructures produced by both matrix- and age-hardening provide only long-range barriers to dislocation motion in BCC metals. The spacing of these barriers occurs on a size scale many times larger than the lattice spacing of the atoms that controls the temperature dependence of the flow properties. Consequently, irradiation cannot influence the temperature dependence of the flow properties, but rather increases the yield strength uniformly at all temperatures, an expectation borne out by ample empirical evidence (see Figure 5.2). This understanding of the effects of irradiation at the micro-scale suggests that the increase in the room temperature yield strength produced by irradiation provides a physically motivated quantification of the degree of irradiation damage imparted to a ferritic steel.

To understand the effect this yield strength increase has on the fracture toughness transition temperature, a model is needed to establish a causal linkage between yield strength increase and the experimentally observed increase in transition temperature. In WRC Bulletin????, the Working Party demonstrated that this increase in yield strength shifts the fracture toughness transition curve along the temperature axis without changing its temperature dependence in the curve shape, an expectation in accord with considerable empirical evidence (see Figure 4.1). Furthermore, available empirical evidence exhibits a linear relationship between the level of irradiation damage, as measured by the increase in the yield strength, and the increase in the fracture toughness transition temperature $T_o$. This relationship, shown in Figure 5.3 using data collected from the literature by the working party, demonstrates that equivalent levels of irradiation damage (i.e., yield strength increase) produce equivalent levels of shift in

‡ As noted previously, non-hardening embrittlement is not expected for US RPV alloys and so is not discussed here.

the toughness transition temperature irrespective of product form. The lack of product form dependence in this relationship can also be anticipated physically because the use of shift values removes the differences in initial state that could explain a product form dependency.

While providing significant insights regarding the fundamental nature of irradiation damage and the trends that can be expected in toughness data, this physically-based understanding of irradiation damage does not yet provide a quantitative relationship that directly links composition and irradiation variables to the amount of toughness transition temperature shift caused by irradiation. The form of such a relationship can be anticipated based on this physical understanding. However, current data limitations require that the coefficients in the relationship be established using CVN data. The physically motivated, empirically calibrated quantitative model proposed by the Working Party is summarized in the following section.

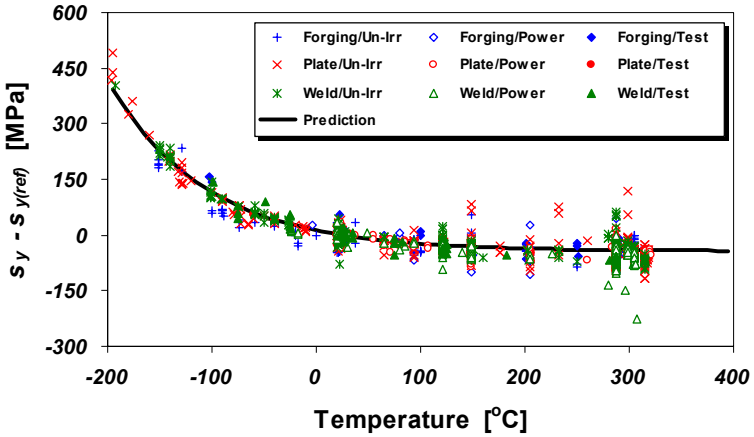


Figure 5.2: Comparison of 0.2% offset yield strength ($s_y$) for nuclear RPV steels to the Zerilli / Armstrong constitutive relation (line labled "prediction"). $s_{y(ref)}$ is the ambient temperature yield strength.

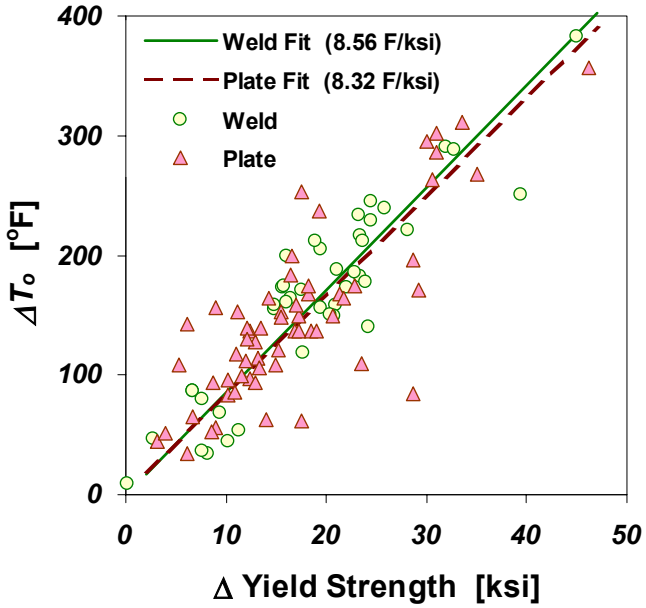


Figure 5.3: Relationship between the change in the fracture toughness index temperature ($\Delta T_o$) and the elevation in the room temperature yield strength ($\Delta\sigma_{ys}$) produced by irradiation. The difference in the fit slopes is not statistically significant.

### 5.2.2 Model Suggested for Use in the PTS Re-Evaluation Project (Uncertainty Classification and Quantification)

#### 5.2.2.1 Relationship Between Composition/Irradiation Variables and CVN Energy Shift Data

As discussed previously, irradiation damage of US RPV steels occurs as a consequence of two different hardening mechanisms: matrix hardening and age hardening. Details of these mechanisms are as follows:

1. **Matrix hardening.** Matrix damage develops continuously during irradiation, producing hardening that has a square root dependence on fluence. Matrix damage can be divided into two components: unstable matrix defects (UMD), and stable matrix defects (SMD). Unstable matrix defects are formed at relatively low fluence, and are small vacancy or interstitial clusters, complexed with solutes such as phosphorous, and are produced in displacement cascades. Increasing flux causes increasing hardening due to these defects, but they occur relatively independent of alloy composition. In low copper alloys, at low fluence and high flux, UMD is the dominant source of hardening. However, in high copper steels, these defects delay the copper rich precipitate contribution to hardening by reducing the efficiency of radiation-enhanced diffusion. Stable matrix features form at high fluence, and include nanovoids and more highly complexed clusters. These defects cause hardening that increases with the square root of exposure and is especially important at high fluences.
2. **Age hardening.** Radiation accelerates the precipitation of copper held in solid solution, forming copper-rich precipitates (CRPs) that inhibit dislocation motion and, thereby, harden the material. This hardening rises to a peak value and is then unaffected by subsequent irradiation because no copper remains in solid solution to precipitate out and cause damage. The magnitude of this peak depends on the amount of copper initially in solution, and therefore available for subsequent precipitation. Post-weld heat treatment (PWHT) performed before the RPV is placed into service can also precipitate copper, removing its ability to cause further damage during irradiation. Thus, different materials are expected to have different peak hardening values due to differing pre-service thermal treatments. Additionally, the presence of nickel in the alloy further enhances its age hardening capacity. Nickel precipitates together with copper, forming larger second-phase particles that present greater impediments to dislocation motion and, thereby, produce a greater hardening effect.

These physical insights help to establish the functional form of a relationship between basic material composition and irradiation condition variables and measurable quantities such as yield strength increase, Charpy transition temperature shift, and toughness transition temperature shift. Currently, the most expedient means to develop a quantitative relationship is by fitting empirical data. One dataset of sufficient breadth to calibrate such a relationship is the database of Charpy shift values generated in US commercial reactor surveillance programs. Eason and Wright recently developed the following physically motivated fit from these data [Eason 00]. This equation represents model M3 in Figure 5.1. :

Eq. 5-1
$$\Delta T_{30} = A\exp\left(\frac{19310}{T_c + 460}\right)\left(1 + 110P\right)\left(\phi t\right)^{0.4601} + B\left(1 + 2.40Ni^{1.250}\right)f\left(Cu\right)g\left(\phi t\right) + Bias$$

where

$$A = \begin{Bmatrix} 8.86\text{x}10^{-17}, \text{welds} \\ 9.30\text{x}10^{-17}, \text{forgings} \\ 12.7\text{x}10^{-17}, \text{plates} \end{Bmatrix}, \qquad B = \begin{Bmatrix} 230, \text{welds} \\ 132, \text{forgings} \\ 206, \text{plates in CE vessels} \\ 156, \text{other plates} \end{Bmatrix}$$

$$f(Cu) = \left\{ \begin{array}{l} 0, Cu \le 0.072 \text{ wt\%} \\ (\text{Cu} - 0.072)^{0.659}, Cu > 0.072 \text{ wt\%} \end{array} \right\}, \quad g(\phi t) = \frac{1}{2} + \frac{1}{2}\tanh\left[\frac{\log(\phi t + 4.579\text{x}10^{12} t_i) - 18.265}{0.713}\right]$$

$$Cu_{\max} = \left\{ \begin{array}{l} 0.25, \text{for welds with Linde 80 or Linde 0091 flux} \\ 0.305, \text{for everything else} \end{array} \right\}$$

$$Bias = \left\{ \begin{array}{l} 0, t_i < 97000 \text{ h} \\ 9.4, t_i \ge 97000 \text{ h} \end{array} \right\}$$

Table 5.1 summarizes the units associated with all of the numeric variables used in Eq. 5-1.

Table 5.1. Independent Variables in Eq. 5-1.

| Variable | Description | Range (Calibration) | Median | Units |
|---|---|---|---|---|
| *Cu* | Copper content | 0.01 – 0.42 | 0.133 | wt% |
| *Ni* | Nickel content | 0.044 – 1.26 | 0.6 | wt% |
| *P* | Phosphorous content | 0.003 – 0.031 | 0.011 | wt% |
| $\phi t$ | Neutron fluence | $9.26\text{x}10^{15}$ – $1.07\text{x}10^{20}$ | $8.66\text{x}10^{18}$ | n/cm$^2$, E>1MeV |
| $t_i$ | Exposure time | 5556 – 158,840 | 38,025 | Hours |
| $T_c$ | Coolant temperature | 522 - 570 | 545 | °F |

The understanding of the physics of irradiation damage described at the beginning of this Section motivated the form of Eq. 5-1. Specifically, Eq. 5-1 includes the following physically motivated features:

A. Different (additive) terms to reflect the different nature of the physical contributions of matrix hardening ("*A*" term) and age hardening ("*B*" term),
B. In the matrix hardening (*A*) term
    a. A (nearly) square root dependency on fluence,
    b. A dependency on phosphorus, and independency from other embrittling elements, and
C. In the age hardening (*B*) term
    a. A threshold copper level below which no age hardening occurs, leaving the matrix hardening term to completely dominate the irradiation response for low copper alloys.
    b. A saturation in age hardening at high copper levels that, through the use of flux type as an indicator variable, corresponds to differences in PWHT practice.
    c. A synergistic effect between copper and nickel that leads to greater hardening.

Eq. 5-1 also includes a number of features that rely more heavily on either an empirical understanding of irradiation effects, or on a recently emerging physical understanding, including:

A. A synergistic effect of flux and time,
B. A product form dependency (including an effect of vessel manufacturer), and
C. A purely time dependent effect.

Figure 5.4 compares all of the $\Delta T_{30}$ values in the calibration dataset to Eq. 5-1. The "normalized" $\Delta T_{30}$ values shown on Figure 5.4 are the measured $\Delta T_{30}$ values normalized to median values of the independent variables (see Table 5.1) to simulate the appearance of data as if all $\Delta T_{30}$ values were determined from tests conducted under the same conditions. In other words, the "normalized" $\Delta T_{30}$ values are adjusted using Eq. 5-1 to minimize the apparent scatter about the model arising from other

variables that are not plotted. Clearly, the uncertainty reflected in Figure 5.4 is large. In WRC Bulletin????, the Working Party identified the following major sources of uncertainty associated with the use of *any* embrittlement trend curve model:

1. How well the physical processes of irradiation damage are represented by the mathematical form of the embrittlement trend curve,
2. How accurately and consistently the data (i.e. $\Delta T_{30}$ data, chemical composition data, fluence data, and so on) are represented in the dataset used to calibrate the embrittlement trend curve,
3. The process by which single (central tendency) values of Cu, Ni and P are associated with each $\Delta T_{30}$ value, and
4. How heat-specific composition distributions are estimated in FAVOR.

While these uncertainties have both aleatory and epistemic components, the information presented by the Working Party suggests that the epistemic component dominates. It is therefore recommended that the uncertainty in the embrittlement trend curve be modeled as epistemic in FAVOR. This sampling procure involves using the Cu, Ni, and P values in Appendix A to center generic Cu, Ni, and P distributions (Appendix B) [Santos 01], and using a Monte Carlo process to draw individual samples from these distributions.

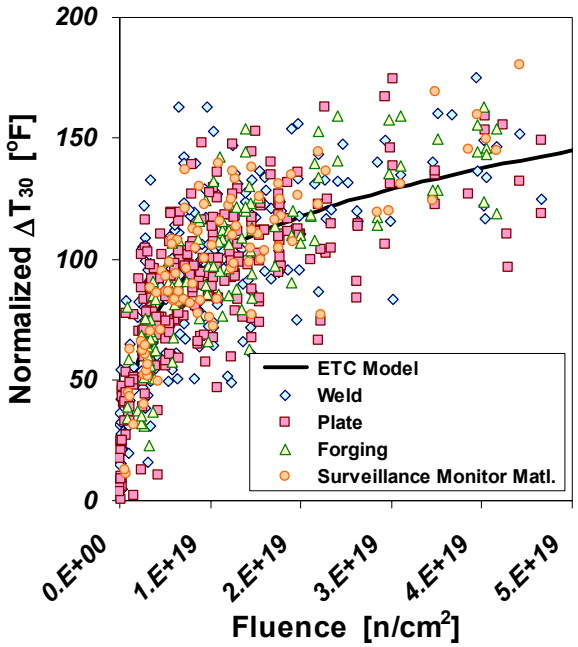


Figure 5.4. Embrittlement trend curve developed by Eason and co-workers.

### 5.2.2.2 Relationship Between CVN Energy Shift and Fracture Toughness Shift Data

Having used information concerning composition and irradiation conditions to estimate the CVN transition temperature shift using Eq. 5-1, it is necessary to convert these $\Delta T_{30}$ values into estimates of the fracture toughness transition temperature (i.e., Model M5 in Figure 5.1 is needed). Figure 5.5 provides an empirical basis for Model M5 using data extracted from the literature by the working party. Least-squares fits to these data are as follows:

Eq. 5-2 $$\Delta T_o = \alpha \cdot \Delta T_{30}$$

Here $\alpha$ = 0.99 for welds and 1.10 for plates. The uncertainty in this relationship is as follows

Eq. 5-3 $$\sigma_{\sigma_{Cu}} = MIN\left\{\frac{\alpha}{3.09023}\cdot\Delta T_{30}, \hat{\sigma}\right\}$$

where $\hat{\sigma}$ is the uncertainty on the linear fits shown in of Figure 5.5. $\hat{\sigma}$ has a value of 25.6°F for welds and 33.9°F for plates. Inadequate data is available for forgings on which to base independently estimated $\alpha$ and $\hat{\sigma}$ values. Consequently, it is recommended (based on inspection of Figure 5.5) that the plate coefficients be adopted for forgings.

In WRC Bulletin????, the Working Party determined that the uncertainties reflected by the data in Figure 5.5 occur primarily due to uncertainties associated with the use of small data sets to define $\Delta T_{30}$ and $\Delta T_o$, and so are primarily epistemic in nature.

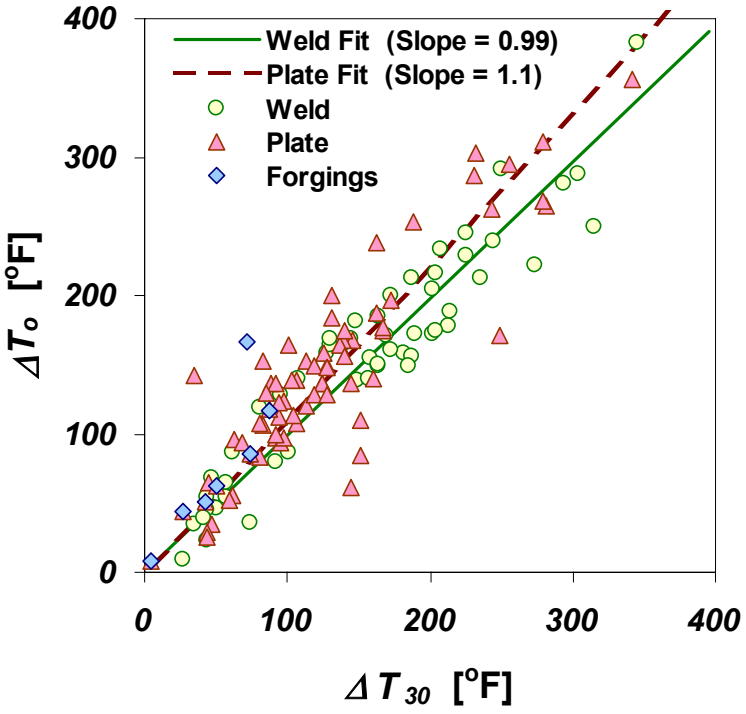


Figure 5.5. Relationship between the change in the fracture toughness index temperature ($\Delta T_o$) change in the 30 ft-lb CVN transition temperature ($\Delta T_o$) produced by irradiation. The difference in the best-fit slopes is statistically significant.

### 5.2.2.3 Complete Relationship

Taken together Eq. 5-1 and Eq. 5-2 relate variables that describe the composition, irradiation, and design of the vessel to the expected shift in the initiation fracture toughness transition temperature. These relationships go through the intermediate step of predicting the shift in the CVN transition curve ($\Delta T_{30}$). The coefficients in Eq. 5-1 and Eq. 5-2 both show a product form dependency whereas there is no product form effect apparent in the physical understanding of irradiation damage (see Section 5.2.1 and Figure 5.3). The working party noted that the differences between the CVN transition temperature shift and the toughness transition temperature shift may explain this apparent inconsistency. Moreover, it is anticipated that the proposed procedure to estimate toughness shift, which first uses Eq. 5-1 (to estimate CVN shift) and then Eq. 5-2 (to estimate toughness transition temperature shift) may predict a product form insensitive toughness shift as expected physically. It is therefore recommended that FAVOR predictions be checked for product form insensitivity (on average) once this procedure is implemented.

It should also be noted that the combined use of Eq. 5-1 and Eq. 5-2 estimates the shift in toughness transition temperature in terms of $T_o$ whereas the $K_{Ic}$ model presented in Eq. 4-4, Eq. 4-5, and Section 4.3 uses $RT_{LB}$ as an index temperature, not $T_o$. However, as illustrated in Figure 4.6, $RT_{LB}$ and $T_o$ differ by only an additive constant, so $\Delta RT_{LB}$ and $\Delta T_o$ will be identical.

## 5.3 Recommended FAVOR Coding Logic

Figure 5.6 illustrates the recommended uncertainty procedure for FAVOR, which is described below:

1. Determine the mean value of the composition variables for a particular heat of material as reported in Appendix A.
2. Around each of these mean values, construct a distribution based on recommendations summarized in Appendix B.
3. Select a single value for Cu, Ni, and P by selecting randomly from each of these distributions.
4. Specify reactor coolant temperature, product form, and vessel manufacturer as deterministic inputs. These values are summarized in Appendix A.
5. Determine the fluence at the inner diameter surface from the fluence map associated with a particular operating time provided by Brookhaven National Laboratories. The recommended treatment of uncertainty on fluence is specified elsewhere [Jones]. Attenuate the fluence from the ID surface to the location of the crack tip using $\phi t = \phi t_{ID} \exp(-0.24 \cdot x)$ where $\phi t$ is fluence (in n/cm$^2$), and $x$ is distance of the inner crack tip from the vessel ID wetted surface (in inches).[§]
6. Use the information from Steps 3, 4, and 5 together with the embrittlement trend curve (Eq. 5-1) to estimate a value of $\Delta T_{30}$ at the inner crack tip of the simulated crack.
7. Convert $\Delta T_{30}$ to $\Delta T_o^*$ using Eq. 5-2. Randomly select a value of $\Delta T_o$ from a normal distribution having a mean value $\Delta T_o^*$ of and a standard deviation defined by Eq. 5-3. This value of $\Delta T_o$ is the best estimate of the shift in the initiation fracture toughness transition temperature produced by irradiation.

[§] This attenuation function is taken from USNRC Reg. Guide 1.99, Revision 2. While it is generally recognized that this relationship produces less attenuation that occurs in practice (i.e. the relationship is conservative), there is insufficient evidence on which to base an improved relationship at this time.

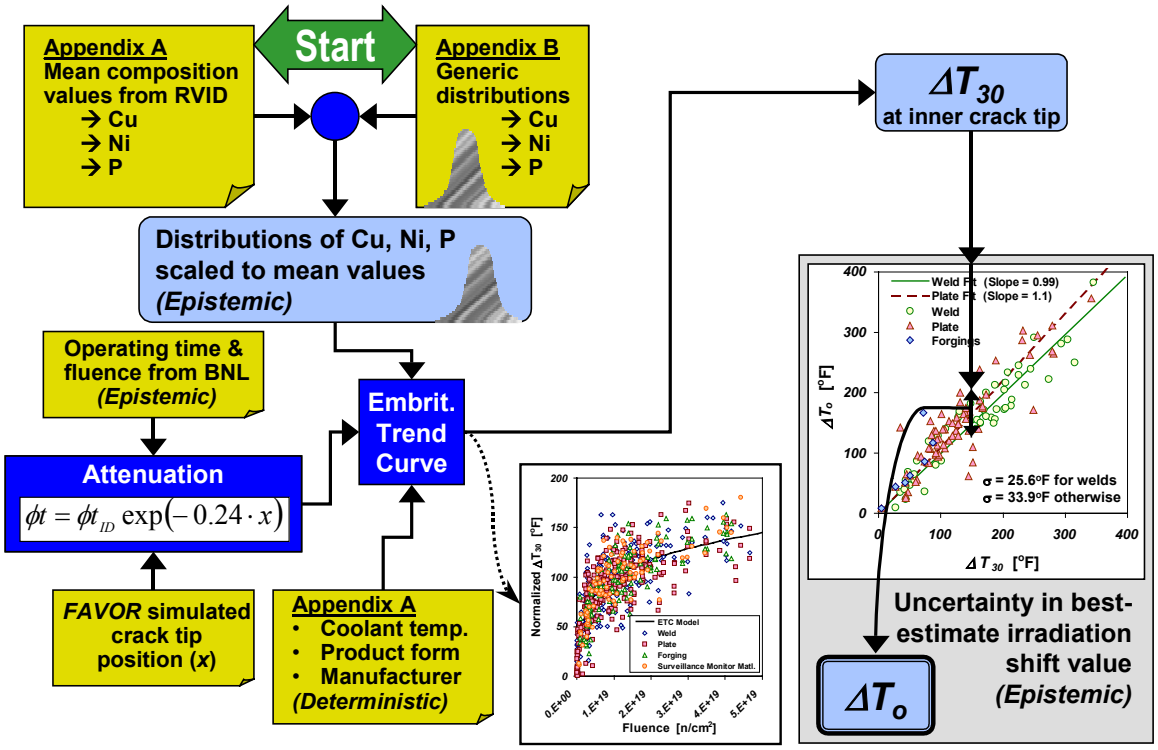


Figure 5.6. Illustration of the proposed procedure to account for irradiation shift uncertainty in FAVOR.

# 6. Model of Crack Arrest Toughness

## 6.1 Requirements of the Model

To enable all commercial operators of pressurized water reactors to assess the state of their RPV relative to the new PTS screening criteria without the need to make new material property measurements, the arrest fracture toughness of the RPV needs to be estimated using only currently available $RT_{NDT}$ values. Moreover, to be consistent with the LEFM principles on which the FAVOR code is based, this model needs to estimate $K_{Ia}$ values. These restrictions suggest that only very limited information, specifically a value of $RT_{NDT}$, is available to define the arrest fracture toughness model appropriate to a particular steel in a particular RPV. Consequently, the temperature dependency and uncertainty of the arrest fracture toughness model will either have to be demonstrated or assumed to be invariant over a wide range of conditions because sufficient information is not available to establish these features on a material heat specific basis.

## 6.2 The Findings of the Working party Presented in WRC Bulletin xxxx

The information presented in WRC Bulletin xxxx suggests that a $K_{Ia}$ model can be defined from the following four elements:

1. A temperature dependency
2. A description of scatter in $K_{Ia}$ data
3. An index temperature that defines the position of the $K_{Ia}$ transition curve on the temperature axis, and
4. A relationship between the index temperatures for the initiation and arrest fracture toughness curves.

As was the case with the initiation fracture toughness model summarized in Section 4.2, the temperature dependency of $K_{Ia}$ data is universal to all reactor pressure vessel steels. Within this class of materials the temperature dependency is insensitive to all individual and combined effects of alloying, heat treatment (and other thermal processing), mechanical processing, and irradiation. These material variables only influence the temperature range over which a particular steel experiences a transition from brittle behavior (at low temperatures) to ductile behavior (at higher temperatures), this being quantified by a heat specific index temperature value. Furthermore, the information presented in WRC Bulletin xxxx suggests that the relationship between the index temperatures for crack initiation and crack arrest toughness is also not expected to be influenced strongly by heat specific factors.

Sections 6.2.1, 6.2.2, and 6.2.3 summarize the physical bases put forward by the Working Party for the following features of a crack arrest toughness model: the temperature dependency of $K_{Ia}$, the scatter in $K_{Ia}$, and the temperature separation between the $K_{Ic}$ and $K_{Ia}$ transition curves. Section 6.2.4 then summarizes a mathematical model that incorporates these features.

### 6.2.1 Physical Basis for a Universal Temperature Dependency in Arrest Fracture Toughness Data

Crack arrest occurs when dislocations can move faster than the crack propagates, which causes crack tip blunting and, thereby, arrest. Dislocation mobility therefore controls the ability of a ferritic steel to arrest a running cleavage crack, and thus its crack arrest toughness. The atomic lattice structure is the only feature of the material that controls the temperature-dependence of the material properties that are controlled by dislocation motion. Consequently, as was the case for crack initiation toughness, the temperature dependency of crack arrest toughness depends only on the short-range barriers to dislocation motion established by the BCC lattice structure. Other features that vary with steel composition, heat treatment, and irradiation include grain size/boundaries, point defects, inclusions, precipitates, and dislocation substructures. These features all influence dislocation motion, and thereby both strength and toughness, but their large inter-barrier spacing relative to the atomic scale associated with the lattice structure makes these effects completely athermal. This understanding suggests that the myriad of metallurgical factors that can influence absolute strength and toughness values, and thereby the transition temperature, exert no control over the temperature dependency of arrest toughness in fracture mode transition. Additionally, since $K_{Ic}$ and $K_{Ia}$ both depend on the ability of the material to absorb energy via dislocation motion, $K_{Ic}$ and $K_{Ia}$ are both expected to exhibit a similar temperature dependence.

### 6.2.2 Physical Basis for a Universal Scatter in Arrest Fracture Toughness Data

As outlined in Section 6.2.1, the occurrence or non-occurrence of crack arrest depends upon the interaction of a rapidly evolving stress state in front of a running crack with the distribution of defects in the material that inhibit dislocation motion. Therefore, scatter in $K_{Ia}$ data occurs as a consequence of the randomness in the distribution of barriers to dislocation motion throughout the material. Barriers to dislocation motion include vacancy clusters, interstitial clusters, coherent and semi-coherent particles, and other dislocations. These dislocation-trapping defects are all of nanometer size and have inter-defect spacings on the same size scale. In WRC Bulletin???? the Working Party noted that the defects that control crack arrest are distributed at a much finer scale throughout the material than are the non-coherent particles responsible for crack initiation, which tend to have inter-defect spacings of sub-micron (1/10 micron) order. The possible variation in local stress state over the microstructural distances that control crack arrest is therefore much smaller than that possible over the microstructural distances that control crack initiation. This smaller stress variation for crack arrest suggests that the scatter in $K_{Ia}$ data should be smaller than in $K_{Ic}$ data, a physically motivated expectation that the Working Party found to agree well with available empirical evidence. However, this physical understanding is not yet sufficiently advanced to rationalize a distribution of crack arrest toughness values that is universal to all ferritic steels.

### 6.2.3 Physical Basis for a Separation Between the $K_{Ic}$ and $K_{Ia}$ Transition Curves

The well-established experimental observation that as a metal is hardened, subsequent tensile tests will exhibit progressively higher yield strengths but have a true stress-strain curve that always overlays the unhardened curve suggests that a universal hardening curve exists for all ferritic steels. This behavior cannot occur unless the hardened material exhibits the same strain-hardening rate as the unhardened material after an equivalent amount of tensile strain. This idea of a universal hardening curve also leads to an invariance of the true stress at maximum load for most hardening mechanisms. In WRC Bulletin???? the Working Party used these ideas to develop the physical basis for the relationship between crack arrest and crack initiation transition temperature. At the time of crack arrest, the material is subjected to a high rate of loading. This loading rate elevation above the quasi-static conditions associated with crack initiation elevates the activation energy required to move dislocations past trapping obstacles, and thus results in an increase in the apparent yield stress of the material in a manner similar to the yield stress elevation produced by prior strain. Figure 6.1 uses the idea of a hardening curve

universal to all ferritic steels to illustrate why the elevation in prior strain caused by the elevated loading rate associated with crack arrest (defined as $\Delta\varepsilon_o$) produces a progressively diminishing elevation in the yield strength as the degree of strain caused by prior hardening ($\varepsilon_o$) increases. Since increases in transition temperature scale with increases in yield strength, this understanding suggests a physical basis for the empirical trend reported by Wallin of a progressively diminishing separation between the crack initiation and crack arrest transition curves for higher transition temperature steels. Moreover, the invariance of the true stress at maximum load that follows directly from the notion of a universal hardening curve suggests that in the limit of very high strength ferritic materials the crack initiation and crack arrest transition curves should approach each other.

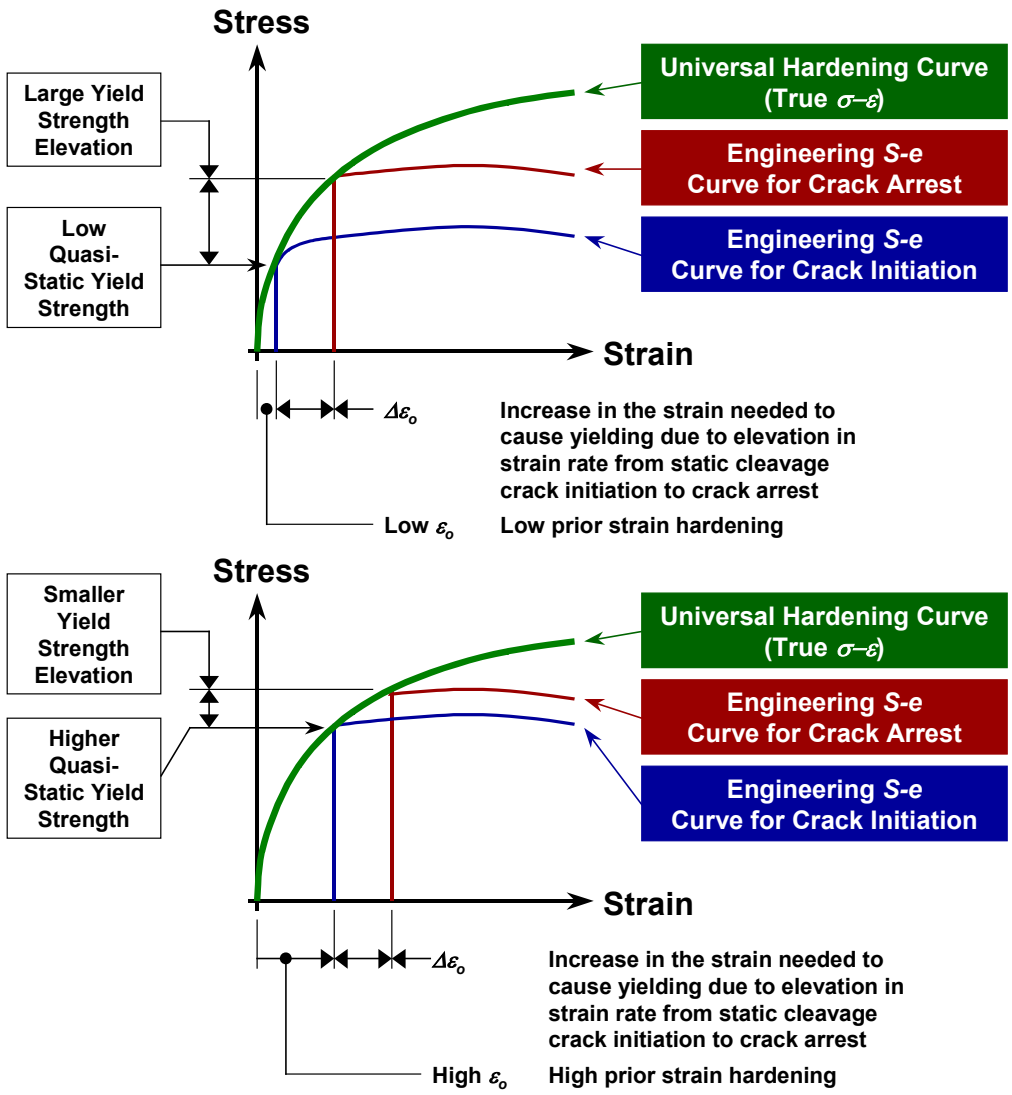


Figure 6.1. An illustration of the effect of strain rate increase on yield strength elevation for materials having different degrees of prior strain hardening.

### 6.2.4 Best Estimate Model

As described in Section 6.2.1, a strong physical basis supports a temperature dependency in arrest fracture toughness data that is universal to all ferritic steels, and has a similar functional form to that of

crack initiation toughness. Mathematically, this characteristic is captured in a model of initiation fracture toughness proposed by Wallin and co-workers [Wallin ALL]:

Eq. 6-1 $$K_{Ia(mean)} = 27.27 + 63.63 \cdot \exp\left[0.0342\left(T - T_{KIa}\right)\right]$$

Eq. 6-1 describes the temperature ($T$) dependency of the mean arrest toughness ($K_{Ja(mean)}$). In this equation, temperature is normalized to the index temperature $T_{KIa}$. $T_{KIa}$ is defined as the temperature at which the mean arrest toughness is 90.9 ksi√in. Figure 6.2 shows the data used by Wallin and co-workers to develop this model. These data demonstrate that when the temperatures associated with crack arrest toughness data are plotted relative to an index temperature derived from the data itself (e.g. $T_{KIa}$ rather than $RT_{NDT}$) that the result anticipated from physics, one of a similar temperature dependency to the crack initiation toughness data, is achieved. Wallin found that a log-normal distribution having a log-normal standard deviation of 0.18 fits these data well.

The physical understanding of the relationship between crack initiation and crack arrest presented in Section 6.2.3 suggests that the temperature separation between the $K_{Ic}$ and $K_{Ia}$ transition curves should progressively diminish as the material is hardened (e.g. by cold work, irradiation, etc.). Available empirical evidence supports this expectation, as illustrated in Figure 6.3. An exponential relationship was selected to represent these data because this relationship has the mathematical form anticipated from physical considerations (i.e. that the separation between the $K_{Ic}$ and $K_{Ia}$ curves diminishes as $T_o$ increases). This fit is as follows:

Eq. 6-2 $$\Delta RT_{ARREST} \equiv T_{K_{Ia}} - T_o = 44.1 \cdot \exp\left\{-0.006\left(T_o - 32\right)/1.8\right\}$$

$\Delta RT_{ARREST}$ is distributed log-normally about the mean values given by the fit of Eq. 6-2, which has an estimated log-normal standard deviation of 0.39.

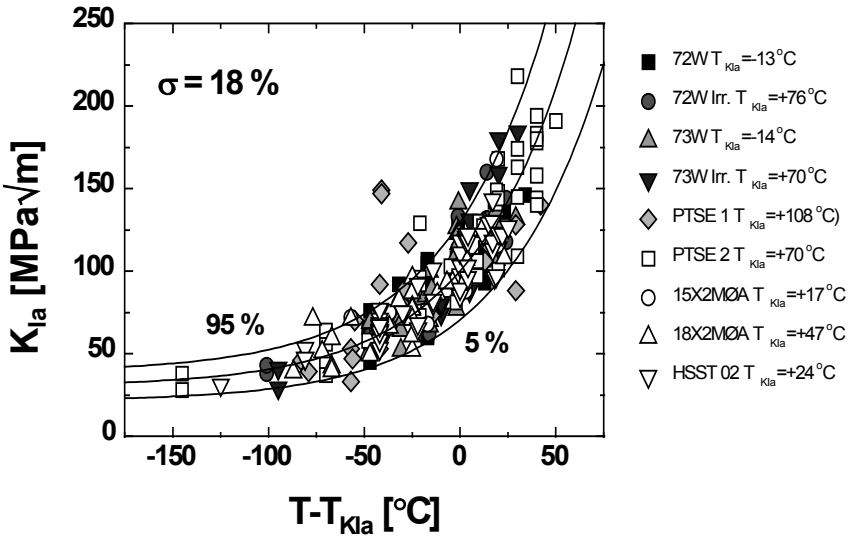


Figure 6.2. Crack arrest transition curves for nine heats of RPV steel. The mean curve has the same temperature dependence as the Master Curve for crack initiation data, i.e. $K_{Ia} = 30 + 70 \cdot \exp\left\{0.019\left[T - T_{KIa}\right]\right\}$.

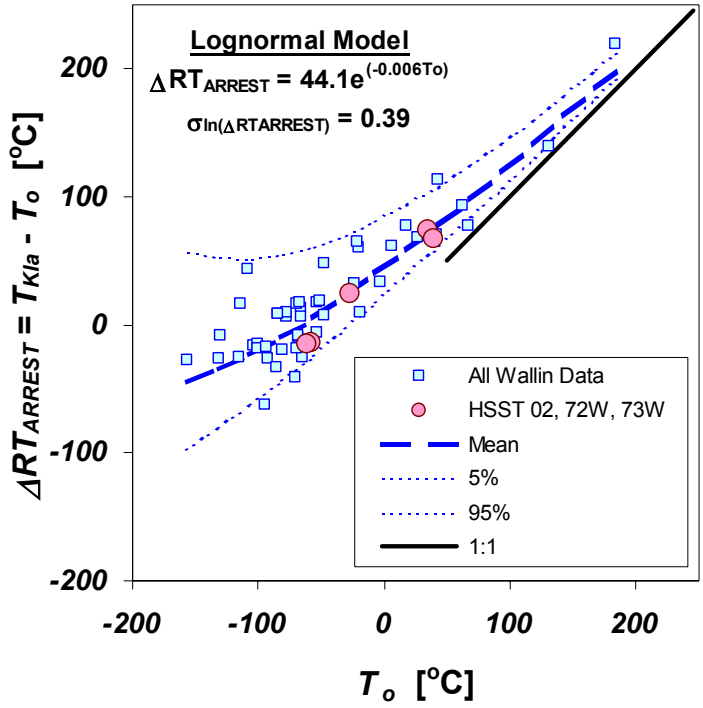


Figure 6.3. Data for RPV and other steels showing the relationship between the crack arrest transition temperature ($T_{KIa}$, vertical axis) and the crack initiation transition temperature ($T_o$, horizontal axis) [Wallin 98b].

### 6.2.5 Crack Arrest Toughness Model Suggested for Use in the PTS Re-Evaluation Effort

The best estimate model presented in Section 6.2.4 requires some modification to enable its use in the PTS re-evaluation project. Specifically, use of the initiation toughness index temperature $T_o$ in Eq. 6-2 is inappropriate because the $K_{Ic}$ model presented in Eq. 4-4, Eq. 4-5, and Section 4.3 uses $RT_{LB}$ as an index temperature, not $T_o$.

To account for these inconsistencies yet still recommend a toughness model that fulfils the needs of the PTS re-evaluation project, the Working party used the insights and physical basis summarized in Sections 6.2.1 through 6.2.4 to classify uncertainty type, and to establish the form of the toughness model, but calibrated the toughness model using only LEFM-valid $K_{Ia}$ data. Their recommendations on the classification and quantification of uncertainty for both the arrest fracture toughness ($K_{Ia}$) and the separation between the initiation and arrest transition curves are summarized in the following sections

#### 6.2.5.1 Arrest Fracture Toughness ($K_{Ia}$) Uncertainty Classification and Quantification

From the physical model of cleavage crack arrest toughness developed by the Working Party in WRC Bulletin????, one concludes that the occurrence or non-occurrence of crack arrest depends upon the interaction of a rapidly evolving stress state in front of a running crack with the distribution of defects in the material that inhibit dislocation motion. The barriers to dislocation motion include vacancy clusters, interstitial clusters, coherent and semi-coherent particles, and other dislocations. These barriers are all of nanometer and have inter-defect spacings on the same size scale. Scatter in $K_{Ia}$ data therefore occurs as a consequence of the randomness in the distribution of barriers to dislocation motion throughout the material. Since the distribution of these barriers throughout the lattice is random and the conditions for

arrest must be satisfied over a significant portion of the advancing crack front for arrest to occur, the uncertainty in $K_{Ia}$ data is irreducible. For this reason the uncertainty in $K_{Ia}$ is treated as aleatory.

As summarized in Section 6.2.1, the physical understanding of the crack arrests suggests that the crack arrest toughness should exhibit a similar temperature dependence to that of crack initiation toughness. The working party found that this similarity can be achieved only if the index temperature used to normalize the $K_{Ia}$ data is determined from the $K_{Ia}$ data itself. For this reason, the working party decided to adopt the $T_{KIa}$ index temperature proposed by Wallin and defined following Eq. 6-1. Also, the working party adopted Wallin's characterization of scatter in $K_{Ia}$ data (a log normal distribution having a standard deviation equal to 0.18), and determined the temperature dependence as a best fit to $K_{Ia}$ data from three RPV steels: HSST Plate 02, and Welds 72W and 73W. These data are depicted along with the model in Figure 6.4 and described mathematically as follows:

Eq. 6-3

$$\mu_{\ln(K_{Ia})}(\Delta T_{RELATIVE}) = \ln\left[\bar{K}_{Ia}(\Delta T_{RELATIVE})\right] - \frac{\sigma^2_{\ln(K_{Ia})}}{2}$$

where

$$\sigma_{\ln(K_{Ia})} = 0.18$$

$$\bar{K}_{Ia}(\Delta T_{RELATIVE}) = 27.302 + 69.962\exp\left[0.006057(\Delta T_{RELATIVE})\right] \quad [\text{ksi}\sqrt{\text{in.}}]$$

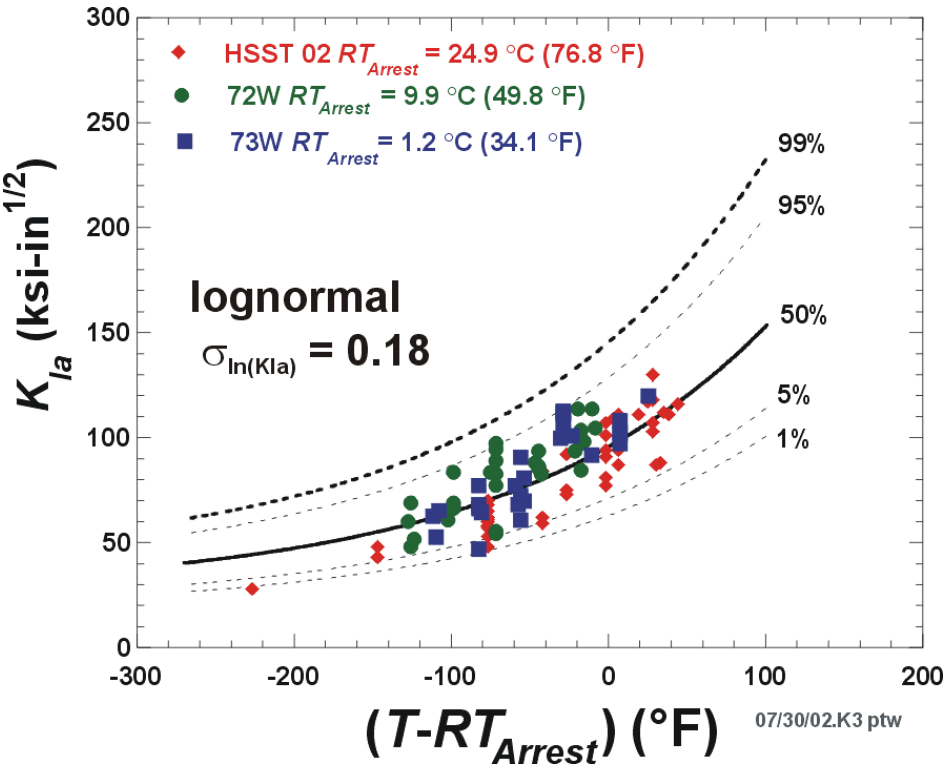


Figure 6.4. $K_{Ia}$ model recommended for use in the PTS re-evaluation effort.

### 6.2.5.2 $K_{Ic}$ to $K_{Ia}$ Curve Separation Uncertainty Classification and Quantification

The physical model developed by the Working Party and described in WRC Bulletin-???? suggests that the temperature separation between the crack initiation and crack arrest transition curves is expected to diminish with increases in the following variables: the level of irradiation damage, or the yield strength, or the crack initiation transition temperature. This expectation is borne out by available experimental data

(see Figure 6.3). The uncertainty evident on Figure 6.3 represents the statistical error in determining both $T_o$ and $T_{KIa}$, which scales in proportion to $1/\sqrt{n}$ where n is the number of fracture toughness specimens tested [ASTM E1921]. This information suggests that the uncertainty in $\Delta RT_{ARREST}$ on Figure 6.3 is reducible, making it epistemic in nature. On this basis the working party recommended that FAVOR treat this uncertainty as epistemic by sampling values from the data shown on Figure 6.3.

As noted earlier, the relationship between $T_o$ and $T_{KIa}$ shown on Figure 6.3 cannot be used directly because the index temperature adopted in the $K_{Ic}$ model of Eq. 4-5 uses $RT_{LB}$ as the index temperature rather than $T_o$. The similarity of the $T_o$- and $RT_{LB}$ -based CDFs depicted in Figure 4.6 was therefore used to relate $RT_{LB}$ to $T_o$. Figure 4.6(b) suggests that, on average,

Eq. 6-4 $$T_o = RT_{LB} - 14.4 \text{ (in °F)}$$

Substuting Eq. 6-4 into Eq. 6-2 then produces the following relationship

Eq. 6-5 $$\Delta RT_{ARREST} \equiv 44.1 \cdot \exp\left\{-0.006\left(RT_{LB} - 14.4 - 32\right)/1.8\right\}$$

Eq. 6-5 now describes the separation between a $K_{Ic}$ curve (indexed to $RT_{LB}$) and a $K_{Ia}$ curve (indexed to $T_{KIa}$). The uncertainty on this estimate is described by a log-normal distribution having an estimated standard deviation of 0.39.

## 6.3 Recommended FAVOR Coding Logic

Figure 6.5 illustrates the procedure recommended for incorporation into FAVOR to represent the uncertainty in crack arrest fracture toughness values:

1. Determine $RT_{INITIATION}$ as per the procedure outlined in Section 4.3.
2. Determine $\Delta RT_{ARREST}$ using the formula $\Delta RT_{ARREST} = 44.1 \cdot \exp\left\{-0.006\left(RT_{INITIATION} - 14.4 - 32\right)/1.8\right\}$. These $\Delta RT_{ARREST}$ values are the means of log-normal distributions having a standard deviation of 0.39. This uncertainty is epistemic.
3. Determine the arrest reference temperature as $RT_{ARREST} = RT_{INITIATION} + \Delta RT_{ARREST}$.
4. Determine the temperature of the vessel at the location of interest relative to $RT_{ARREST}$ as $\Delta T_{ARREST} = T_{VESSEL} - RT_{ARREST}$.
5. The aleatory distribution of $K_{Ia}$ at $\Delta T_{ARREST}$ is established by Eq. 6-3.

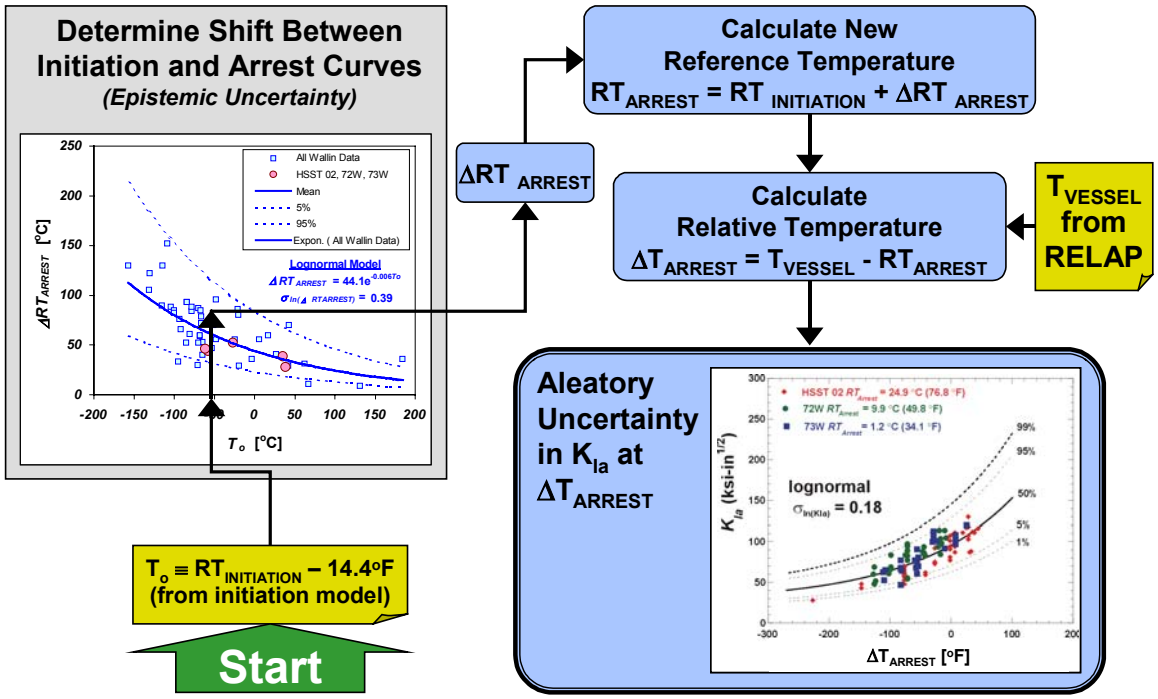


Figure 6.5. Illustration of the proposed procedure to account for uncertainty in the characterization of $K_{Ia}$.

# 7. Summary and Recommendations

In Sections 4, 5, and 6 we summarized the recommendations made by the WRC Bulletin???? Working party concerning best estimate models and treatment of uncertainty for crack initiation toughness, the shift of toughness transition temperature caused by irradiation, and crack arrest toughness, respectively. Each Section concluded with a recommended coding logic for FAVOR (see 4.3, 5.3, and 6.3, respectively). In this Section we address certain additional issues that arise when these recommendations are placed together in FAVOR and used to model the failure of a nuclear RPV (Section 7.1). Finally, while every effort has been made to propose models and input parameters having both a firm physical and empirical justification, on occasion it has been necessary to exercise engineering judgment in the absence of an adequately developed state of knowledge. A natural consequence of this situation is that the judgments are somewhat arbitrary, making alternative conclusions possible. In Section 7.2 we summarize these judgments, thereby identifying them for additional study should the need arise in the future to further refine the FAVOR model.

## 7.1 Additional Issues

### 7.1.1 Double-Counting of Uncertainties

The index temperature for the un-irradiated initiation fracture toughness transition curve, $T_{o(u)}$, is used in several places in the recommended models,

- The accuracy with which $RT_{NDT}$ places the un-irradiated initiation fracture toughness transition curve relative to actual fracture toughness data is assessed using $T_o$ (or its surrogate $RT_{LB}$) in Figure 4.6. A factor to adjust for the bias in $RT_{NDT}$ is developed on this basis (Eq. 4-4). Here $T_{o(u)}$ is used to estimate the error term $\{RT_{NDT(u)} - T_{o(u)}\}$.
- The accuracy with which the shift in the CVN transition temperature ($\Delta T_{30}$) approximates the irradiation induced shift in fracture toughness data ($\Delta T_o$) involves the use of an un-irradiated value of $T_o$ in the $\Delta T_o$ calculation (see Figure 5.5 and Eq. 5-2). Here $T_{o(u)}$ is used to estimate the error term $\{\Delta T_{30} - \Delta T_o\}$.

This use of $T_{o(u)}$ in different parts of the toughness model introduces the potential for including the same uncertainty multiple times in the FAVOR calculation. To determine if this is happening we investigate correlations between $\{RT_{NDT(u)} - T_{o(u)}\}$ and $\{\Delta T_{30} - \Delta T_o\}$ is presented in Figure 7.1. Very few domestic RPV steels have all of $RT_{NDT(u)}$, $T_{o(u)}$, $\Delta T_{30}$, and $\Delta T_o$ available (just HSST-02, Weld 72W, and Weld 73W) so additional data was obtained from recent irradiation studies conducted in Japan [Onizawa 01] and in Belgium [SCK/CEN 01]. The data in Figure 7.1 demonstrate that there is no systematic relationship between the error in the un-irradiated initiation fracture toughness transition temperature and the error

in the irradiation-induced transition temperature shift, suggesting that the uncertainty treatment proposed in Eq. 4-4 and Eq. 5-2 requires no modification.

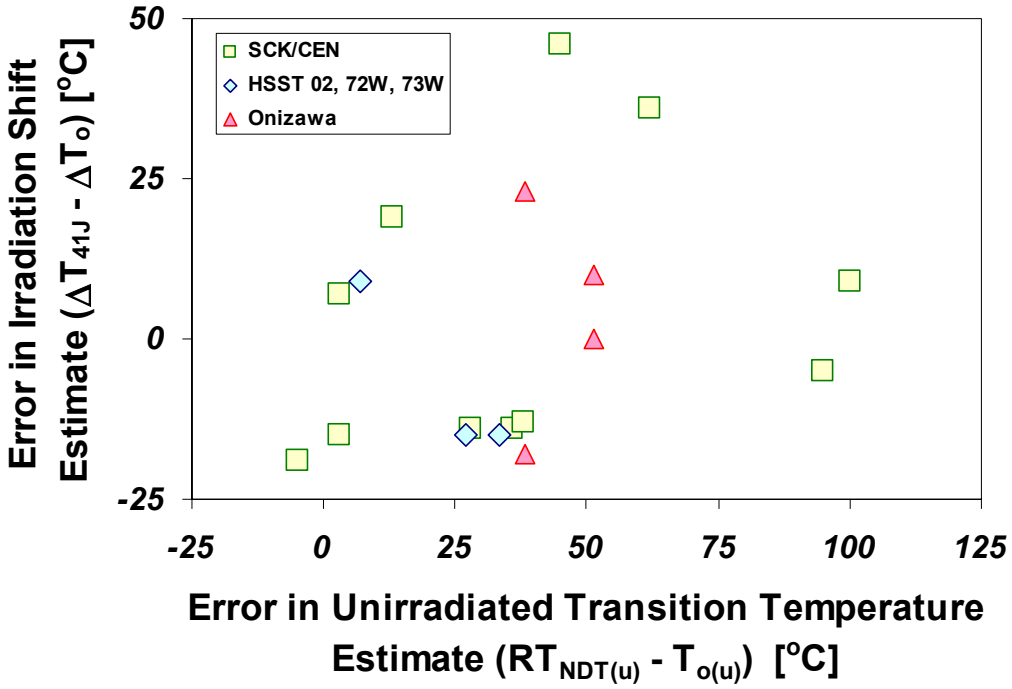


Figure 7.1. Relationship between the error in the un-irradiated initiation fracture toughness transition temperature and the error in the irradiation-induced transition temperature shift.

### 7.1.2 Modelling of Crack Initiation, Arrest, and Re-Initiation

#### 7.1.2.1 Relationship Between Crack Initiation and Crack Arrest Model

When performing a probabilistic fracture calculation, cracks may initiate, arrest, and re-initiate in the same simulation run. Consequently, a relationship is needed between $K_{Ic}$ and $K_{Ia}$ data for the same material. Certainly the information in Figure 6.3 is needed as this specifies the temperature separation between the $K_{Ic}$ and $K_{Ia}$ curves. However, mathematical simulation of crack initiation, arrest, and subsequent re-initiation also requires the following information:

- For the arrest calculation: Are the permissible values of $K_{Ia}$ influenced in any way by the value of $K_{Ic}$ at which the crack initiated?
- For the re-initiation calculation: Are the permissible values of $K_{Ic}$ influenced in any way by the value of $K_{Ia}$ at which the crack arrested?

These questions are addressed in the following sections.

##### 7.1.2.1.1 Influence of $K_{Ic}$ on Subsequent $K_{Ia}$ Values

Crack arrest toughness is undefined at values above the crack initiation toughness because the fact that the crack has initiated means that arrest was not possible. Thus, the value of crack initiation toughness (say $\hat{K}_{Ic}$) establishes the maximum allowable $K_{Ia}$ for temperature at which crack initiation occurred (say $\hat{T}$). As the crack propagates deeper into the vessel wall the temperature increases above $\hat{T}$ for PTS

loadings, so restricting the maximum allowable $K_{Ia}$ to $\hat{K}_{Ic}$ is no longer appropriate. For temperatures exceeding $\hat{T}$ the maximum allowable $K_{Ia}$ therefore cannot exceed the $K_{Ia}$ value of the same percentile as the value $\hat{K}_{Ic}$ occupies in the $K_{Ia}$ distribution at temperature $\hat{T}$. Figure 7.2 provides an illustration of these ideas.

Having established a physical rationale supporting adoption of the percentile corresponding to ( $\hat{K}_{Ic}$ , $\hat{T}$ ) as the maximum value of the $K_{Ia}$ distribution, it is also necessary to specify how the distribution of $K_{Ia}$ values in Eq. 6-3 below this limit is altered. The following two methods were considered:

Method #1. Truncate the $K_{Ia}$ distribution established in Eq. 6-3 at the percentile corresponding to ( $\hat{K}_{Ic}$ , $\hat{T}$ ), but make no other changes to the distribution.

Method #2. Scale the $K_{Ia}$ distribution established in Eq. 6-3 so that some high percentile value (in the compressed distribution) corresponds to the percentile at ( $\hat{K}_{Ic}$ , $\hat{T}$ ) (in the un-scaled distribution).

The Working Party was unable to develop any physical insight to suggest the technical superiority of one method over the other. For this reason, it is recommended that FAVOR adopt Method #2 for the purpose of computational efficiency.

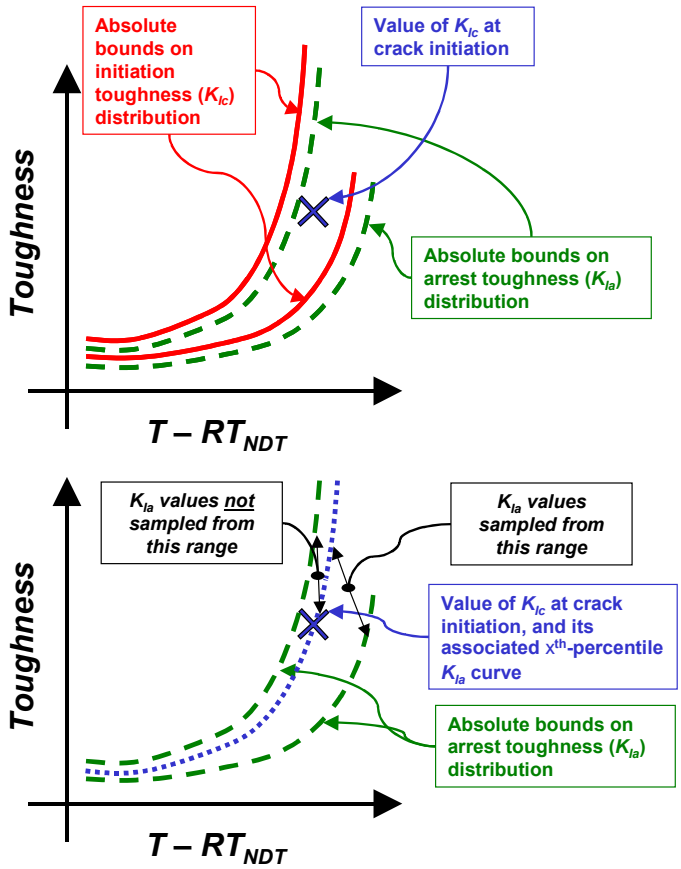


Figure 7.2. Illustration of the proposed procedure to limit $K_{Ia}$ values dependent upon the $K_{Ic}$ value that started the simulation.

#### 7.1.2.1.2 Influence of $K_{Ia}$ on Subsequent $K_{Ic}$ Values

Crack initiation toughness is undefined at values below the crack arrest toughness because the fact that the crack has arrested means that it could no longer propagate. This idea is supported by the experimental observation that the crack arrest toughness transition curve always falls below the crack initiation toughness transition curve. This physical argument establishes the value of crack arrest toughness (say $\tilde{K}_{Ia}$) as the minimum allowable $K_{Ic}$ for temperature at which crack arrest occurred (say $\tilde{T}$). As the transient continues after crack arrest, the temperature at the arrest location falls below $\tilde{T}$. Consequently restricting the minimum allowable $K_{Ic}$ to $\tilde{K}_{Ia}$ is no longer appropriate. Therefore, for temperatures below $\tilde{T}$ the minimum allowable $K_{Ic}$ therefore cannot exceed the $K_{Ia}$ value of the same percentile as the value $\tilde{K}_{Ia}$ occupies in the $K_{Ia}$ distribution at temperature $\tilde{T}$.

The argument presented in the preceding paragraph establishes the physically admissible bounds on the $K_{Ic}$ distribution presuming that a value of $K_{Ia}$ is known for the material. Were FAVOR modeling crack arrest probabilistically, these bounds would establish the limits of the $K_{Ic}$ distribution. However, in FAVOR the aleatory uncertainty in crack arrest data toughness is simulated using a Monte Carlo approach wherein a large number of deterministic crack arrest analyses are performed to estimate what fraction of the flaws that initiate can be expected to extend through the wall and fail the vessel. In this context, the only consistent choice for $K_{Ic}$ when checking for crack re-initiation is the $K_{Ic}$ value having the same percentile as the $K_{Ic}$ value that initiated the crack to begin with. This value of $K_{Ic}$ falls within the physically admissible bounds on the $K_{Ic}$ distribution because of the restrictions placed on the $K_{Ia}$ distribution in Section 7.1.2.1.1.

### 7.1.2.2 Vessel Failure Criteria

FAVOR considers a vessel to have failed if **either** of the following occurs:

A. The crack fails to experience a stable arrest at a depth of less than 90% of the vessel wall thickness, or if
B. At any stage during it's propagation through the vessel wall the ligament remaining between the advancing crack front and the outer diameter of the vessel experiences a load causing general plastic flow in the ligament.

The second criteria suggests that the vessel failure probability depends not only on the crack arrest toughness of the material as discussed in Section 6, but also on the material flow properties since these control resistance to failure by plastic collapse. Ligament collapse, and consequently vessel failure, is considered to have occurred whenever the pressure-induced membrane stress exceeds the instability stress. These values are calculated as follows:

Eq. 7-1 $$\sigma_{MEMBRANE} = p_i \frac{r_i + a}{\beta \cdot (t - a)}$$

Eq. 7-2 $$\sigma_{INSTABILITY} = \sigma_{FLOW}$$

Here, $\beta$ is 1 for hoop stress and 2 for axial stress, $p_i$ is the internal pressure, $r_i$ is the inner radius of the vessel, $\sigma_{FLOW}$ is defined as the average of the yield and the ultimate strengths of the material, $a$ is the crack depth, and $t$ is the thickness of the vessel wall. This collapse model assumes that the presence of the crack simply produces a vessel having a wall that is thinner by the amount of the crack depth. No account is taken of the stress intensification produced by the presence of the crack on plastic flow in the vessel.

A way to estimate flow stress that accounts for the effects of irradiation hardening, and uncertainty in the flow stress values is needed to provide input to Eq. 7-2. This can be done by first estimating the value of $\Delta T_{30}$ for the material of interest (using the embrittlement trend curve, Eq. 5-1). This $\Delta T_{30}$ value is converted to a $\Delta\sigma_{flow}$ value as follows:

1. Convert $\Delta T_{30}$ to $\Delta\sigma_{ys}$ using the relationship in Figure 7.3. These data were compiled by the Working Party from data in the open literature, and are the same information as presented previously in Figure 5.3 and Figure 5.5.
2. Recently Natishan, et al. have noted a striking consistency in the hardening behavior of all ferritic steels, a consistency that can be anticipated on theoretical grounds [Natishan 01b]. Figure 7.4 provides empirical evidence supporting their conclusion. Of direct relevance here, the data in Figure 7.4 suggest that the ultimate tensile strength exceeds the yield strength by 16.5 ksi (114 MPa) on average. This information suggests that the estimate of the increase in yield strength produced by irradiation (from Figure 7.3) should provide a reasonable estimate of the increase in flow strength produced by irradiation.

In summary, the irradiated flow strength of a ferritic RPV steel can be estimated as follows:

Eq. 7-3 $$\sigma_{FLOW(I)} = \sigma_{FLOW(U)} + \gamma \cdot \Delta T_{30}$$

where

| | |
|---|---|
| $\sigma_{flow(u)}$ | is the un-irradiated flow strength from Appendix A. |
| $\Delta T_{30}$ | is estimated using Eq. 5-1, and |
| $\gamma$ | is 0.112 ksi/°F for welds, and 0.131 ksi/°F for plates. |

The uncertainty in this relationship is as follows

Eq. 7-4 $$\sigma_{\sigma_{Cu}} = MIN\left\{\frac{\gamma}{3.09023}\cdot\Delta T_{30}, \hat{\sigma}\right\}$$

where $\hat{\sigma}$ is the uncertainty on the linear fits shown in Figure 7.3. $\hat{\sigma}$ has a value of 4.22 ksi welds and 2.91 ksi for plates. Inadequate data is available for forgings on which to base independently estimated $\gamma$ and $\hat{\sigma}$ values. Consequently, it is recommended (based on inspection of Figure 7.3) that the plate coefficients be adopted for forgings. In some sense Eq. 7-3 is backwards because the increase in flow strength due to irradiation is estimated from a toughness transition temperature shift, whereas it is well established that it is the increase in flow strength that *causes* the toughness transition temperature shift. Nevertheless, this approach is recommended for use in FAVOR to maintain consistency with the embrittlement trend curve model.

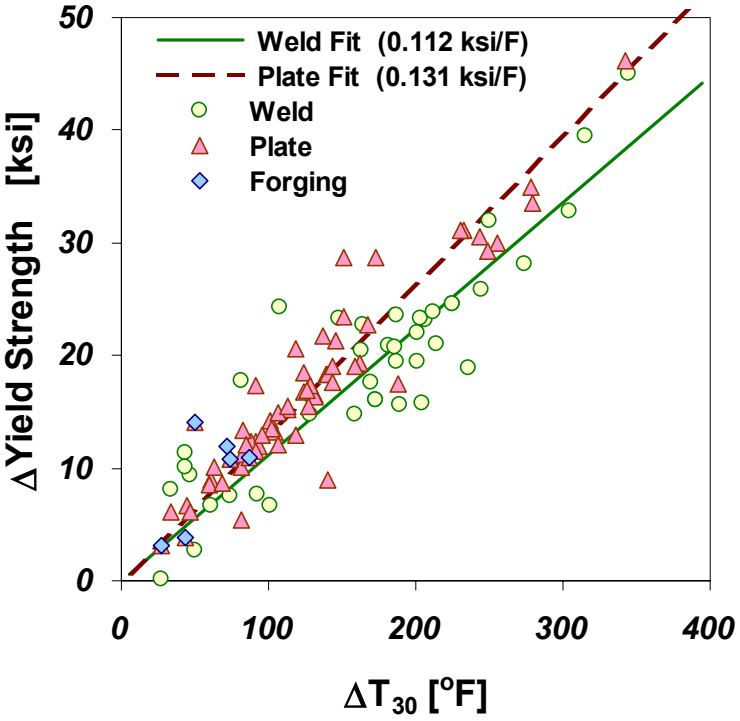


Figure 7.3. Relationship between the shift in the 30 ft-lb CVN transition temperature and the increase in yield strength produced by irradiation.

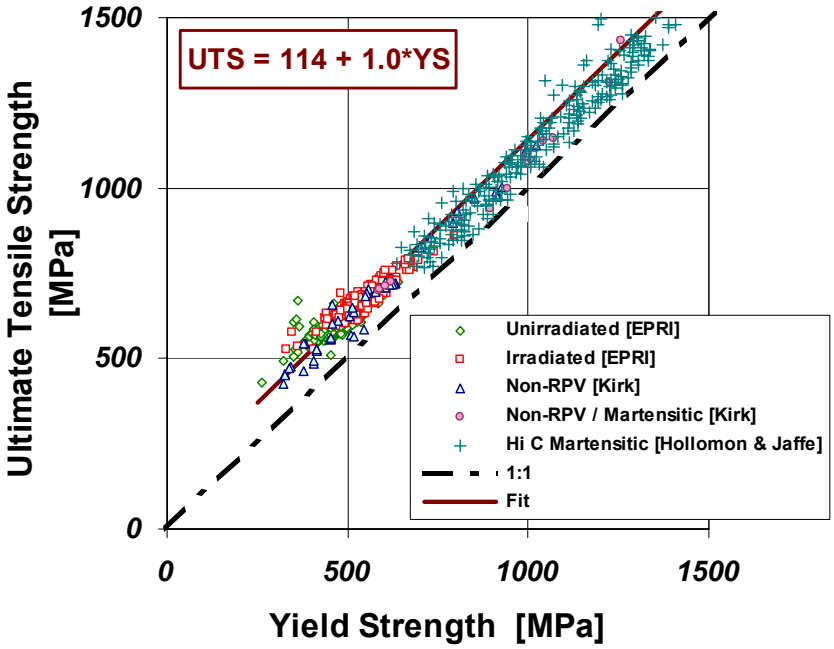


Figure 7.4. A consistent relationship between yield strength and ultimate tensile strength for a wide variety of steels [Natishan 01b].

### 7.1.2.3 Through-Wall Property Gradients

In the early years of nuclear RPV construction in the United States it was common manufacturing practice in the United States to copper-coat the welding wires used in RPV fabrication to inhibit corrosion. By the early 1970s the damaging effects of copper on a steel's resistance to irradiation damage was recognized, and so the practice of copper coating was abandoned. However, all of the early production vessels, those that now lie closest to the PTS screening limits, were fabricated with copper coated weld wires[**]. The copper coating process was not well controlled, which led to varying amounts of copper being deposited on different spools of welding wire. As a consequence of the limited size of these spools and the large volume of weld metal needed to make a PWR weld, it was generally not possible to complete the welding of either the axial seams or the girth welds using a single spool of wire. Evidence of this can be seen in through-thickness compositional surveys [CEOG ???]. Thus, to model appropriately the fracture resistance of the welds in these early vessels it is important that FAVOR account for the effects of variations in copper content through the thickness of an RPV weld.

The number of layers in an RPV weld that can each be expected to have a consistent copper content because the weld metal in the layer was deposited all from the same spool of weld wire can be estimated using the following information:

1. The vessel wall thickness
2. The vessel diameter
3. The dimensions of the weld prep
4. The amount of wire in a single spool, and
5. Details of the welding process, including
    a. Whether tandem or single wire feed was used, and
    b. Information regarding the welding sequence (i.e. how may welds were made simultaneously.

Table 7.1 summarizes this information for the welds in the four plants being modeled, and uses it to estimate (in the last column) the number of distinct layers in these RPV welds. The number of layers was determined by dividing $T_{WD}$ by $t_{wall}$, rounding to the nearest integer, and adding 1. Rounding off and adding 1 accounts for the use of less than full spools of welding wire at the beginning of fabrication.

To simulate the effect of distinct weld layers on vessel integrity, the following procedure is recommended for implementation in FAVOR:

1. Determine the number of layers in the weld of interest from the information in Table 7.1. Divide the vessel thickness evenly into this number of weld layers.
2. During the course of a crack arrest analysis (see Section 7.1.2) crack propagation is simulated through the vessel wall. When the crack tip passes into a new weld layer, new values of chemistry (Cu, Ni, and P) should be re-drawn from the mean and standard deviation values associated with the weld region the crack is located in (formulas in Appendix B describe the distributions of Cu, Ni, and P).
3. A new value of irradiation shift is determined using these new composition values and the procedure detailed in Section 5.3.
4. Because the steel in the new weld layer has different material properties than those in the preceding weld layer, all restrictions on the $K_{Ic}$ and/or $K_{Ia}$ distribution established based on initiation and arrest events that occurred in the preceding layer (see Section 7.1.2.1) are

[**] The four plants being analyzed as part of the PTS re-evaluation effort were all early production vessels, and so were all manufactured using copper coated weld wire.

eliminated because the physical rationale that justified these restrictions applies only to the material in which crack initiation and/or crack arrest occurred.

Table 7.1. Layers of uniform copper content expected in RPV welds.

| Plant | Weld ID | # Welds Made at One Time, $N_{WELD}$ | # of Arcs, $N_{ARC}$ | Vessel Thick., $t_{WALL}$ [in] | Weld Length, $L$ [in] | Weld Width, $W$ [in] | Full Spool Weld Layer Thickness, $T_{WL}$ [in] | Likely Number of Layers in the RPV Weld, $N_{WL}$ |
|---|---|---|---|---|---|---|---|---|
| **CE Fabrication, Coil Weight ($W_{COIL}$) = 250 lbs., Coil Volume ($V_{COIL}$) = 880 cu-in.** | | | | | | | | |
| Palisades | Intermediate Axial | 3 | 2 | 8.5 | 96.00 | 1.4375 | 4.25 | 3 |
| | Lower Axial | 3 | 2 | | 92.72 | 1.4375 | 4.40 | 3 |
| | All Circumferential | 1 | 1 | | 553.71 | 1.3125 | 1.21 | 8 |
| Calvert Cliffs 1 | Intermediate Axial | 3 | 2 | 8.625 | 96.75 | 1.375 | 4.41 | 3 |
| | Lower Axial | 3 | 2 | | 97.38 | 1.375 | 4.38 | 3 |
| | All Circumferential | 1 | 1 | | 553.90 | 1.25 | 1.27 | 8 |
| Beaver Valley 1 | Intermediate Axial | 2 | 2 | 7.875 | 100.63 | 1.375 | 6.36 | 2 |
| | Lower Axial | 2 | 2 | | 100.63 | 1.375 | 6.36 | 2 |
| | All Circumferential | 1 | 1 | | 505.60 | 1.25 | 1.39 | 7 |
| **B&W Fabrication, Coil Weight ($W_{COIL}$) = 350 lbs., Coil Volume ($V_{COIL}$) = 1,234 cu-in.** | | | | | | | | |
| Oconee 1 | Intermediate Axial | 2 | 1 | 8.44 | 30.00 | 1.625 | 12.64 | 2 |
| | Lower & Upper Axial | 2 | 1 | | 73.19 | 1.625 | 5.18 | 3 |
| | All Circumferential | 1 | 1 | | 536.40 | 1.625 | 1.41 | 7 |

Formulas:

$$\rho = 0.284 lbs / in^3$$

$$V_{COIL} = W_{COIL} / \rho$$

$$T_{WL} = \frac{V_{COIL} \cdot N_{ARC}}{N_{WELD} \cdot L \cdot W}$$

$$N_{WL} = ROUND\left(T_{WL} / t_{WALL}\right) + 1$$

## 7.2 Engineering Judgments

In preparing these recommendations, every effort has been made to propose models and input parameters having both a firm physical and empirical justification. However, on occasion it was necessary to exercise engineering judgment in the absence of an adequately developed state of knowledge to fully specify programming logic for FAVOR. A natural consequence of this situation is that these judgments are somewhat arbitrary, making alternative conclusions possible. Here we summarize these judgments, thereby identifying them for additional study should the need arise in the future to further refine the FAVOR model.

A. Throughout these recommendations
   - Distribution Truncation: In various places throughout this report statistical distributions are specified that do not have finite bounds. Values simulated from such distributions will occasionally deviate significantly from any physically expected or experimentally observed value. To guard against such excessive extrapolations all non-finite statistical distributions will be truncated at the 0.1% and at the 99.9% confidence limits. The selection of 0.1% and 99.9% as truncation limits is arbitrary.

- Distribution Modification: When simulating small values of a parameter based on experimentally derived statistical distributions it is possible to simulate physically unrealistic values of the parameter. In these situations (see Figure 5.5, Figure 7.4, and Figure B.3) the value of the standard deviation is reduced to prevent simulation of physically unrealistic values.

B. In the initiation toughness model
   - $K_{min}$: The Working Party was unable to develop a physical expectation regarding either the minimum value of fracture toughness or its temperature dependence, and so recommended a temperature dependent value of $K_{min}$ based on a fit to available $K_{Ic}$ data. Other toughness models (e.g. the Master Curve) adopt a temperature invariant value for $K_{min}$.

C. In the irradiation embrittlement model
   - Embrittlement trend curve: While the form of the recommended embrittlement trend curve is largely consistent with a physical understanding of irradiation damage mechanics, certain terms in the embrittlement trend curve rely heavily on empirical justification to support their inclusion. Furthermore, the inclusion of some terms has been justified with the intent of producing a conservative characterization of irradiation embrittlement. These terms include the following:
     - Product-form dependent coefficients in the stable matrix damage term: A statistically insignificant effect included to obtain a more conservative characterization of irradiation embrittlement.
     - Manufacturer dependent coefficients in the copper rich precipitate term: A statistically significant effect having no known physical basis. The appropriateness of this term cannot be assessed using independent data because the appropriate value of the "CE-manufactured?" variable is un-defined unless the steel in question has been made into a pressure vessel, and all available data of this type have been used to calibrate Eq. 5-1.
     - Long-term bias: A statistically significant effect having no known physical basis. This term was included to obtain a more conservative characterization of irradiation embrittlement.
     - Synergistic effect of flux and time: A statistically marginal effect premised on a physical justification that is not universally accepted by experts in the irradiation damage community. This term was included to obtain a more conservative characterization of irradiation embrittlement.

     An embrittlement trend curve containing none of these features is available [Server 2001]. A recently published study demonstrates that this alternative trend curve predicts independently developed irradiation shift data with greater accuracy than does Eq. 5-1 which, on average, predicts $\Delta T_{30}$ values 14% above those measured experimentally [Gunawardane 2001].
   - Attenuation: The function recommended to account for attenuation of fluence through the vessel wall is recognized to be conservative. Moreover, this function reflects a belief that irradiation damage correlates better with damage measured in terms of displacements-per-atom (dpa) than with damage measured in terms of fluence. This belief has yet to be conclusively validated using mechanical property data.

D. In the arrest toughness model
   - Universal scatter: Currently there is no physical rationale supporting a distribution of $K_{Ia}$ that is universal to all RPV steels, however a universal distribution is assumed in the crack arrest model recommended for implementation in FAVOR.
   - Modification of $K_{Ia}$ distribution in crack run/arrest determination: The recommended modification of the $K_{Ia}$ distribution below the physically established upper limit of $K_{Ic}$ is arbitrary, made without the aid of physical insight regarding what the distribution should be.

## 7.3 Recommendations Not Incorporated into the October 2001 Version of FAVOR

The recommendations made in Section 7.1.2.1 regarding the relationship between crack initiation and crack arrest models and in Section 7.1.2.3 regarding through-wall property gradients are not adopted into the October 2001 version of FAVOR. While justifiable physically, the recommendations made in these Sections require substantial changes to the program structure of FAVOR. Such features can be incorporated into future versions of FAVOR, however they were not implemented in the October 2001

version due to schedule constraints associated with the PTS re-evaluation project. When determining if a running cleavage crack will arrest, the October 2001 version of FAVOR restricts the $K_{Ia}$ distribution in all weld layers based on $K_{Ia}$ percentile associated with the $K_{Ic}$ value that caused crack initiation, not just for the weld layer the crack initiated in (as was recommended). Relative to the physical understanding of crack arrest detailed in Sections 7.1.2.1 and 7.1.2.3, this procedure makes crack arrest less likely because $K_{Ia}$ values that exceed the $K_{Ia}$ percentile associated with $K_{Ic}$ are not permitted to occur throughout the entire thickness of the RPV. The October 2001 version of FAVOR also assumes that all welds have four layers, rather than using the weld-specific recommendations of Table 7.1. Assigning four weld layers to the critical axial welds (rather than the two to three layers suggested in Table 7.1) gives these welds more arrest capacity than they actually have. Thus, the two differences between the October 2001 version of FAVOR and the recommendation provided herein have offsetting effects on the (modeled) arrest capacity of the RPV.

# 8. References


| | |
|---|---|
| 10CFR5061 | Code of Federal Regulation 10CFR50.61, "Fracture Toughness Requirements for Protection Against Pressurized Thermal Shock Events." |
| 10CFR50G | Code of Federal Regulation 10CFR50 Appendix G, "Fracture Toughness Requirements {for Normal Operation}." |
| ASME NB2331 | ASME NB-2331, 1998 ASME Boiler and Pressure Vessel Code, Rules for Construction of Nuclear Power Plants, Division 1, Subsection NB, Class 1 Components. |
| ASTM E1921 | ASTM E1921-97, "Test Method for Determination of Reference Temperature, $T_o$, for Ferritic Steels in the Transition Range," ASTM, 1998. |
| Bowman 00 | Bowman, K.O. and Williams, P.T., "Technical Basis for Statistical Models of Extended $K_{Ic}$ and $K_{Ia}$ Fracture Toughness Databases for RPV Steels, ORNL/NRC/LTR-99/27, February 2000. |
| BWOG | "Response to Request for Additional Information (RAI) Regarding Reactor Vessel Integrity," BAW-2325 Revision 1, January 1999. |
| CEOG | "Best Estimate Copper and Nickel Values in CE Fabricated Reactor Vessel Welds," CE NPSD-1039 Revision 2, June 1997. |
| CE-944 | CE NPSD-944-P Rev 2. |
| Dickson 99 | Dickson, T.L., Malik, S.N.M., Bryson, J.W., and Simonen, F.A., "Revisiting the Integrated Pressurized Thermal Shock Studies of an Aging Pressurized Water Reactor," ASME PVP-Volume 388, Fracture, Design Analysis of Pressure Vessels, Heat Exchangers, Piping Components, and Fitness for Service, ASME, August, 1999. |
| Eason 00 | Eason, E. and Wright, J., "Updated Transition Temperature Shift Model," USNRC Internal Document, July 2000. |
| Gunawardane 01 | "Effect Of Irradiation on Yield and Fracture Toughness of Ferritic Steels," MS Thesis, University of Maryland, August 2001. |
| Jones 01 | ??? |
| Nanstad 93 | Nanstad, R.K., Keeney, J.A., and McCabe, D.E., 1993, "Preliminary Review of the Bases for the $K_{Ic}$ Curve in the ASME Code," ORNL/NRC/LTR-93/15, Oak Ridge National Laboratory, Oak Ridge, TN. |
| Natishan 01a | Natishan, M., Kirk, M., Modarres, M., Li, F., Williams, P., Nanstad, R., Bass, R., Merkle, J., and Dickson, T., "Evaluation and Characterization of Uncertainty in Fracture Toughness Models for Ferritic Reactor Pressure Vessel Steels," *in publication*. |
| Natishan 01b | Natishan, M., Kirk, M., Gunawardane, H., and Wagenhofer, M., "More Information from a Hardness Test than You Ever Thought Possible," *Small Specimen Test Techniques: Fourth Volume, ASTM STP-1418,* M. Sokolov, J. |

Landes, and G. Lucas, Eds., American Society for Testing and Materials, West Conshohocken, PA, 2001.

PREP4 "PREP4: Power Reactor Embrittlement Program, Version 1.0", Electric Power Research Institute, 1996: SW-106726.

RPVDATA Electric Power Research Institute Reactor Vessel Materials Database.

RVID Nuclear Regulatory Commission Reactor Vessel Integrity Database, Version 2.1.1, July 6, 2000.

Onizawa 01 Onizawa, K., Personal Communication.

Santos 01 Santos, C., Kalinousky, D., Abramson, L., and Mitchell, M., "Development of Statistical Distributions for Copper, Nickel, and Phosphorus for the PTS Re-Evaluation Program," NRC Internal Document, February 2001.

SCK/CEN 01 E. Lucon, Personal Communication.

SECY82465 SECY-82-465, United States Nuclear Regulatory Commission, 1982.

Server 01 Server, W., English, C., Naimon, D., and Rosinski, S., "Charpy Embrittlement Correlations – Status of Combined Mechanistic and Statistical Bases for U.S. RPV Steels," PWR Materials Reliability Project Report 1000705, May 2001.

Siu 99 "Uncertainty Analysis and Pressurized Thermal Shock, An Opinion," United States Nuclear Regulatory Commission, 1999.

Siu 01 Siu, N., Malik, S., Bessette, D., Woods, R., Mosleh, A. and Modarres, M. "Treating Aleatory and Epistemic Uncertainties in Analyses of Pressurized Thermal Shock," Proceedings of PSAM 5, International Conference on Probabilistic Safety Assessment and Management, Osaka, Japan, November 27-December 1, 2000, pp. 377-382.

VanDerSluys 77 VanDerSluys, W.A., Seeley, R.R., and Schwabe, J.R., "An Investigation of Mechanical Properties and Chemistry within a Thick MnMoNi Submerged Arc Weldment," EPRI Report NP-373, February 1977.

Wallin 84a Wallin, K., Saario, T., and Törrönen, K., "Statistical Model for Carbide Induced Brittle Fracture in Steel," *Metal Science*, Vol. 18, January 1984, 13-16.

Wallin 84b Wallin, K., Saario, T., Törrönen, K., and Forsten, K., "Mechanism-Based Statistical Evaluation of the ASME Reference Fracture Toughness Curve," 5th International Conference on Pressure Vessel Technology, Vol. II, Materials and Manufacturing, San Francisco, California, ASME, 1984.

Wallin 84c Wallin, K., "The Scatter in $K_{IC}$ Results," *Engineering Fracture Mechanics*, **19**(6), pp. 1085-1093, 1984.

Wallin 84d Wallin, K., "The Size Effect in $K_{IC}$ Results," *Engineering Fracture Mechanics*, **22**, pp. 149-163, 1985.

Wallin 93a Wallin, K., "Irradiation Damage Effects on the Fracture Toughness Transition Curve Shape for Reactor Vessel Steels," In*t. J. Pres. Ves. & Piping*, **55**, pp. 61-79, 1993

WRC 175 PVRC Ad Hoc Group on Toughness Requirements, "PVRC Recommendations on Toughness Requirements for Ferritic Materials." Welding Research Council Bulletin No. 175, August 1972.

Yoon 01 Yoon, K.K., Hall, J.B., VanDerSluys, W.A., Higuchi, M., Iida, K., "Japanese Fracture Toughness Data Analysis Using Master Curve Method," 2001 ASME Pressure Vessels and Piping Conference July 23-26, 2001 - Atlanta, Georgia, USA

→ **Last Revised on Monday, October 03, 2001 at 1038 hrs, MTK** **10-3-01.doc**
→ **Last Opened on 1/3/03**

**VERSION FOR NRC STAFF CONCURRANCE REVIEW**

# Appendix A Summary of values for use in FAVOR calculations.

| Product Form | Heat | Beltline | $\sigma_{flow(u)}$ [ksi] | $RT_{NDT(u)}$ [°F] | | | Composition(2) | | |
|---|---|---|---|---|---|---|---|---|---|
| | | | | $RT_{NDT(u)}$ Method | $RT_{NDT(u)}$ Value | $\sigma_{(u)}$ Value | Cu | Ni | P |
| **Beaver Valley 1, (Designer: Westinghouse, Manufacturer: CE) Coolant Temperature = 547°F, Vessel Thickness = 7-7/8 in.** | | | | | | | | | |
| PLATE | C4381-1 | INTERMEDIATE SHELL B6607-1 | 83.8 | MTEB 5-2 | 43 | 0 | 0.14 | 0.62 | 0.015 |
| | C4381-2 | INTERMEDIATE SHELL B6607-2 | 84.3 | MTEB 5-2 | 73 | 0 | 0.14 | 0.62 | 0.015 |
| | C6293-2 | LOWER SHELL B7203-2 | 78.8 | MTEB 5-2 | 20 | 0 | 0.14 | 0.57 | 0.015 |
| | C6317-1 | LOWER SHELL B6903-1 | 72.7 | MTEB 5-2 | 27 | 0 | 0.2 | 0.54 | 0.01 |
| LINDE 1092 WELD | 305414 | LOWER SHELL AXIAL WELD 20-714 | 75.3 | Generic | -56 | 17 | 0.337 | 0.609 | 0.012 |
| | 305424 | INTER SHELL AXIAL WELD 19-714 | 79.9 | Generic | -56 | 17 | 0.273 | 0.629 | 0.013 |
| LINDE 0091 WELD | 90136 | CIRC WELD 11-714 | 76.1 | Generic | -56 | 17 | 0.269 | 0.07 | 0.013 |
| **Calvert Cliffs 1, (Designer and Manufacturer: CE) Coolant Temperature = 545°F, Vessel Thickness = 8 5/8-in.** | | | | | | | | | |
| PLATE | B-8489-1 | LOWER SHELL D-7207-3 | 78.8 | MTEB 5-2 | -20 | 0 | 0.11 | 0.53 | 0.008 |
| | B-8489-2 | LOWER SHELL D-7207-2 | 80.3 | MTEB 5-2 | -10 | 0 | 0.11 | 0.56 | 0.009 |
| | C-4351-2 | INTERMEDIATE SHELL D-7206-1 | 74.7 | MTEB 5-2 | 20 | 0 | 0.11 | 0.55 | 0.011 |
| | C-4420-1 | LOWER SHELL D-7207-1 | 78.0 | MTEB 5-2 | 10 | 0 | 0.13 | 0.54 | 0.01 |
| | C-4441-1 | INTERMEDIATE SHELL D-7206-3 | 78.5 | ASME NB-2331 | 10 | 0 | 0.12 | 0.64 | 0.011 |
| | C-4441-2 | INTERMEDIATE SHELL D-7206-2 | 82.6 | ASME NB-2331 | -30 | 0 | 0.12 | 0.64 | 0.011 |
| LINDE 1092 WELD | 20291/12008 | INTERMEDIATE SHELL AXIAL WELD 2-203 | 78.8 | ASME NB-2331 | -50 | 0 | 0.22 | 0.83 | 0.01 |
| | 21935 | LOWER SHELL AXIAL WELD 3-203A/C | 78.6 | Generic | -56 | 17 | 0.18 | 0.72 | 0.015 |
| LINDE 0091 WELD | 33A277 | INT. TO LOWER SHELL CIRC. WELD 9-203 | 78.6 | ASME NB-2331 | -80 | 0 | 0.24 | 0.16 | 0.014 |
| **Oconee 1, (Designer and Manufacturer: B&W) Coolant Temperature = 556°F, Vessel Thickness = 8.44-in.** | | | | | | | | | |
| FORGING | AHR54 (ZV2861) | LOWER NOZZLE BELT | (4) | B&W Generic | 3 | 31 | 0.16 | 0.65 | 0.006 |
| PLATE | C2197-2 | INTERMEDIATE SHELL | (4) | B&W Generic | 1 | 26.9 | 0.15 | 0.5 | 0.008 |
| | C2800-1 | LOWER SHELL | (4) | B&W Generic | 1 | 26.9 | 0.11 | 0.63 | 0.012 |
| | C2800-2 | LOWER SHELL | 69.9 | B&W Generic | 1 | 26.9 | 0.11 | 0.63 | 0.012 |
| | C3265-1 | UPPER SHELL | 75.8 | B&W Generic | 1 | 26.9 | 0.1 | 0.5 | 0.015 |
| | C3278-1 | UPPER SHELL | (4) | B&W Generic | 1 | 26.9 | 0.12 | 0.6 | 0.01 |
| LINDE 80 WELD | 1P0962 | INTERMEDIATE SHELL AXIAL WELDS SA-1073 | 79.4 | B&W Generic | -5 | 19.7 | 0.21 | 0.64 | 0.025 |
| | 299L44 | INT./UPPER SHL CIRC WELD (OUTSIDE 39%) WF-25 | (4) | B&W Generic | -7 | 20.6 | 0.34 | 0.68 | (3) |
| | 61782 | NOZZLE BELT/INT. SHELL CIRC WELD SA-1135 | (4) | B&W Generic | -5 | 19.7 | 0.23 | 0.52 | 0.011 |
| | 71249 | INT./UPPER SHL CIRC WELD (INSIDE 61%) SA-1229 | 76.4 | ASME NB-2331 | 10 | 0 | 0.23 | 0.59 | 0.021 |
| | 72445 | UPPER/LOWER SHELL CIRC WELD SA-1585 | (4) | B&W Generic | -5 | 19.7 | 0.22 | 0.54 | 0.016 |
| | 8T1762 | LOWER SHELL AXIAL WELDS SA-1430 | 75.5 | B&W Generic | -5 | 19.7 | 0.19 | 0.57 | 0.017 |
| | 8T1762 | UPPER SHELL AXIAL WELDS SA-1493 | (4) | B&W Generic | -5 | 19.7 | 0.19 | 0.57 | 0.017 |

| | | | | | | | | | |
|---|---|---|---|---|---|---|---|---|---|
| | 8T1762 | LOWER SHELL AXIAL WELDS SA-1426 | 75.5 | B&W Generic | -5 | 19.7 | 0.19 | 0.57 | 0.017 |
| **Pallisades, (Designer and Manufacturer: CE) Coolant Temperature = 532°F, Vessel Thickness = 8½ in.** | | | | | | | | | |
| PLATE | A-0313 | D-3803-2 | (4) | MTEB 5-2 | -30 | 0 | 0.24 | 0.52 | 0.01 |
| | B-5294 | D-3804-3 | (4) | MTEB 5-2 | -25 | 0 | 0.12 | 0.55 | 0.01 |
| | C-1279 | D-3803-3 | (4) | ASME NB-2331 | -5 | 0 | 0.24 | 0.5 | 0.011 |
| | C-1279 | D-3803-1 | 74.7 | ASME NB-2331 | -5 | 0 | 0.24 | 0.51 | 0.009 |
| | C-1308A | D-3804-1 | (4) | ASME NB-2331 | 0 | 0 | 0.19 | 0.48 | 0.016 |
| | C-1308B | D-3804-2 | (4) | MTEB 5-2 | -30 | 0 | 0.19 | 0.5 | 0.015 |
| LINDE 0124 WELD | 27204 | CIRC. WELD 9-112 | 76.9 | Generic | -56 | 17 | 0.203 | 1.018 | 0.013 |
| LINDE 1092 WELD | 34B009 | LOWER SHELL AXIAL WELD 3-112A/C | 76.1 | Generic | -56 | 17 | 0.192 | 0.98 | (3) |
| | W5214 | LOWER SHELL AXIAL WELDS 3-112A/C | 72.9 | Generic | -56 | 17 | 0.213 | 1.01 | 0.019 |
| | W5214 | INTERMEDIATE SHELL AXIAL WELDS 2-112 A/C | 72.9 | Generic | -56 | 17 | 0.213 | 1.01 | 0.019 |

Notes:

(1) Information taken directly from the July 2000 release of the NRCs Reactor Vessel Integrity (RVID2) database.
(2) These composition values are as reported in RVID2. In FAVOR calculations these values should be treated as the central tendency of the Cu, Ni, and P distributions detailed in Appendix B.
(3) No values of phosphorus are recorded in RVID2 for these heats. A generic value of 0.012 should be used, which is the mean of 826 phosphorus values taken from the surveillance database used by Eason et al. to calibrate the embrittlement trend curve.
(4) No values strength measurements are available in PREP4 for these heats [PREP]. A value of 77 ksi should be used, which is the mean of other flow strength values reported in this Appendix.

# Appendix B Generic Distributions of Cu, Ni, and P

While there is considerable information available concerning the composition of the steels used in US nuclear RPV construction [RVID, RPVDATA], the heats for which sufficient information exists on which to estimate the statistical distribution of the chemical composition are considerably more limited. However, such information is needed as input to the probabilistic fracture mechanics code FAVOR to assess the effects of material variability on the probability of vessel failure. In this Appendix we review available data sets wherein multiple composition measurements have been made on the same heat of steel, and use these data to derive generic distributions for Cu, Ni, and P. In FAVOR these distributions will be assumed to apply to all RPV steels.

A RPV is divided into different **regions**, each corresponding to a unique heat of steel, be it of a weld, plate, or forging. Figure B.1 illustrates these various regions. In the FAVOR analysis, each region is further divided into **sub-regions** of approximately constant fluence (based on the fluence maps provided by Brookhaven National Laboratory), with each sub-region having an approximately constant value of fluence within it. The average Cu, Ni, and P for each of these regions is based on the information in the RVID database, and was summarized in Appendix A. In this Appendix we use available data to estimate the distribution of chemical composition about these best-estimate values using available information.

To model appropriately the uncertainty in chemical composition, we define composition variability at two different levels:

1. Variability Within a Region: The possible composition variability within a region is defined based on multiple measurements taken from widely varied locations within a heat of steel, and is addressed in Section 8.1.
2. Variability Within a Sub-Region: In any given RPV, FAVOR simulates the existence of thousands of flaws. It is therefore possible that two (or more) of these flaws will be simulated to exist within the same sub-region. The greatest physical separation that these multiple flaws could have from each other is on the order of 3-in. because (a) once a flaw is placed within a sub-region its location is specified only by its location through the wall thickness, (b) flaws are simulated to exist only in the inner 3/8-T of the vessel wall, and (c) PWR vessel walls tend to be on the order of 8-in. thick. Thus, for sub-regions the possible composition variability is defined based on multiple measurements made close together, as detailed in Section 8.2.

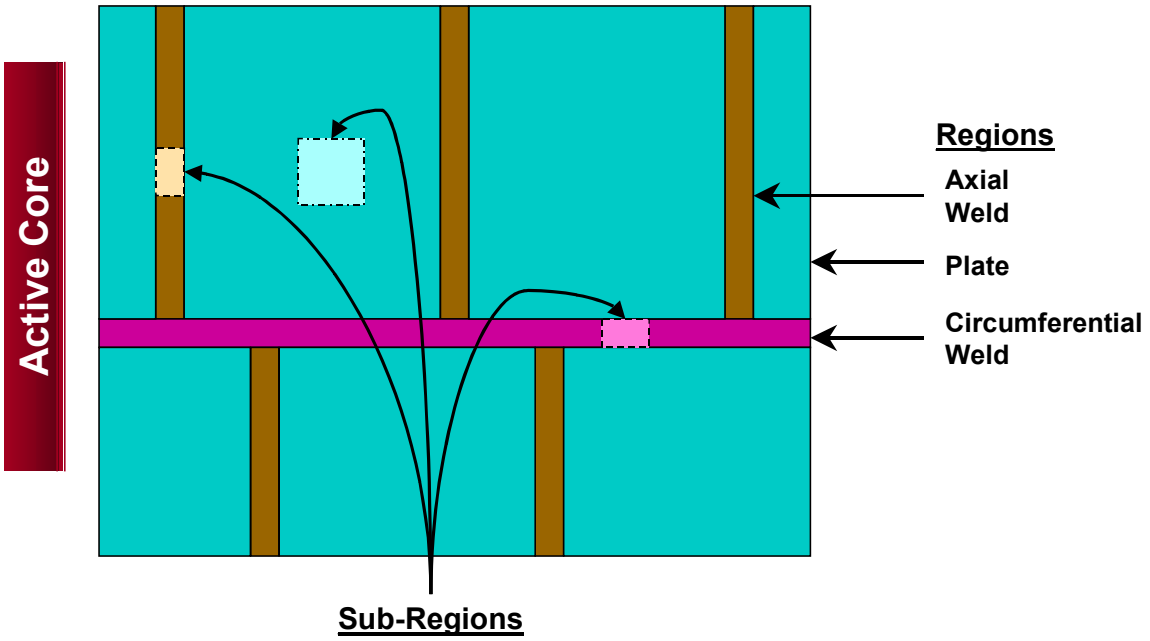


Figure B.1. Designation of material regions and sub-regions in an "un-wrapped" view of a RPV.

## 8.1 Variability Within a Region

### 8.1.1 Welds

#### 8.1.1.1 Copper and Nickel

The raw data used to quantify the variability of Cu and Ni within a particular weld region was obtained from reports published by the CEOG and the B&WOG that organize individual measurements of chemical composition in terms of the hierarchy illustrated in Figure B.2 [CEOG, BWOG]. Within each **heat** of material, data may be available for several different **weld-pieces**. A weld-piece is a separately identifiable weld, such as a nozzle drop-out, a surveillance weld, a weld qualification block, etc. For each weld-piece some number of **independent-measurements** of chemical composition are made. In this appendix we report mean and standard deviation values at the heat level. These parameters are defined according to the following procedure:

Step 1. Identify all of the independent measurements and weld-pieces associated with a particular weld wire heat.
Step 2. Determine the mean Cu, Ni, and P for each weld-piece as the average of all of the independent measurements for that weld-piece.
Step 3. Determine the mean Cu, Ni, and P for the heat as the average of all of the weld-piece means (calculated in Step 2).
Step 4. Determine the standard deviation of Cu, Ni, and P for the heat as the standard deviation of all of the weld-piece means (calculated in Step 2).

This procedure weights the data from each weld-piece equally regardless of the number of independent-measurements made on that weld-piece. Table B.1 and Table B.2 provide the data for Cu and Ni, respectively. Statistical representations of these data are provided in Figure B.3 and Figure B.4. These fits are as follows:

o For Copper: The best estimate on the standard deviation for Cu ($\sigma_{Cu}$) is 0.167 of the mean Cu value taken from Appendix A (i.e., $\sigma_{Cu} = 0.167 \cdot \mu_{Cu}$). The distribution of $\sigma_{Cu}$ about this best estimate is distributed normally. Values of the standard deviation on $\sigma_{Cu}$ are as follows

$$\sigma_{\sigma_{Cu}} = MIN\left\{\frac{0.167}{3.09023} \cdot \mu_{Cu}, 0.0185\right\}$$

This distribution is illustrated in Figure B.3. In FAVOR the standard deviation on copper for a particular heat should be simulated by drawing randomly from the distribution illustrated in Figure B.3. The standard deviation depends on the heat mean copper, as illustrated in the figure.

o For Nickel: The best estimate on the standard deviation for Ni ($\sigma_{Ni}$) is 0.029, and is independent of the mean Ni value taken from Appendix A. The distribution of $\sigma_{Ni}$ about this best estimate is distributed normally. The standard deviation on $\sigma_{Ni}$ is 0.0165. This distribution, truncated at the 5% and 95% quantiles, is illustrated in Figure B.4[††]. In FAVOR the standard deviation on nickel for a particular heat should be simulated by drawing randomly from the distribution illustrated in Figure B.3. This standard deviation is independent of the heat mean nickel, as illustrated in the figure.

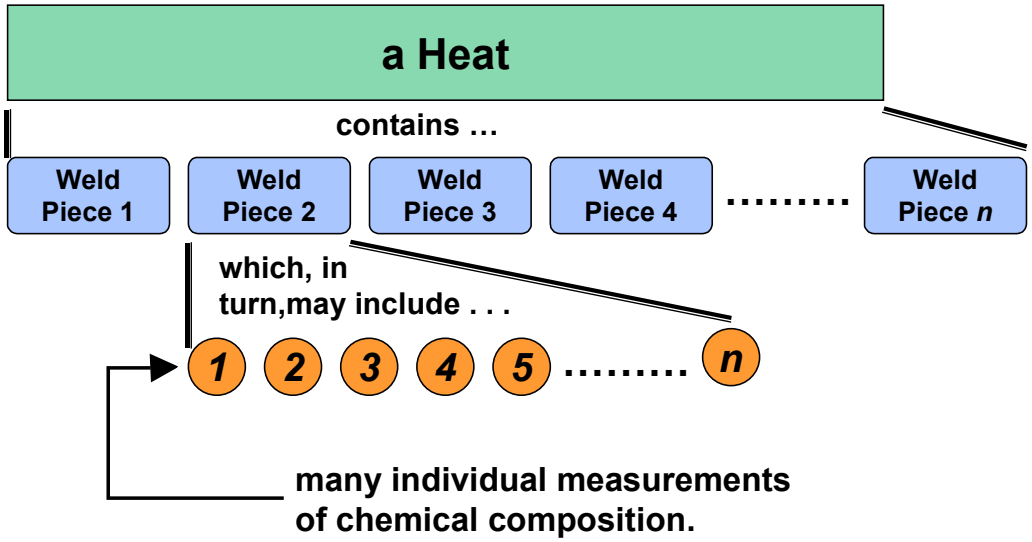


Figure B.2. Hierarchy for composition measurements.

Table B.1. Copper data.

| Vendor | PTS Plant? | Heat # | Number of Weld Pieces | for this Heat | |
|---|---|---|---|---|---|
| | | | | Mean | Std. Dev. |
| CE | Y | 33A277 | 25 | 0.258 | 0.048 |
| CE | Y | 90136 | 15 | 0.269 | 0.076 |
| BW | Y | 61782 | 13 | 0.232 | 0.042 |
| BW | N | 72105 | 12 | 0.323 | 0.048 |
| BW | Y | 71249 | 10 | 0.234 | 0.046 |
| CE | Y | W5214 | 10 | 0.225 | 0.062 |
| CE | N | 51912 | 10 | 0.156 | 0.012 |

[††] Here 5%/95% truncation limits are selected rather than the 1% / 99% values used in the remainder of the document to avoid simulation of negative values of standard deviation.

| | | | | | |
|---|---|---|---|---|---|
| CE | N | 2P5755 | 10 | 0.210 | 0.036 |
| CE | N | 90099 | 9 | 0.209 | 0.043 |
| CE | N | 5P5622 | 9 | 0.153 | 0.031 |
| BW | Y | 72445 | 8 | 0.218 | 0.029 |
| BW | Y | 299L44 | 8 | 0.336 | 0.062 |
| CE | N | 4P6519 | 8 | 0.133 | 0.049 |
| CE | N | 1P3571 | 7 | 0.295 | 0.078 |
| BW | N | 406L44 | 7 | 0.270 | 0.033 |
| BW | Y | 8T1762 | 6 | 0.192 | 0.023 |
| CE | Y | 27204 | 6 | 0.203 | 0.020 |
| CE | N | 10137 | 6 | 0.216 | 0.010 |
| CE | N | 51874 | 6 | 0.147 | 0.034 |
| CE | N | 1248 | 6 | 0.206 | 0.035 |
| BW | N | 821T44 | 6 | 0.237 | 0.033 |
| CE | Y | 21935 | 5 | 0.183 | 0.033 |
| BW | N | 72442 | 5 | 0.260 | 0.033 |
| CE | N | 86054B | 5 | 0.214 | 0.023 |
| CE | N | 1P2815 | 5 | 0.316 | 0.093 |
| CE | Y | 305414 | 4 | 0.337 | 0.023 |
| BW | N | 8T1554 | 4 | 0.160 | 0.019 |
| CE | N | 6329637 | 4 | 0.205 | 0.026 |
| CE | Y | 12008,20291 | 3 | 0.199 | 0.037 |
| CE | Y | 34B009 | 3 | 0.192 | 0.011 |
| CE | Y | 305424 | 3 | 0.289 | 0.019 |
| BW | N | 1P0815 | 3 | 0.167 | 0.059 |
| BW | N | T29744 | 3 | 0.207 | 0.037 |
| CE | N | 12008,21935 | 3 | 0.213 | 0.011 |
| CE | N | 13253 | 3 | 0.221 | 0.071 |
| BW | N | 1P0661 | 2 | 0.165 | 0.025 |
| CE | N | 20291 | 2 | 0.191 | 0.043 |
| CE | N | 12008,305414 | 2 | 0.300 | 0.028 |
| BW | Y | 1P0962 | 1 | 0.210 | 0.033 |
| BW | N | 8T3914 | 1 | 0.180 | |
| CE | N | 3277 | 1 | 0.247 | |
| CE | N | 51989 | 1 | 0.170 | |
| CE | N | 12008,13253 | 1 | 0.210 | |

Table B.2. Nickel data.

| Vendor | PTS Plant? | Heat # | Number of Weld Pieces | for this Heat | |
|---|---|---|---|---|---|
| | | | | Mean | Std. Dev. |
| CE | | 4P6052 | 33 | 0.049 | 0.027 |
| CE | | 3P7317 | 30 | 0.067 | 0.031 |
| CE | | 4P7869 | 23 | 0.095 | 0.025 |
| BW | Y | 61782 | 12 | 0.516 | 0.053 |
| BW | | 72105 | 12 | 0.578 | 0.020 |
| BW | Y | 71249 | 10 | 0.590 | 0.033 |
| CE | | 90077 | 10 | 0.055 | 0.017 |
| CE | | 2P5755 | 10 | 0.058 | 0.008 |
| BW | Y | 72445 | 9 | 0.543 | 0.057 |
| BW | Y | 299L44 | 8 | 0.676 | 0.038 |
| CE | | 83650 | 8 | 0.087 | 0.027 |
| CE | | 89476 | 8 | 0.069 | 0.023 |
| CE | | 89833 | 8 | 0.054 | 0.023 |
| CE | | 90130 | 8 | 0.133 | 0.073 |
| CE | | 4P6519 | 8 | 0.060 | 0.017 |
| CE | | 83642 | 7 | 0.078 | 0.027 |
| CE | | 83653 | 7 | 0.102 | 0.035 |

| | | | | | |
|---|---|---|---|---|---|
| CE | | 88114 | 7 | 0.187 | 0.026 |
| CE | | 90071 | 7 | 0.074 | 0.032 |
| CE | | 1P3571 | 7 | 0.755 | 0.045 |
| BW | | 406L44 | 7 | 0.589 | 0.006 |
| CE | Y | 33A277 | 6 | 0.165 | 0.013 |
| BW | Y | 8T1762 | 6 | 0.567 | 0.059 |
| CE | | 10120 | 6 | 0.063 | 0.037 |
| CE | | 90069 | 6 | 0.076 | 0.059 |
| CE | | 90146 | 6 | 0.082 | 0.038 |
| CE | | 90209 | 6 | 0.111 | 0.042 |
| CE | | 5P5622 | 6 | 0.077 | 0.031 |
| CE | | 86054B | 6 | 0.046 | 0.004 |
| BW | | 821T44 | 6 | 0.628 | 0.009 |
| CE | Y | 27204 | 5 | 1.018 | 0.047 |
| CE | | 83637 | 5 | 0.066 | 0.033 |
| CE | | 83640 | 5 | 0.088 | 0.031 |
| CE | | 87005 | 5 | 0.151 | 0.032 |
| CE | | 1P2815 | 5 | 0.724 | 0.021 |
| CE | | BOLA | 5 | 0.910 | 0.020 |
| BW | | 72442 | 5 | 0.602 | 0.020 |
| CE | Y | 305414 | 4 | 0.609 | 0.022 |
| CE | | 10137 | 4 | 0.043 | 0.026 |
| CE | | 51874 | 4 | 0.038 | 0.005 |
| CE | | 51912 | 4 | 0.059 | 0.025 |
| CE | | 83648 | 4 | 0.130 | 0.018 |
| CE | | 90144 | 4 | 0.043 | 0.006 |
| BW | | 8T1554 | 4 | 0.568 | 0.068 |
| CE | Y | 305424 | 3 | 0.630 | 0.018 |
| CE | Y | 12008,20291 | 3 | 0.846 | 0.026 |
| CE | | 13253 | 3 | 0.732 | 0.007 |
| CE | | 88112 | 3 | 0.188 | 0.045 |
| CE | | HODA | 3 | 0.938 | 0.051 |
| BW | | 1P0815 | 3 | 0.523 | 0.037 |
| BW | | T29744 | 3 | 0.653 | 0.017 |
| CE | Y | 21935 | 2 | 0.704 | 0.034 |
| CE | Y | 90136 | 2 | 0.070 | 0.000 |
| CE | | 12420 | 2 | 1.023 | 0.033 |
| CE | | 12008,305414 | 2 | 0.765 | 0.035 |
| CE | | 12008/27204 | 2 | 0.980 | 0.000 |
| BW | | 1P0661 | 2 | 0.640 | 0.010 |
| BW | | 8T3914 | 2 | 0.625 | 0.035 |
| BW | Y | 1P0962 | 1 | 0.640 | |
| CE | | 9565 | 1 | 0.080 | |
| CE | | 20291 | 1 | 0.737 | |
| CE | | 51989 | 1 | 0.165 | |
| CE | | 12008,13253 | 1 | 0.083 | |
| CE | | 12008,21935 | 1 | 0.867 | |
| CE | | 12008/305424 | 1 | 0.810 | |
| CE | | 1P2809 | 1 | 0.770 | |
| CE | | 39B196 | 1 | 1.200 | |
| CE-Ni+ | | 1248 | 4 | 1.073 | 0.142 |
| CE-Ni+ | | 1248/661h577 | 2 | 1.105 | 0.021 |
| CE-Ni+ | Y | 34B009 | 3 | 0.888 | 0.299 |
| CE-Ni+ | Y | W5214 | 12 | 1.025 | 0.137 |

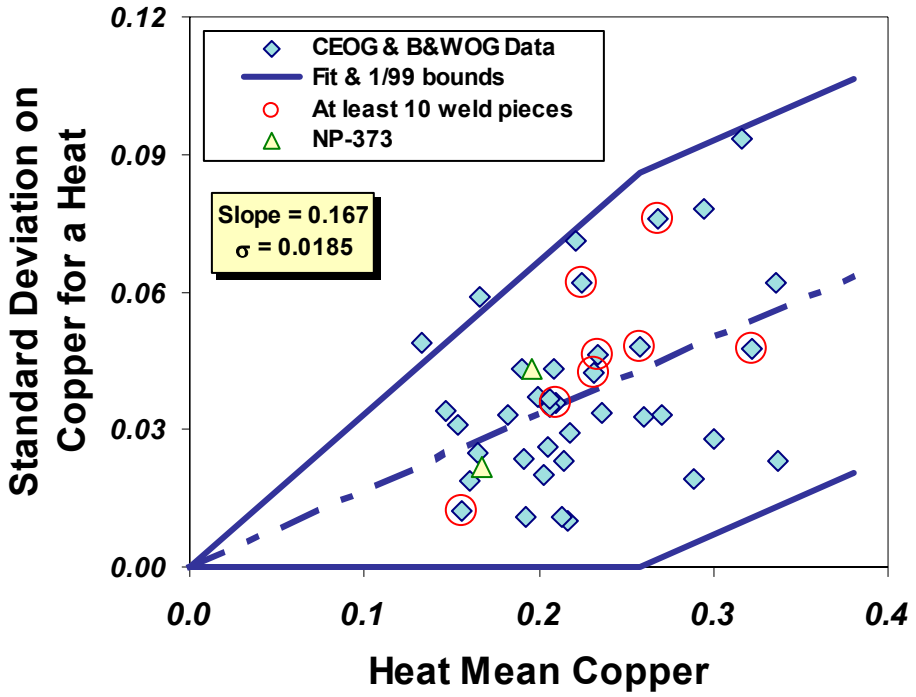


Figure B.3. Copper variability within a region for welds.

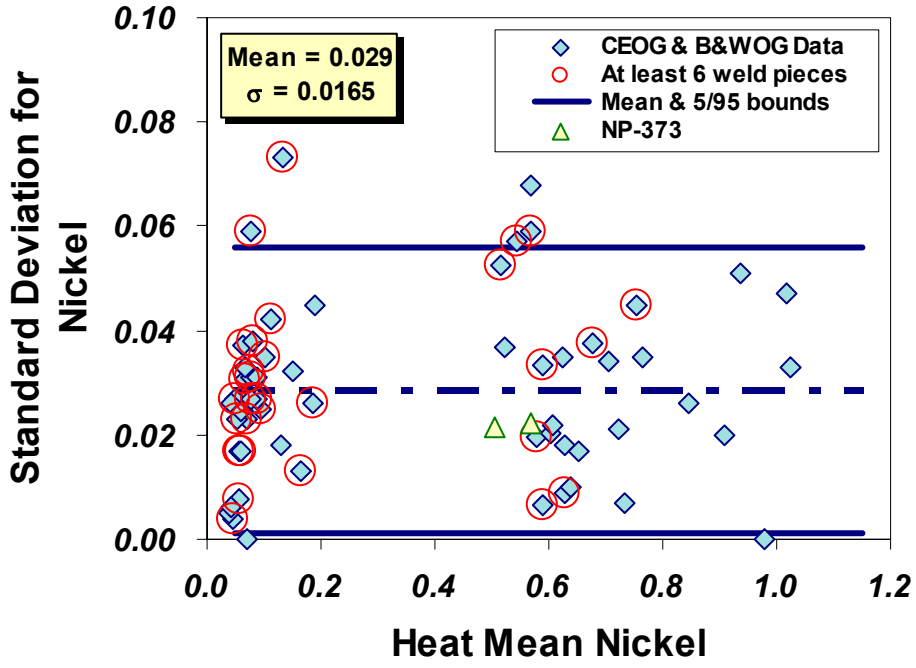


Figure B.4. Nickel variability within a region for non-nickel addition welds

#### 8.1.1.2 Phosphorus

The data used to quantify the variability of phosphorus within a particular weld region was obtained from a 1977 EPRI report concerning a comprehensive chemical survey of a single Linde 80 weldment made by Babcox and Wilcox [VanDerSluys 77]. Figure B.5 provides the welding details and illustrates the chemical sampling plan used in this study. In total 56 independent measurements of composition were made on the weld metal while 35 were made in the surrounding A503 Cl. 2 forging. Figure B.3 and Figure B.4 show the Cu and Ni data from these two weld wire heats analyzed in the manner detailed in Section 8.1.1.1 overlaid on the larger dataset for Cu and Ni. This comparison suggests that the data reported in EPRI NP-373 is similar to that available for the larger population of domestic RPV welds. The phosphorous data for both the forging and for the two weld heats is illustrated in Figure B.6. The estimated standard deviation values for weld wire heats A and B are 0.0010 and 0.0014, respectively while the forging has an estimated standard deviation on phosphorus of 0.0016. Lacking more detailed information it is recommended that FAVOR adopt the same standard deviation for phosphorus in all product forms, that being the average of these three experimental observations, or 0.0013. Use of the weld and forging data together to establish a generic statistical distribution for phosphorus is justified since phosphorus is an impurity element, and so is not added intentionally to any product form.

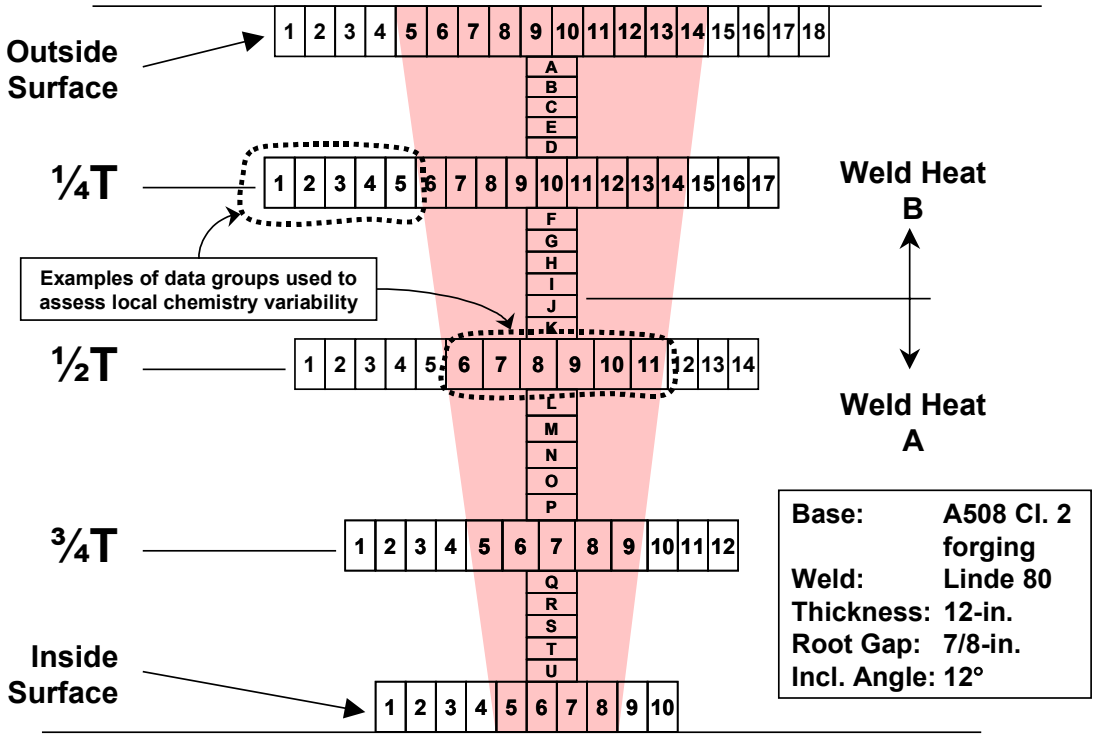


Figure B.5. Chemistry sampling plan from EPRI NP-373.

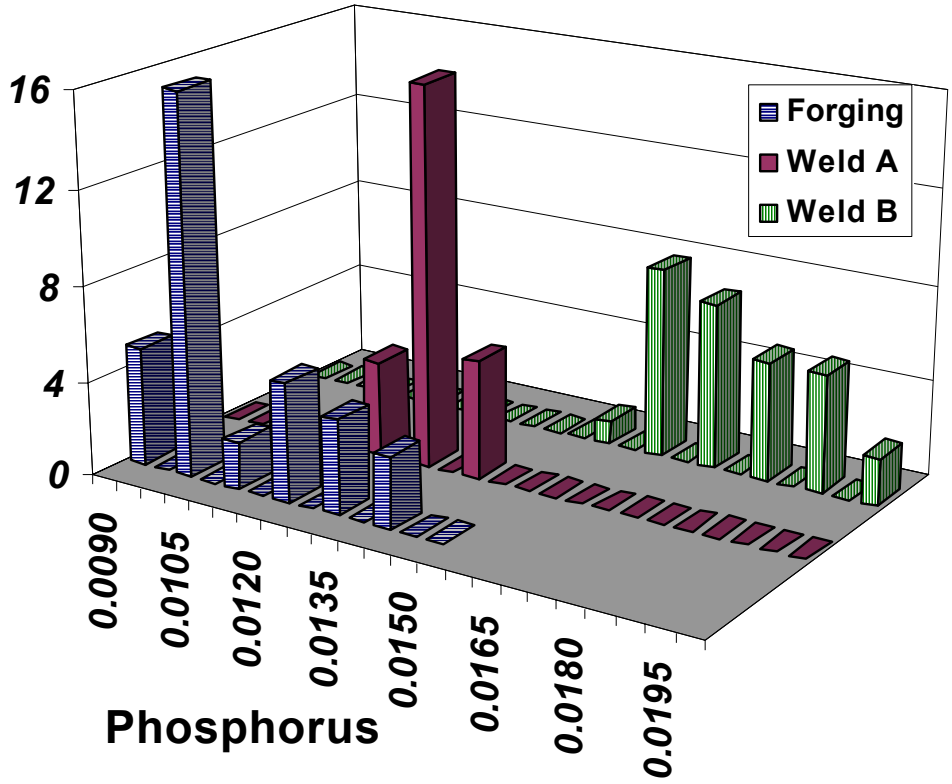


Figure B.6. Phosphorus data reported in EPRI NP-373 (the vertical axis reflects the number of independent measurements made).

### 8.1.2 Plates and Forgings

The data reported in EPRI NP-373 is the most detailed chemical survey of a domestic production RPV weldment that the staff has been able to locate. For this reason, the distributions of Ni and Cu determined from the 35 composition measurements made in the forging are used to assess the statistical distributions that should be assumed for Cu, Ni, and P for both plates and forgings. Figure B.7 and Figure B.8 summarize the Cu and Ni data respectively (the P data was presented previously in Figure B.6). Based on these data, the following distributions are recommended for use in FAVOR to represent the chemical composition variability in all plate and forging regions:

- For Copper: Normal with a standard deviation of 0.0073.
- For Nickel: Normal with a standard deviation of 0.0244.
- For Phosphorus: Normal with a standard deviation of 0.0013 (see Section 8.1.1.1).

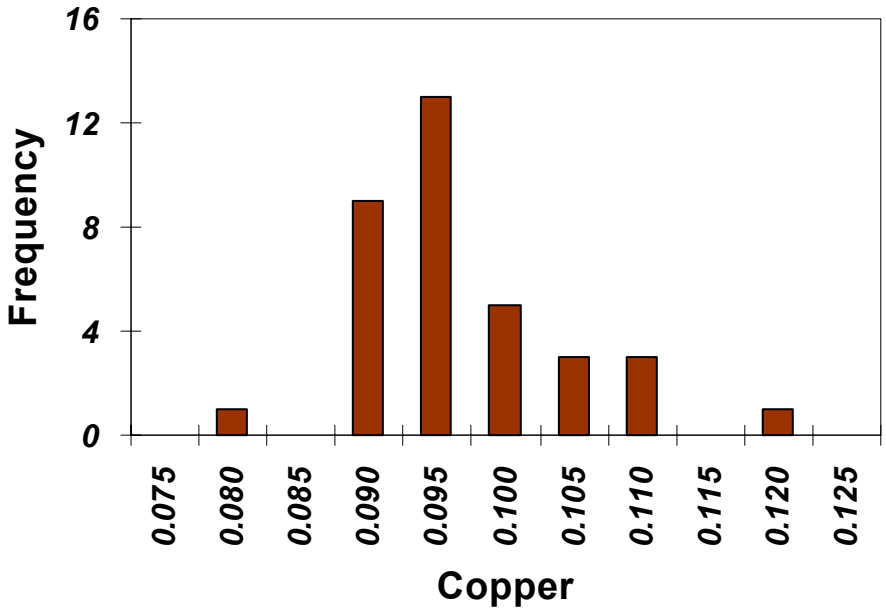


Figure B.7. Copper data reported in EPRI NP-373 for an A508 Cl. 2 forging (the vertical axis reflects the number of independent measurements made).

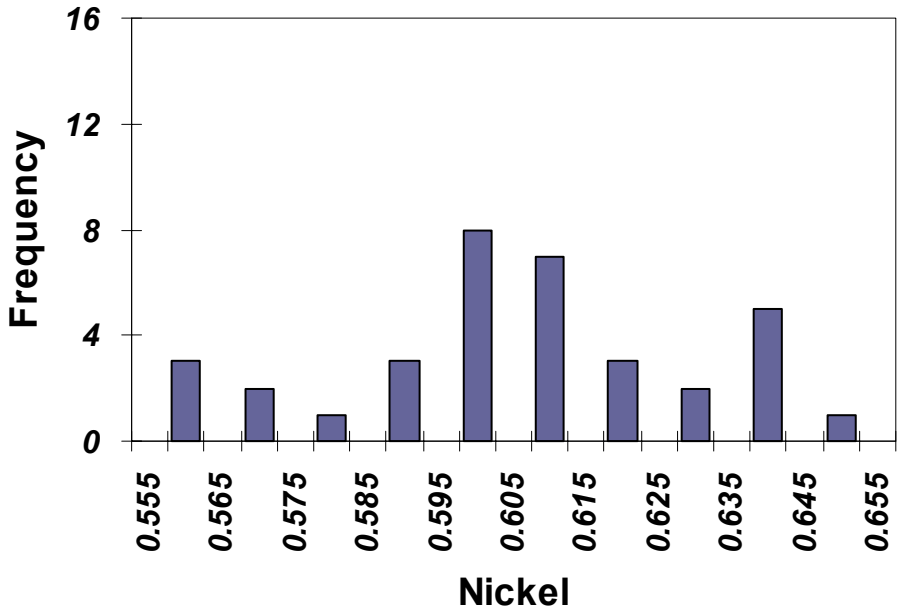


Figure B.8. Nickel data reported in EPRI NP-373 for an A508 Cl. 2 forging (the vertical axis reflects the number of independent measurements made).

### 8.2 Variability Within a Sub-Region

To quantify the variability in Cu, Ni, and P that could be expected to occur should FAVOR simulate more than one flaw to exist within the same sub-region, data sets were assembled from the literature wherein multiple measurements of chemistry were made close together (i.e. within the area covered by a few square inches). Two data sources were identified:

- o CE-NPSD-944: Five measurements of weld chemistry (Cu and Ni) were made at the ¼T location on eight different samples of weld, these samples having been removed from a total of 7 weld wire heats.
- o EPRI NP-371: As illustrated in Figure B.5, many groupings of chemistry measurements taken from this comprehensive study of chemistry can be used to assess the local variability of plate and weld chemistry.

To use all of these data together, the mean values of Cu, Ni, and P were first calculated for each local grouping. The deviation of each weld measurement from this local mean was then calculated, and a normal distribution fit to the deviation values to quantify the local variability in chemistry. These standard deviations are summarized in Table B.3, while Figure B.9 provides histograms of the underlying data. Should FAVOR simulate multiple flaws to exist within the same sub-region, normal distributions having the standard deviations from Table B.3 should be sampled, and then this sampled value added to the previously simulated mean values of chemistry for that sub-region.

Table B.3. Standard deviations to quantify local weld variability.

| | For Welds | For Plates and Forgings |
|---|---|---|
| Copper | 0.0131 | 0.0035 |
| Nickel | 0.0119 | 0.0124 |
| Phosphorus | 0.0008 | 0.0005 |

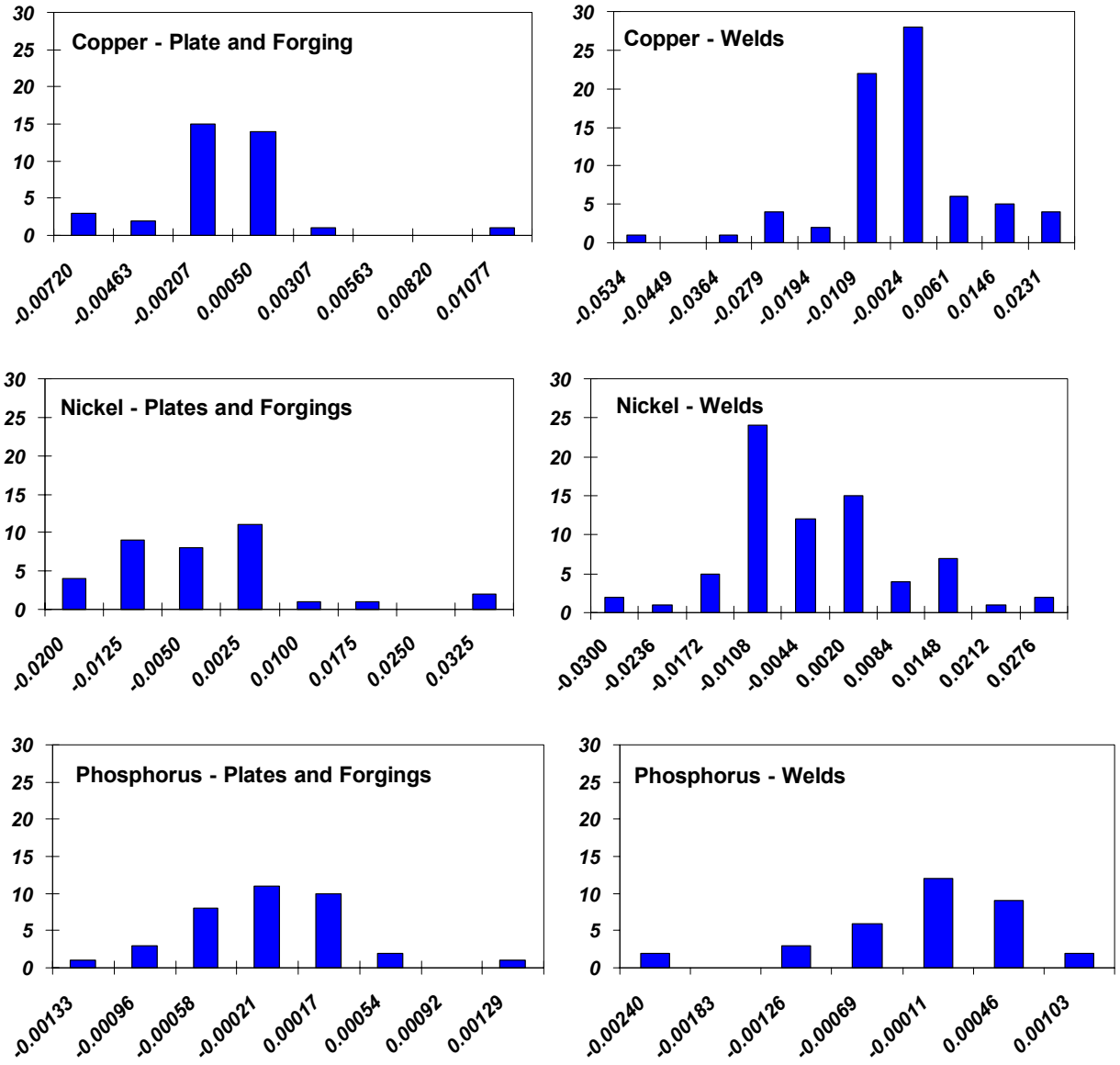


Figure B.9. Local chemistry variability histograms.